Exposure to Engineered Nanomaterial Results in Disruption of Brush Borders in Epithelia Models *in vitro*

by

James J. Faust

A Dissertation Presented in Partial Fulfillment
of the Requirements for the Degree
Doctor of Philosophy

Approved November 2014 by the
Graduate Supervisory Committee:

David Capco, Chair
Debra Baluch
Douglas Chandler
Richard Herman
Tatiana Ugarova

ARIZONA STATE UNIVERSITY

December 2014

ABSTRACT

Engineered nanoparticles (NP; 10^{-9} m) have found use in a variety of consumer goods and medical devices because of the unique changes in material properties that occur when synthesized on the nanoscale. Although many definitions for nanoparticle exist, from the perspective of size, nanoparticle is defined as particles with diameters less than 100 nm in any external dimension. Examples of their use include titanium dioxide added as a pigment in products intended to be ingested by humans, silicon dioxide NPs are used in foods as an anticaking agent, and gold or iron oxide NPs can be used as vectors for drug delivery or contrast agents for specialized medical imaging. Although the intended use of these NPs is often to improve human health, it has come to the attention of investigators that NPs can have unintended or even detrimental effects on the organism. This work describes one such unintended effect of NP exposure from the perspective of exposure via the oral route. First, this Dissertation will explain an event referred to as brush border disruption that occurred after nanoparticles interacted with an *in vitro* model of the human intestinal epithelium. Second, this Dissertation will identify and characterize several consumer goods that were shown to contain titanium dioxide that are intended to be ingested. Third, this Dissertation shows that sedimentation due to gravity does not artifactually result in disruption of brush borders as a consequence of exposure to food grade titanium dioxide *in vitro*. Finally, this Dissertation will demonstrate that iron oxide nanoparticles elicited similar effects after exposure to an *in vitro* brush border expressing model of the human placenta. Together, these data suggest that brush border disruption is not an artifact of the material/cell culture model, but instead represents a bona fide biological response as a result of exposure to nanomaterial.

ACKNOWLEDGMENTS

I wish to express my sincere gratitude to Professor David Capco for fostering my intellectual development over the years. I am sincerely grateful to Dr. Brian Koeneman for the training he provided during my undergraduate studies. I am particularly thankful to Professor Paul Westerhoff for his input in these studies, and financial support. I am indebted to his former and current students: Dr. Kyle Doudrick, Dr. Robert Reed, Dr. Yu Yang, and Mr. Xiangyu Bi for their expert characterization of the food grade titanium dioxide employed in a substantial portion of this work. I also wish to thank Dr. Yongsheng Chen from Georgia Institute of Technology for generously supporting the work related to α-Fe_2O_3 in Chapter 5. Dr. Wen Zhang is acknowledged for synthesizing and characterizing α-Fe_2O_3 nanoparticles used in chapter 5 of this Dissertation.

I thank David Lowry for his assistance and ongoing patience in the W.M. Keck Electron Microscopy Facility at ASU, and Dr. Karen Sweazea for the use of Sigma Stat. The microarray and quantitative PCR data shown in Chapter 5 of this work would not have been possible if it were not for the assistance provided by Dr. Scott Bingham in the DNA Core Facility at ASU.

Finally, I wish to thank the members of my supervisory committee for their technical advice, support of this work, and guidance in preparing me for future endeavors.

TABLE OF CONTENTS

CHAPTER Page

Page

LIST OF TABLES

Table Page

LIST OF FIGURES

Figure Page

Figure Page

Figure Page

CHAPTER 1

INTRODUCTION

Overview

Engineered nanoparticles (NP; < 100 nm) offer unique advantages in consumer goods and medicine compared to their bulk (> 100 nm) counterparts due to the material properties that change when synthesized on the nanoscale. Although NPs are used in consumer goods including human foods and in medicine, there exists little information about their potential side effects. From the standpoint of exposure, and because of their small size, NPs have the potential to interact with cells individually and organized as tissue in fundamentally different ways than their bulk counterparts. This dissertation describes one such side effect referred to as brush border disruption within the context of exposure via the oral route. Chapter 1 provides the reader with the information necessary to understand the experimental Chapters 2-5 in context; Chapter 2 describes the human intestinal cell lines used for the majority of experiments necessary to complete this Dissertation. Chapter 2 further describes the molecular architecture of the brush border cytoskeleton, and concludes with analytical methods necessary to conduct studies related to NP exposure within the context of brush border disruption. Chapter 3 describes methods used in order to isolate NP directly from consumer goods intended to be ingested. Chapter 4 reveals an effect of exposure to food grade TiO_2, and shows disruption of the intestinal brush border independent of sedimentation *in vitro*. Chapter 5 characterizes the effects of exposure to α-Fe_2O_3 NPs and shows brush border disruption in a cell culture model of the human placenta. Chapter 6 provides a conclusion to this Dissertation and suggests that NP exposure at the intestinal epithelium may elicit similar effects compared to enteropathic bacteria.

The Definition of Nanomaterial

At present the term "nano" can be inappropriately broad and can elicit a positive or negative connotation depending on the context. Encyclopedia Brittanica (Schrödinger, 2009) defines nanoparticle (nano·par·ti·cle) as: "a microscopic particle whose size is measured in nanometers." Nanometer is a unit of length in the metric system whose SI symbol is "nm" whereby 1 nm is equivalent to $1x10^{-9}$ meters. Put simply, 1 nm is equivalent to one billionth of a meter. To put this small size into context, it is known that the human fingernail on average grows at a rate of 1 nm/s (Initiative, 2006), the diameter of deoxyribonucleic acid (DNA) is 2.5 nm, and a piece of paper is 100,000 nm thick (Initiative, 2006). Arguably the most widely used definition of NP is any particle with external dimensions between 1- and 100 nm (Dunphy Guzman, Taylor, & Banfield, 2006; Roco, 2007)

Particle size is not the only criterion that defines the word "nanoparticle." Auffan and coworkers (2009) argue that the change in physico-chemical properties that occur only below a specified size are the cause of toxicity, whereas particles above the 20-30 nm threshold typically behave similar to larger (i.e., bulk) particles of identical chemical composition. Using a variety of examples the authors illustrate that inorganic metal and metal oxide NPs (e.g., gold, titanium dioxide, alumina oxide, etc.) below 20-30 nm in diameter have novel material properties that could negatively affect biological systems (Auffan et al., 2009). Although there is relevance to the definition set forth by Auffan et al., (2009) other (Kreyling, Semmler-Behnke, & Chaudhry, 2010) argue that volume specific surface area should be the defining criterion. The authors put forth the definition in part because of the fact that many small particle tend to aggregate or agglomerate due to their high surface free-energy. These aggregated/agglomerated materials contain a collection of particles that can have heterogeneous sizes. Although

this collection of material as an agglomerate/aggregate is usually in the micrometer (μm; $1x10^{-6}$ m) range, primary particles can undergo desorption from the agglomerate over time (Auffan et al., 2009) and interfere with normal biochemical processes.

Although these definitions are pleasing to the physical chemist, the biologist might not see the need for such specific definitions. Rather, early studies related to toxicology of NPs have shown that the principal issue related to the detrimental effects of the material is the inability of the body to clear the material from the tissue. This is best exemplified in the case of carbon or asbestos exposure within the mining community (Oberdörster, Stone, & Donaldson, 2007). As miners were chronically exposed to the material, the immune system was unable to clear the inorganic material, but still produced effects associated with disease (i.e., inflammation, fibrosis, etc.). This in turn led to detrimental effects to the body over the long term. Therefore, from a purely biological perspective, surface reactivity, the ability to act as a catalyst, and paramagnetism are irrelevant if the body has no means to remove the material from site of exposure. Therefore, this dissertation has opted to define nanoparticle based on sizes that are most readily internalized by the cell culture models employed in this work. Loosely speaking, and as defined in this dissertation, nanoparticles are <100 nm in diameter, whereas bulk particles are >100 nm in diameter.

Finally, some investigators elect to define the word nanoparticle based on the peculiar notion that biomolecules are nanoparticles. For example, some define lipid-based delivery vehicles used as vectors for small molecule drugs or DNA/RNA as nanoparticles. Although these vesicles can be made ≤100 nm in diameter, they are composed largely of organic material that the body can breakdown. Furthermore, their particokinetics are dictated largely by diffusional forces and Browian motion (Einstein, 1956). In the case of inorganic metal and metal oxide nanoparticles, many additional

physical forces contribute to particokinetics during *in vitro* and *in vivo* exposure assessment (Teeguarden, Hinderliter, Orr, Thrall, & Pounds, 2007). In the case of inorganic metal and metal oxide nanoparticles, not only do the cells within the body have few defenses against excess metal as nanoparticles, but biological identity can be conferred to inorganic nanoparticles due to their high surface free-energy. Indeed, the concept of the nanoparticle corona (Lundqvist et al., 2008; Monopoli, Åberg, Salvati, & Dawson, 2012) which will be described in Chapter 6 of this dissertation, further underscores the complexity of inorganic nanoparticles and the importance of defining "nano" based on the biologists view within the context of exposure assessment.

The Uses of Nanomaterial

As illustrated in Chapter 2 of this dissertation, it is coming to the attention of investigators that consumer goods contain nanoparticles. The most widely cited example detailing the physico-chemical parameters of TiO_2 isolated directly from consumer goods came from a study conducted in the Westerhoff laboratory (Weir, Westerhoff, Fabricius, Hristovski, & von Goetz, 2012). The study (Weir et al., 2012) showed that a number of foods contained nanoparticles as TiO_2, and Monte Carlo simulations were conducted in order to determine the amount of titanium (Ti) ingested. These analyses indicated that children in the US are the highest consumers of food grade Ti at concentrations between 1-2 mg/kg body weight/day. However, because of its high refractive index and texture modifying properties TiO_2 is commonly added to products such as milk, toothpaste, and candies including chewing gum (Weir et al., 2012). TiO_2 was approved as a color additive for use in human food products by the Food and Drug Administration in 1966 with the stipulation that it not to exceed 1% by weight. TiO_2 as a food grade additive has the European Union Classification # E171. Color and texture are not the only reasons nanoparticles are used to modify human foods. Because of its abundance (10% of the

earth's crust) and chemical properties silicon dioxide (SiO_2) NPs have found use in a plethora of food products (Chaudhry et al., 2008; Tiede et al., 2008). SiO_2 was categorized as E551, and is commonly used as an anticaking agent. Recent studies have found silver NPs on the surface of pears (Z. Zhang, Kong, Vardhanabhuti, Mustapha, & Lin, 2012). Silver is a known antibacterial agent used in a number of consumer products (Rai, Yadav, & Gade, 2009).

Aside from human foods there are a number of medically relevant uses for engineered NPs. Cadmium/telluride NPs encapsulated by a zinc sulfide shell and further decorated with capping ligands have unique optical properties. These so called quantum dots have a number of advantages over organic fluorophores including increased brightness and lengthened fluorescent "on" states (Leutwyler, Bürgi, & Burgl, 1996; Michalet et al., 2005). Furthermore, the emission profile of the NP semiconductors can be tailored based on the diameter of the NP. Smaller quantum dot nanocrystals emit blue light, while larger quantum dots emit red light. Because of their small size, and resistance to photobleaching these NPs offer unique advantages over traditional organic fluorophores. Quantum dots are not the only exciting imaging advancement that can be achieved when certain materials are synthesizes on the nanoscale. Iron oxide nanoparticle crystals (i.e., γ-Fe_2O_3, Fe_3O_4) undergo a change in magnetism when synthesized below 20 nm in diameter (Ajay Kumar Gupta & Gupta, 2005). This change in magnetism to superparamagnetism results in NPs that can be used for magnetic resonance imaging (MRI; Ajay Kumar Gupta & Gupta, 2005). However, their larger counterparts offer little use for MRI.

NPs can also be used for tumor therapy. As the diameter of the particle is made smaller, there is an increase in the surface-area-to-volume ratio. On the nanoscale this results in a large number of atoms on the surface of the particle. Investigators have

exploited the fact that the surface atoms can be further chemically modified, a process referred to as functionalization, to permit attachment of a wide variety of bioactive compounds. Modifications to the particle surface results in covalent attachment of a range of chemical moieties from simple amine and carboxyl groups to change the surface charge, to antibodies, or even lipid-based varieties (Han, Ghosh, & Rotello, 2007; Lu, Salabas, & Schüth, 2007), and by no means is this list comprehensive. Because of the ability to functionalize the surface of nanoparticles with various chemical moieties, it is possible to attach small molecule chemotherapeutic drugs to locally deliver drugs to tumors. Specificity of the treatment is one central barrier to chemotherapeutic agents. Therefore, the ability to couple antibodies in addition to chemotherapeutic drugs to the surface of the nanoparticle permits localized treatment of cancerous cells while minimizing off-target effects due to the high degree of specificity antibodies endow.

In addition to their use as vectors for delivery, investigators have further taken advantage of the inherent changes in material properties that occur when the material is synthesized on the nanoscale. As indicated in the preceding text, iron oxide NPs can undergo a change to superparamagnetism when synthesized below 20 nm in diameter. If an alternating magnetic field is applied to these superparamagnetic iron oxide nanoparticles (SPIONs), under the right conditions these changes in magnetic field produce local heating of the SPIONs. Localized heating of tissue (i.e., thermal ablation) can result in tissue death, which adds a synergistic component; Tissue imaging through MRI, specificity through surface functionalized antibodies, local drug delivery, and thermal ablation indeed provide a multi-faceted approach to tumor treatment. In addition to SPIONs, gold NPs offer similar advantages because of the material properties on the nanoscale. Gold NPs can be pulsed with a tuned two-photon laser in the near infrared region to produce localized hyperthermia (Terentyuk et al., 2009). The

advantage of this system is the fact that near infrared light is much less phototoxic compared to the visible wavelengths of light necessary to normally heat gold NPs. Furthermore, the two photon pulse permits deep penetration compared to conventional lasers. In addition, short laser pulses result in vaporization of a thin layer of the NP. This in turn imparts mechanical force on the surrounding tissue which acts analogous to an explosion in the immediate vicinity of the vaporized NP. These phototherapy approaches are only made possible because of the absorption of light resulting in surface surface plasmon resonance and tunability of gold NPs (X. Huang, Jain, El-Sayed, & El-Sayed, 2007, 2008).

By no means should the aforementioned list of NP uses be considered exhaustive. Iron NPs have been used to remediate groundwater contaminated with arsenic and chlorinated species (Cundy, Hopkinson, & Whitby, 2008). TiO_2 nanotubes have been employed to split water into hydrogen and oxygen (Lin, Lu, Hsieh, & Chien, 2009). Gold NPs have been used to produce colormetric reactions capable of detecting elements such as lead (Z. Wang, Lee, & Lu, 2008), and silver NPs have been applied to wound dressings in order to promote anti-microbial effects (Maneerung, Tokura, & Rujiravanit, 2008). Because of their uses in consumer goods, in medicine, and in the environment, it appears that NPs have become an integral part of our economy.

Routes of Nanomaterial Exposure in the Human Body

It has become clear that NPs are ingrained in our society because of the multifaceted benefits of their production and use. However, due to their small size, reactivity, and surface-area-to-volume ratio, a number of unintended and off-target side effects of NP exposure have been documented. Before the effects of NP exposure observed as studies in this dissertation are shown, it is necessary to describe first the principal routes of NP exposure in humans. As detailed in the proceeding text, the four

major routes of exposure are: Inhalation, dermal, direct injection, and oral. Inhalation, dermal and direct injection will be discussed briefly, whereas the focus of the text will be exposure via the oral route. Although some consider ocular exposure a portal for NP entry, these discussions can be found elsewhere (Warheit, Sayes, Reed, & Swain, 2008).

Arguably the most widely studies route of NP exposure is inhalation. This is largely due to the causal role of particle and fiber dust that was found to affect the mining community and elicit disease (Donaldson, Murphy, Schinwald, Duffin, & Poland, 2011; Oberdörster et al., 2007). Studies have shown also that burning wood releases NPs that can be inhaled by humans and affect the lung (Lipsky & Robinson, 2006). More recently, it has come to the attention of scientific community that burning diesel or combustion-based gas products results in the release of ultrafine (10 Å - 10 nm) particles (Donaldson et al., 2005; Oberdörster & Utell, 2002). Once these particles are introduced to lung tissue, the body initiates an immune response. Long term and repeated exposure to certain types of micro- and nano-scale particles can result in tissue fibrosis or even lung cancers (Davis et al., 1986; Hodgson & Darnton, 2000; Selikoff, Churg, & Hammond, 1964). As a consequence of these studies there has been a shift from assessing the effects of exposure after a clear link to toxicity has been made, to employing small animal and cell culture models in order to determine if NPs could result in toxicity (Donaldson & Seaton, 2012). Although the body has evolved several defenses to deny access to the lung, high concentrations, the size of the particle or fiber, and duration of exposure play a role in actual concentrations that reach the lung.

Dermal application represents another major route of NP exposure. Due to its ability to refract light in the ultraviolet range, TiO_2 has found use as a physical barrier in sunscreens (Abbott & Maynard, 2010; Crosera et al., 2009). Moreover, when TiO_2 is synthesized on the nanoscale and subsequently applied to skin, the whiteness of the

material diminishes and the application appears natural (i.e., not white, but skin-tone). The use of TiO_2 NPs in sunscreen is further underscored by the fact that surface modifications can make the NPs hydrophobic. Altering the wetting properties of the material makes the sunscreen "water-proof," and not easily removed from skin. These properties of TiO_2 that only occur when synthesized as NPs have made TiO_2 NPs a major additive to sunscreens and cosmetics (Sadrieh et al., 2010). Zinc oxide and alumina oxide are applied also to various cosmetics and health and beauty products (Nohynek, Dufour, & Roberts, 2008).

As indicated in the preceding text, one major use of NPs can be in diagnostics and medicine. When used for potential therapeutic intervention, the NPs are directly injected to the site of interest. This includes intravenous, intraperitoneal, intracranial, etc., and can result in higher NP concentrations at the injection site compared to other exposure routes. Although injection of NPs in humans as a route of NP exposure is limited to clinical trials, the possibility exists that NPs will be injected as therapeutic options for human disease or diagnosis in the future. Furthermore, injection of NPs as a route of exposure in small animal studies has been widely adopted (Semmler‐Behnke et al., 2008; Takeda et al., 2009; Yamashita et al., 2011). Therefore, inject of NPs as a route of exposure must be considered also.

Although there is a considerable body of literature related to inhalation, dermal, and direct injection as exposure routes, relatively less is known regarding exposure to NPs via the oral route. This comes as a surprise given the fact that NPs are additives in human foods (Weir et al., 2012) or even in drink supplements (R.B. Reed et al., 2014). However, there has recently been a paradigm shift from studying NPs purchased from chemical companies to employing food grade or even NPs isolated directly from foodstuffs (Athinarayanan, Periasamy, Alsaif, Al-Warthan, & Alshatwi, 2014; J. J. Faust,

Doudrick, Yang, Westerhoff, & Capco, 2014). This is due to the fact that semi-conductor type NPs or those used in cosmetics are unlikely to be intentionally ingested by humans. In order to understand the potential sites of exposure, the proceeding text will briefly outline the anatomical features of the alimentary tract and describe how foodstuffs which can contain NPs are taken into the body.

The Passage of Foodstuffs through the Alimentary Tract

Mastication begins as the teeth physically sheer and grind foodstuffs into small pieces. This is done in order to create a bolus that is fragmented and lubricated with saliva for swallowing. The bolus is passed from the oral cavity to the esophagus and into the stomach, where fragmentation completes and digestion ensues. The initial stage of digestion is accomplished by muscular contractions in the stomach in concert with the low pH environment of the stomach to produce chyme. Chyme is passed from the stomach into the duodenum of the small intestine where pancreatic enzymes and bicarbonate, and bile from the liver mix with chyme to neutralize pH, digest complex macromolecules, and emulsify fat. The small intestine has a number of anatomical features that give rise to additional surface area. First, the gut is thrown into folds known as plicae; second, mound-like structures known as villi decorate the plicae; third the epithelial cells that line the luminal region of the villi contain an apical cell specialization known as microvilli. These cells are endowed with 1,000 to 3,000 microvilli depending on the anatomical position of the cells within the gastrointestinal (GI) tract. Microvilli in quantities as great at 1,000-3,000 microvilli per cell are referred to as brush borders. Cells containing brush borders exist in the small and large intestine, in the kidney proximal tubule, and in the placental syncytiotrophoblast. The tiers of anatomical features that create surface area greatly aid in nutrient absorption. The bolus proceeds through the jejunum and ileum of the small intestine with aid from

longitudinal and circular contractions of the muscle lining the gut, an event referred to as peristalsis. Absorption is completed as the bolus passes into the large intestine where water is reabsorbed. Feces are excreted from the body via defecation through the anal canal. The regional architecture of the GI tract is based on similar functional layers from the esophagus to the anus, and a detailed histological plan can be found elsewhere (Young, Woodford, & O'Dowd, 2013). However, it should be noted that the luminal regions of the GI tract are most likely to come in contact with inorganic NPs as part of foodstuffs since the epithelia that line the lumen are responsible for protection, secretion and absorption.

In particular, the main function of the small intestine is nutrient absorption. Although a number of physical barriers exist in the human body to prohibit direct contact between the cells within the epithelium and chyme, the epithelium of the small intestine is most likely to encounter the majority of ingested NPs within foodstuffs. This is because nutrient digestion is completed and absorption begins in the duodenum as enzymes breakdown complex macromolecules into smaller parts only after the stomach has liquefied the bolus. Further, peristalsis churns chyme in an effort to maximize the amount of chyme that comes in contact with the absorptive epithelium. These concerted events, coupled with the small size of NPs, and the fact that the epithelium is a gateway to the body makes the absorptive epithelium of the small intestine a fascinating model that has been employed by investigators in order to determine if engineered NPs elicit toxic events in this cell system.

Disruption of the Intestinal Brush Border as a Consequence of NP Exposure

The remainder of this dissertation focuses on an event referred to as brush border disruption. The first study to describe brush border disruption was by Koeneman and cowrokers (2010). This event was identified after exposure to TiO_2 NPs (Koeneman

et al., 2010), but has been shown also to be a consequence of exposure to iron oxide NPs (Madhavi Kalive, Wen Zhang, Yongsheng Chen, & David G Capco, 2012; W. Zhang, Kalive, Capco, & Chen, 2010). Brush border disruption is defined as a loss and/or reorganization of the brush border microvilli. Under normal conditions brush border microvilli are well ordered, standing straight off the surface of the cells, and dense in number. However, the study by Koeneman et al., (2010) revealed a change in the normal structure of the microvilli such that exposure to TiO_2 NPs resulted in a loss in the total number of microvilli, and an altered surface morphology. Since microvilli exist to provide additional cell surface area, a reduction in the total number and organization of brush border microvilli could result in malnutrition or diarrhea.

The goal of this dissertation was to identify whether or not disruption of the brush border was an artifact of *in vitro* exposure. That is, because human tissue is difficult and costly to procure, investigators have turned to immortalized cell lines that can be grown in culture. These cell lines retain many of the morphological and biochemical features of cells within the body, but offer a simple system as a first step in identifying whether or not NPs affect the normal engineering of human cells. Although cell culture has revolutionized cell biology, many investigators have not used comparable cell lines, and analytical techniques necessary to detail interactions of NPs in cell culture models of the gut. Therefore, Chapter 2 of this dissertation describes the Caco-2 BBe1 cell line and provides several hypotheses regarding possible mechanisms that might account for brush border disruption as a consequence of NP exposure. The brush border cytoskeleton that permits the normal number and morphology of microvilli is described in detail. In addition, procedures are outlined for the normal growth of the cell line and methods to image the cells using scanning and transmission electron microscopy. One main barrier that exists is employing material that is relevant for *in vitro* studies.

Therefore, Chapter 3 identifies several sources that can be used to isolate food grade TiO_2 and provides a simple method to separate bulk (> 100 nm) from nanoparticles (< 100 nm) in complex mixtures of TiO_2. Furthermore, at least one criticism of employing cell culture is the fact that a number of physical forces exist in the body that are difficult to recreate during *in vitro* analysis. Chapter 4 utilizes relevant food grade sources of TiO_2, and provides evidence that brush border disruption is not an event dependent on sedimentation of agglomerated food grade TiO_2 due to *in vitro* analysis. Although brush border disruption occurs in human intestinal cells, do other brush border expressing models result in similar finding *in vitro*? Chapter 5 describes size-dependent effects of 3 different diameters of a model iron oxide (α-Fe_2O_3) NP, and shows that brush border disruption is not an event exclusive to human intestinal cells. Chapter 6 concludes this work by discussing the significance of these findings and outlines future perspectives.

CHAPTER 2

ENGINEERED NANOPARTICLES INDUCED BRUSH BORDER DISRUPTION IN A HUMAN MODEL OF THE INTESTINAL EPITHELIUM

Nanomaterials and Exposure to the Human Body

This chapter defines engineered nanomaterials as nanoparticles (NPs) deliberately constructed to exploit the unique characteristics of the material on the nanoscale (10^{-9} m in diameter), and not those NPs that exists due to natural environmental processes. Further, a nanoparticle is defined within this chapter as materials that have a diameter of 1-100 nm in any external dimension (Dunphy Guzman et al., 2006; Foss Hansen, Larsen, Olsen, & Baun, 2007). In this chapter this definition includes NP agglomerates as the state of agglomeration can change depending on the location in the human body, and since the surface free-energy of individual NPs may still exist. Engineered NPs can take on a variety of geometries, crystal structures, or elemental composition(s) depending on their intended use. The excitement these NPs encourage is highlighted by the fact that the physico-chemical parameters can be tailored if the surface of the nanomaterials is chemically functionalized through conjugation chemistry. That is, a number of physical interactions (e.g. covalent or noncovalent bonding) can be exploited at the NP surface to chemically "tailor" NPs. Examples for the use of engineered NPs include drug delivery (Arruebo, Fernández-Pacheco, Ibarra, & Santamaría, 2007), tissue contrast enhancement for MRI (Mahmoudi, Sant, Wang, Laurent, & Sen, 2011; Oh & Park, 2011), wavelength specific probes for fluorescence imaging (Howarth, Takao, Hayashi, & Ting, 2005; Resch-Genger, Grabolle, Cavaliere-Jaricot, Nitschke, & Nann, 2008), cancer targeting (Gao, Cui, Levenson, Chung, & Nie, 2004) and ablation (H.-C. Huang, Rege, & Heys, 2010), environmental remediation of toxic compounds (Sylvester, Westerhoff, Möller, Badruzzaman, & Boyd, 2007), and this

list is by no means comprehensive. It is thus increasingly acknowledged that engineered NPs are an integral part of medical diagnostics, treatments, and consumer goods now and in the future.

While NPs have summoned considerable excitement within the scientific community because of the aforementioned characteristics, concern has been raised since some NPs act as a double-edged sword. Arguably the most widely known example of such a double-edged sword effect was exacted by the nanofiber, asbestos. Because of the material properties inherent to this nanofiber included tensile strength, and resistance to damage, it was ubiquitously used as components of construction materials. However, those human subjects chronically exposed to the nanofiber asbestos acquired respiratory pathologies such as mesothelioma. As a consequence of the aforementioned aftermath of human exposure to NPs, investigators have begun to characterize potential health-related effects of engineered NPs in a variety of *in vitro* cell culture models (Donaldson and Seaton, 2012). In such models, investigators employ cell systems that mimic the major site of tissue exposure for a given potential route of exposure, and this has lead to a number of insights concerning NPs in cell biology and medicine.

Due to the small size, three predominant routes by which NPs can intentionally or unintentionally enter the human body exist: These include inhalation, dermal, and exposure via the oral route. Concerning the latter, a great number of investigations have focused on understanding the uptake and subsequent transport of NPs through the gastrointestinal tract to improve bioavailability of pharmacological drugs, whereas few have investigated exposure in an effort to understand the response of individual cells in their social context. The remainder of this work will not address systemic transport of NPs from the gastrointestinal tract as systemic transport is beyond the scope of this chapter. Rather this work will flush out some of the unintended health effects NPs

provoke as ingested components of consumer goods or as part of a medical application with a focus on TiO_2 NPs. First, there is an extensive body of work, at the ultrastructural, biochemical, and molecular levels that set the foundation for understanding of effects of NPs on the cells of the gastrointestinal tract, and specifically, on the absorptive enterocytes that pass nutrients into the body. These components will be briefly reviewed as they provide key markers of assessing both gross and subtle effects of nanomaterials taken in by the oral route. Second, this chapter will describe an emerging nanotoxicity research paradigm; NP-induced brush border disruption. Finally, this chapter provides a detailed methods section which lays the basic framework for handling the principle model cell culture system for the absorptive cells of the gut including; a) proper cell culture and technique, and; b) scanning electron microscopy for the human brush border expressing cell line, Caco-2 BBe1. Inappropriate application of these techniques have resulted in several inconsistencies in results reported in the literature and have begun to confound the understanding of the system.

The Molecular Components of the Cytoskeletal Apparatus of the Intestinal Brush Border

Intestinal microvilli and the brush border.

When specimens are transversely sectioned through the long axis of the polarized enterocyte as part of the gut epithelium, the so-called microvilli appears as thin, "finger-like" projections emanating from the apical cell surface. While several different eukaryotic cells types assemble microvilli on their apical surface only those cells of the digestive tract and the kidney proximal tubule contain such an abundance of microvilli that early morphologists referred to these regions as brush borders (or striated borders). This cell specialization has captured the attention of investigators for decades, and its importance is underscored by the morphological and function redundancy found in

mammals including humans, to simple invertebrates such as the fruit fly, Drosophila (Figure 1).

Depending on the location within the gut, the dimensions of microvilli can vary since an increase in the length and number of microvilli results in increased cell surface area. For example, absorptive cells of the small intestine have microvilli with a length of approximately 1-2 μm and a diameter of 100 nm. In contrast, those cells of the colon have fewer microvilli per cell, and the length of each microvillus is around 500-1,000 nm. Further, within the Crypts of the small intestine exist undifferentiated cells that contain a sparse number of microvilli at the cellular apex (TM Mukherjee & Williams, 1967). In light of the fact that microvilli on their luminal/apical surface contain integral membrane proteins responsible for absorption of complex macromolecules (e.g., carbohydrates, peptides, etc.) it is not surprising that the small intestine, acting as the principal site of nutrient absorption contains cells with a robust number of microvilli, while the colon functioning to reabsorb water contains relatively fewer. The story related to the morphometry of microvilli is complicated by the fact that dietary changes can result in a decreased length of the microvilli (Misch, Giebel, & Faust, 1980), and that some molecular components of the microvilli continuously undergo states of assembly and disassembly (Stidwill, Wysolmerski, & Burgess, 1984). Since microvilli increase the cell surface area, it can be deduced that the cells of the small intestine have a greater surface area than cells of the large intestine. These facts indicate that studies related to NP-induced brush border disruption are complicated by both the anatomical location within the gastrointestinal tract, and the cell type employed, since these regions are variable.

Around the time the transmission electron microscope (TEM) became commercially available for biological samples, investigators captured the first detailed

glances of the brush border with high spatial resolution (Granger & Baker, 1950; Miller & Crane, 1961; TM Mukherjee & Williams, 1967; Palay & Karlin, 1959; Trier, 1963). Later with improved technique in chemical fixation of biological samples McNabb and Sandborn (1964) described filamentous structures at the core of the microvilli. In the early 1970 through the use of model organisms such as *Xenopus*, salamander, and chicken the formation and elongation of microvilli of the brush border was examined in detail, a process referred to as brush border morphogenesis. These model organisms were employed in part due to their ability to experimentally manipulate brush borders *in vitro*, and the gradual morphogenesis process unique to these models. Further, the ability to decorate actin filaments with heavy meromyosin (or the S-1 subfragment) enabled investigators to begin to identify the polarity of actin filaments in a variety of cell types (Ishikawa, Bischoff, & Holtzer, 1969). In a hallmark study, Tilney and Mooseker (1971) isolated brush borders and imaged decorated filamentous components of the microvilli with heavy meromyosin. Biochemical analysis through the use of SDS-PAGE indicated that the most abundant protein of isolated brush borders migrated in a manner identical to purified chicken actin. Together these data were the first to indicate unambiguously that actin is the major (i.e., the most abundant) cytoskeletal protein component of microvilli (Tilney & Mooseker, 1971). These early studies spurred a flurry of subsequent investigations focused on identifying the molecular components underlying the process of brush border morphogenesis (Arpin & Friederich, 1992; Bretscher, 1983a; Coudrier, Kerjaschki, & Louvard, 1988; Hirokawa & Heuser, 1981; Mooseker, 1985; Shibayama, Carboni, & Mooseker, 1987), which has been the focus of exhaustive reviews (Bement & Mooseker, 1996; Heintzelman & Mooseker, 1992).

The microvillar region.

Anatomically the brush border is separated and historically defined as the microvilli and terminal web regions (Heintzelman and Mooseker, 1992; see Figure 2). Within the microvillus core exists ~20 actin filaments organized as parallel bundles in a hexagonal array that extend into, and are supported by, the terminal web region. The electron-dense tip is the site where the addition of actin monomers to F-actin occurs, and these filaments were found to have uniform polarity with minus ends enmeshed within the terminal web (Begg, Rodewald, & Rebhun, 1978; Hirokawa & Heuser, 1981; Hirokawa, Tilney, Fujiwara, & Heuser, 1982). There are a number of proteins that secure F-actin bundles to one another. The first and most abundant is a 68-kDa protein known as fimbrin (Bretscher & Weber, 1980a), which is also referred to in the literature as plastin 1, I-plastin,or I-fimbrin. The second most abundant protein that bundles F-actin is the 95-kDa protein, villin which is stoichiometrically the minor to fimbrin (Bretscher & Weber, 1979). Finally the 30-kDa splice variant of espin acts to further crosslink axial bundles (Bartles, Zheng, Li, Wierda, & Chen, 1998). Each core bundle of actin filaments is laterally tethered in a helical arrangement to the plasma membrane by brush border myosin 1 (Myo1A), composed of a 110-kDa heavy chain and 4-5 calmodulin light chains (Garcia et al., 1989; Glenney Jr, Osborn, & Weber, 1982; Howe & Mooseker, 1983). Another protein that fastens the core bundle to the plasma membrane is the 80-kDa protein ezrin (Bretscher, 1983b; Bretscher, Reczek, & Berryman, 1997), although this result has been questioned recently through the use of molecular modeling techniques (Brown & McKnight, 2010). In cultured LLC-PK1 cells ezrin was found to interact with the Rho-GEF, PLEKHG6, to promote apical rearrangement of the actin cytoskeleton via Rho-G (D'Angelo et al., 2007). Furthermore, in an impressive display of microscopy, Zwaenepoel and coworkers (2012) elucidated the role of novel ezrin-

interacting partners of the Eps8 family responsible for proper brush border morphogenesis. Through the use of a yeast two-hybrid screen the authors found the novel protein Esp8L1a that interacts with phosphorylated ezrin and is a component of the brush border in LLC-PK1 cells. This novel component (Esp8L1a) of the porcine absorptive brush border was found to regulate microvilli length by capping F-actin at the plus tips (Zwaenepoel et al., 2012).

The terminal web region.

The terminal web is a support structure within which the F-actin core rootlets terminate (Figure 2). Structurally it is composed of the non-erythroid spectrins, fodrin and TW260/240 (Glenney, Glenney, & Weber, 1983), and myosin II that link adjacent core bundles (Hirokawa, Cheney, & Willard, 1983; Hirokawa et al., 1982). The actin bundles are further stabilized along the length of core filaments by tropomyosin (Mooseker, 1976). Within this meshwork α-actinin, a 95-kDa structural protein, associates with the microvillar rootlets and circumferential actin band (Bretscher & Weber, 1978). Beneath the interconnecting fine fibrils within the terminal web region is the intermediate filament network, which extends from intercellular junctions (Hirokawa et al., 1983; Hirokawa & Heuser, 1981; Hirokawa et al., 1982). Through immunohistochemical analysis fimbrin has also been shown to interact with cytokeratin 19, but not cytokeratin 8, in the terminal web (Grimm-Günter et al., 2009). Further, in fimbrin knockout mouse model Grimm-Gunter et al., (2009) demonstrated a role for fimbrin in the terminal web. Through the use of TEM the authors (Grimm-Gunter et al.) showed that these knockout mice have shorter microvilli with a disorganized and less densely packed terminal web region. The organelle-free zone, a region occupied, and extended by the terminal web, was significantly shorter in fimbrin deficient mice. For these reasons the authors suggest that fimbrin, aside from its classical role as a F-actin

bundling protein in the microvillus core, is an essential component of the terminal web that may act to stabilize the core actin rootlets to the intermediate filament network (Grimm-Günter et al., 2009). In the differentiated enterocyte just beneath the intermediate filament network exists the microtubule network organized as parallel columns from the apical to the basolateral domain of the cell (Achler, Filmer, Merte, & Drenckhahn, 1989; Gilbert, Le Bivic, Quaroni, & Rodriguez-Boulan, 1991; Halbleib, Sääf, Brown, & Nelson, 2007).

Molecular Targets Putatively Responsible for Brush Border Disruption

Several, as of yet, putative targets for the NP-induced disruption of the brush border exist. One mechanism is dependent on the inherent charge of the nanomaterial. The surface of any given nonfunctionalized (i.e., naked) NP contains large amounts of free energy due to the small size of the material. This free energy at the NP interface attracts oppositely charged components within its immediate environment. When naked (i.e., nonfunctionalized) NPs are in solution, this region is referred to as the electric double layer, and when the solution contains an abundance of proteins these layers are referred to as the hard and soft coronas. These corona proteins bound to the NPs can elicit a number of biological responses (Monopoli et al., 2012) one of which is the ability of NPs to reorganize the lipid bilayer (B. Wang, Zhang, Bae, & Granick, 2008). It is well known that under normal physiological conditions the concentration of intracellular-free calcium ($[Ca^{2+}]i$) in intestinal cells is at least five orders of magnitude lower than that of the extracellular environment. As a downstream consequence of a "leaky" plasma membrane a rapid increase in $[Ca^{2+}]i$ from the extracellular milieu could occur and activate the calcium-dependent protein, villin. Villin is versatile protein that was identified as an exclusive protein in brush borders. When $[Ca^{2+}]i$ levels are in the nanomolar concentrations, villin acts as a F-actin bundling protein. However, should

the $[Ca^{2+}]i$ concentrations reach the micro-to millimolar range villin converts to an F-actin severing protein. Further, under certain circumstances villin assumes the role of capping F-actin. It was thus predicted by Koeneman and coworkers (2010) to be the causal agent responsible for the NP-induced brush border disruption accompanying exposure to a 70/30% (anatase/rutile) mixture of TiO_2 NPs. This prediction was based on the fact that a dose-dependent disruption of the microvilli was observed as well as a dose-dependent increase in $[Ca^{2+}]i$. This prediction may be corroborated in part by siRNA disruption of villin; employing an antisense approach the authors (De Beauregard et al.) permanently down-regulated villin and observed what was referred to as "limp" microvilli. That is, the microvilli appeared to fall over and become parallel, and not perpendicular to the horizontal axis of the plasma membrane. This limp morphology was rescued by cDNA encoding a partial sense villin RNA (De Beauregard, Pringault, Robine, & Louvard, 1995) indicating that villin could play a role in the disruption observed by Koeneman and coworkers (2010). The report (Koeneman et al., 2010) was notable in that it was the first to indicate that TiO_2 NPs, although classically considered to be relatively inert, have the ability to disrupt microvilli of the brush border after exposure to an *in vitro* model of the human intestine (the Caco-2 BBe1 cell model). This work has since prompted subsequent investigations into the potential effects TiO_2 NPs instigate after exposure in the Caco-2 cell model.

Brush Border Disruption as a Result of Exposure to NPs in Consumer Goods

There are number of benefits for the use of TiO_2 NPs in medicine and consumer goods. One example is the addition of TiO_2 NPs in sun screens, in part due to the fact that TiO_2 is highly reflective and acts as a protective physical barrier between human skin and the sun. However, under certain conditions ultraviolet light can interact with the TiO_2 NP surface and results in photocatalytic production of oxygen radicals. In an

effort to reduce the photocatalytic effects, TiO_2 NPs that are components of sun screens can be encapsulated with aluminum oxide. After the aluminum oxide encasing, the NPs can be further functionalized to improve hydrophobicity. However, it has also become clear that NPs undergo changes thoughout, what is referred to as a "life cycle." The life cycle of NPs is defined as changes that can occur as the NP is modified by different conditions in the environment which can include different parts of the human body. The life cycle begins at the time NPs are manufactured and can be altered by temperature, pH, and light among other things, as their local physical environment is altered - for example, NPs in pure neutral water (pH 7.2) do not behave the same as they would in the acid conditions in the stomach (pH ~1-4). One study (Fisichella et al., 2012) set out to investigate the life cycle of functionalized TiO_2 NPs that are components of these sun screens and subsequently the downstream effects in the Caco-2 cell model. The authors treated the NPs with acid in an effort to mimic the effects of passage through the stomach as well as incubating replicate NPs in water while applying ultraviolet light, and assessed the physico-chemical changes accompanying these treatments. The study found that gastric or environmental conditions degraded the hydrophobic polydimethylsiloxane (PDMS) surface modification such that these NPs became hydrophilic and agglomerated over time. After degradation of the PMDS organic layer, the authors claimed that theseTiO_2 NPs are not taken up by Caco-2 cells, and further, that they do not disrupt the brush border of Caco-2 cells at a concentration of 100 μg/mL after a 72 hour exposure. However, other studies have clearly shown that nonfunctionalized TiO_2 NPs are internalized in the Caco-2 cell model, and this internalization was confirmed through the use of mass balance analysis (Koeneman et al., 2010). Furthermore, recent studies suggest that a change in the NP life cycle from human skin to chlorine containing water sources such as swimming pools results in a

rapid degradation of the protective aluminum shell (Virkutyte, Al-Abed, & Dionysiou, 2012).

While the study by Koeneman and colleagues (2010) was the first, it is not the only study to indicate a disruption of the brush border as a result of NP exposure. Employing a model iron oxide NP (hematite; α-Fe_2O_3) first Zhang et al., (2010) and later Kalive et al., (2012) demonstrated a NP-induced disruption of the brush border in Caco-2 cells. The study by Zhang and coworkers (2010) suggested that the interaction between the NP surface and plasma membrane resulted in adsorption of hematite to the cell surface. The authors hypothesized that movement of the brush border microvilli permitted access for the NPs to "wedge" between individual microvilli. The authors proposed that this wedging caused the arrays of microvilli to whorl around a central point at their microvillar tips when viewed by scanning electron microscopy (SEM) after NP exposure (W. Zhang et al., 2010). Although individual microvilli do not oscillate to move materials in the gut under normal conditions, they do contain a number of molecular motors that act to stabilize both the microvillar and terminal web regions. Studies have shown that injection of antibodies directed against myosin II in a brush border expressing porcine cell line (LLC-PK1) result in microvilli that apparently became limp (Temm-Grove, Helbing, Wiegand, Honer, & Jockusch, 1992). Through DNA microarray analysis it was found by Kalive et al., (2012) that a number of genes responsible for the production of intermediate filament proteins, some of which are components of the terminal web, are upregulated. Further regarding the microvillar region it was found that the gene responsible for the production of the actin capping protein CapZ (typed in their publication as CAPZA) which is a known component of the plus tips of the microvilli was upregulated (Madhavi Kalive et al., 2012). Data shown in Chapter 5 of this dissertation corroborate upregulation of *CapZ* as a result of NP

exposure, albeit in an established, brush border expressing model of the human placenta. Taken together these results suggest at least two independent mechanisms by which the NPs disrupt the archetypical organization of the brush border. First, structural components integral to terminal web continuity are altered at the gene level as a result of NP exposure. Since microvilli cannot exist without a supporting structure from which F-actin bundles exert force to deform the apical plasma membrane, it can be predicted that gross changes in the organization and composition of the terminal web at the protein level result in brush border disruption. Second, actin capping at the plus tips of the microvilli could induce a retraction of the brush border since the individual actin filaments continuously undergo a state of flux with addition of monomers at their plus tips.

More recently it has come to the attention of investigators that NPs are common additives to a number of ingested consumer goods (Weir et al., 2012). The study by Weir et al., (2012) surveyed a number of food products and found P25 and E171 TiO_2 NPs in food. The latter is a pigment approved by the United State Food and Drug Administration in 1966 as a color additive for use in human food (FDA, 2010). The authors (Weir et al., 2012) found that 36% of this pigment contained particles with one external dimension <100 nm in diameter. The study subsequently calculated dietary exposure and found that children under the age of 10 years in the United States and the United Kingdom are the greatest consumers of ingested TiO_2 NPs at concentrations of 1-2 mg TiO_2 per kilogram of body weight per day and 2-3 mg TiO_2 per kilogram of body weight per day, respectively (Weir et al., 2012). These data highlight the need to assess the effects of food-grade NPs after exposure to models of the human gut, since studies indicate that TiO_2 NPs disrupt the human enterocyte brush border, and that food-grade pigments are being consumed as NPs.

Procedures to Procure Differentiated Brush Borders Using the Caco- 2BBe1 Cell Model.

Introduction to cell culture and the Caco-2 BBe1 cell line.

The procedures in the proceeding text describe routine maintenance of Caco-2 BBe1 cells from the date they are purchased, through cell culture, and conclude with a protocol to procure publication quality scanning electron micrographs of brush borders. While these methods seem straightforward, it is advised that only those investigators that have experience with cell culture and cell biology attempt to employ this model for studies related to materials science and engineering of nanomaterials as slight deviations from routine electron microscopy protocols or careless culture technique result in brush borders that appear in poor health. If untreated brush borders are in poor health then it becomes impossible to determine if NPs have an effect on the brush border. As a consequence, investigators have questioned whether or not these control brush borders are representative, and some have begun to show unhealthy epithelia as control specimens, albeit employing unorthodox cell culture or electron microscopy techniques. These differences highlight the need to standardize protocols to obtain accurate and comparable results between investigators.

In order to permit adequate resolution of brush borders and the subtle changes that may accompany brush border disruption, investigators commonly employ SEM and image at high magnification. The field of view in a scanning electron micrograph at high magnification can be the diameter of the average Caco-2 BBe1 cell after the 17-21 days of differentiation. Figure 3 is a representative scanning electron micrograph after the 17-21 days of proper aseptic technique and culture conditions required to permit brush border morphogenesis. When viewed as a scanning electron micrograph the apical surface of the Caco-2 BBe1 epithelium decorated with a well-ordered array of the finger-like

projections known as microvilli (Figure 3). The micrograph (Figure 3 A) was captured at a magnification of 1,500x in an attempt to balance resolution of individual microvilli with the number of cells in the field of view. At this magnification of 1,500x the intercellular borders become difficult to see. However, the telltale sign of the cell to cell interface is the slight interdigitation of microvilli outlined by white arrows (Figure 3 A). The micrographs shows 3 different regions directly surrounded by the oval, square, and triangle in Figure 3 A corresponding to 3 different cells imaged as higher (5,000x) magnification views (Figure 3 B-D) to illustrate in detail the archetypical organization of the human enterocyte brush border (Caco-2 BBe1 epithelia). It is important for the investigator to choose random areas when conducting morphometric analysis of brush borders. Further, the investigator must choose at least 3 random 1 μm^2 regions to count microvilli in order to procure statistical analysis from three independent experiments. Finally, if control specimens do not appear well organized as shown in Figure 3, the entire experiment must be culled from analysis as the result from the experimental exposure would be ambiguous.

Details related to basic cell culture and aseptic technique are beyond the scope of this methods section. However, it is highly recommended that the investigator practice cell culture techniques as described in the Freshney text (Freshney, 2005). Historically, the parental Caco-2 cell line designated by American Type Culture Collection (ATCC) as HTB-37™ was employed to study the uptake and pharmacokinetics of novel drugs (Artursson, Palm, & Luthman, 2012; Hidalgo, Raub, & Borchardt, 1989); for the first time a simplified model of the human gastrointestinal tract could be grown in culture and used in high throughput to screen materials. This cell line allured investigators as it could be propagated continuously in culture eliminating the expense and ethical concerns associated with procuring fresh human tissue. Further, a large number of cells

can be grown for experimental analysis and used in standardized assays. While HTB-37™ sparked interest for its use as a predictor of small molecule transport, it was limited in that epithelia formed from this cell line were found to be relatively heterogeneous, and some cells within this epithelium did not produce brush borders at all. In 1992 Peterson and Mooseker subcloned HTB-37™ and called these cell lines brush border expressing 1 and 2 (BBe1 and BBe2). This was, in part, first due to a need for a human cell line that faithfully mimicked the *in vivo* brush borders at the morphological and biochemical levels. And second, the need for an *in vitro* model that sustained gradual morphogenesis of the brush border in order to understand the molecular events accompanying brush border morphogenesis. Since that time there have been numerous investigators that have employed the Caco-2 BBe1 cell system to exploit the archetypical organization of the brush border *in vitro* (Bement, Forscher, & Mooseker, 1993; J.J. Faust & Capco, 2012; Halbleib et al., 2007; Koeneman et al., 2009; M. D. Peterson & Mooseker, 1993).

One benefit of *in vitro* cell systems is that the investigator can screen various NP diameters, concentrations, physico-chemical parameters, etc., for those NPs that result in relatively few toxic effects. For these reasons investigators have employed the Caco-2 BBe1 cell model in order to understand the effects NPs elicit after exposure via the oral route. The use of the Caco-2 cell model has been recommended by the International Life Science Institute Research Foundation/Risk Science Institute (ILSI RF/RSI) Nanomaterial Toxicity Screening Working Group as an attractive option to understand potential deleterious effects of NPs after exposure to the human gastrointestinal tract (Oberdörster et al., 2005), However, recent studies indicate that care should be exercised concerning interpretation of experimental data procured from the use of Caco-2 (HTB-37™) for the aforementioned reasons (J.J. Faust, Zhang, Koeneman, Chen, & Capco, 2012; Fisichella et al., 2012; Koeneman et al., 2010); First, it is essential that

investigators clearly indicate which Caco-2 cell line was used during experimentation as many fail to report this critical piece of information; Second, and most disconcerting are control images shown by some that are not comparable to a plethora of reports in the literature dating back to 1992. Such results show the need for a standardize set of cell culture and microscopy preparation techniques, otherwise observations will become confounding.

The following text describes routine maintenance of the commercially available Caco-2 BBe1 cell line (ATCC, CRL-2102™) starting from thawing frozen, token ampules, to establishing user stocks. This methods section is concluded with a procedure that can be employed should the investigator wish to produce publication quality scanning electron micrographs of Caco-2 brush borders.

Procedure for thawing Caco-2 BBe1 cells from frozen cryogenic ampules.

1. Purchase 1-3 validated Caco-2 BBe1 cell lines from a geographically convenient cell repository at a low passage number. It was found that the archetypical structure of the brush border remains consistent until passage number 68 (M. D. Peterson & Mooseker, 1993).

2. After placing the order for the cell line, begin by preparing sterile complete culture medium. The medium of choice for Caco-2 BBe1 cells is Dulbecco's Modification of Eagle's Medium (DMEM; Cellgro, 10-013), supplemented with 10 μg/mL human transferrin (Invitrogen; 0030124SA), 10,000 I.U./mL penicillin, 10,000 μg/mL streptomycin and 25 μg/mL amphotericin (Cellgro; 30-004-CI), and 10% fetal bovine serum (Biosera; FBS2000). Cellgro supplies their medium in volumes of 500- or 1000 mL. The Nalgene® plastic that contains the DMEM permits the additional volume of supplements. The complete culture medium is inverted in the Nalgene® plastic 3-5

times to make the mixture uniform and subsequently apportioned (100 mL each) into 125 mL Wheaton glass bottles. Under no circumstances should the medium come in contact with the tops of Wheaton glass bottles as the medium may become contaminated. These sterile, pre-labeled 125 mL glass bottles can be stored at 4°C for up to 8 weeks.

3. Upon arrival of the cells immediately warm the complete culture medium to 37°C in a recirculating water bath. This commonly takes 15 minutes to equilibrate the medium from 4° to 37°C. Once equilibrated the closed bottle of complete culture medium is sprayed with 70% ethanol and placed on the grating of the air curtain to dry. Proceed to the next step immediately.

4. Remove the cryogenic ampule containing the cells from the packaging, ensure that the cap is tightly sealed, and begin to thaw the contents by gently swirling the frozen ampule in a pre-equilibrated (37°C) water bath. Inspect the ampule and continue to thaw with swirling until there appears a piece of ice that approximates the diameter of a pen tip. This thawing process takes about 2 minutes and should not be prolonged. It is advised that a trained member of the laboratory completes the thawing process. Proceed to the next step immediately.

5. Sterilize the external surface of the ampule with 70% ethanol and it place on the grating of the air curtain. Situate all necessary materials within the working area of the biological safety cabinet only after the 70% ethanol has air dried. Proceed to the next step immediately.

6. Transfer 9 mL of pre-equilibrated (37°C) complete culture medium to a sterile 15 mL centrifuge tube, add the thawed cells, and centrifuge at 125 g for 5 minutes to pellet the cells. Proceed to the next step immediately.

7. Aspirate the supernatant, gently resuspend the cells in 1 mL of complete culture medium, and transfer 1 mL into a T-75 culture vessel. Add 9 mL of additional pre-

equilibrated complete culture medium and gently rock the culture vessel five times to distribute the cells. Label the culture vessel with the investigator's name, the date, the cell type (Caco-2 BBe1), and the cell passage number. Quickly inspect the culture with an inverted phase-contrast microscope. The cells should appear as phase-bright spheres. Proceed to the next step immediately.

8. Transfer the culture vessels to a humidified cell culture incubator equilibrated to maintain a constant temperature of 37°C with an atmosphere of 5% CO_2 in air. The following day the cells should be inspected and the culture medium should be changed to remove nonviable cells.

Procedure for feeding Caco-2 BBe1 cells.

For routine maintenance, complete culture medium should be replenished every 3 days with 10 mL per T-75 culture vessel. To remove cell culture medium aseptically, aspirate the old medium used by the cells and pipet fresh, pre-equilibrated, sterile medium.

1. Set the culture vessel and pre-equilibrated complete culture medium on the air grate of the biological safety cabinet while waiting for ethanol to dry from gloved hands, and the complete culture medium bottle. This typically takes 2 minutes.

2. Aseptically aspirate the used cell culture medium, and pipet fresh, pre-equilibrated complete culture medium. This typically takes 2 minutes.

3. Return the culture vessels to the cell culture incubator.

The number of cells that occupy the percent area of the culture vessel surface is defined as the "percent confluence." In other words, if 80% of the culture vessel surface is occupied by cells, the culture is said to be 80% confluent. Once 80% confluence is reached the cells should be subcultured to prevent cell differentiation due to overcrowding of the cells.

Procedure for subculturing Caco-2 BBe1 cells.

1. Place the following in a recirculating 37°C water bath for 15 minutes: Ca^{2+}/Mg^{2+}-free phosphate buffered saline (PBS; Cellgro, 20-031-CV), complete culture medium, and 0.25% trypsin/2.21 mM EDTA in Hanks Balanced Salt Solution (Cellgro, 25-050-Cl).

2. Place all materials including the cell culture vessels in the hood as described in the paragraphs in the text above.

3. Aspirate the complete growth medium from the culture vessel. Proceed to the next step immediately.

4. Rinse the cells once with Ca^{2+}/Mg^{2+}-free PBS (3 mL per T-75). Aspirate the PBS. Proceed to the next step immediately.

5. Apply 3 mL of 0.25% trypsin/2.21 mM EDTA in Hanks Balanced Salt Solution, and return the T-75 culture vessel to the cell culture incubator for 5 minutes. Proceed to the next step immediately.

6. Pipet 3 mL of complete culture medium into the T-75 culture vessel to inactivate the trypsin, and transfer the entire volume (6 mL total) to a 15 mL centrifuge tube. Proceed to the next step immediately.

7. Centrifuge at 150 g for 5 minutes to pellet the cells. During this 5 minute wait, label new sterile culture vessels with the appropriate information, and add complete growth medium to the new culture vessel. Proceed to the next step immediately.

8. Aspirate the supernatant to remove any residual trypsin, and resuspend the cell pellet in 1 mL of complete culture medium; gently mix to randomize the cells. Transfer 100 µL of the suspension to the new culture vessel and gentle agitate to distribute the cells. This results in a 1:10 dilution.

9. Return the cells to the cell culture incubator. The cells will become adherent within 12 hours and will require additional subculturing after approximately 1 week in culture.

Procedure for establishing Caco-2 BBe1 user stocks.

The procedures described up to this point detail the routine culture of Caco-2 cells starting from a newly purchased cell line. This newly purchased cell line is hereafter referred to as the "token stock," as it is the lowest passage, validated cell line. There are 4 stages of cell lines that should be maintained in a cell culture laboratory and those include, 1) token stocks, 2) seed stocks, 3) distribution stocks, and finally 4) user stocks. The fine details of each of these classifications are described in the Freshney text (2005). Under no circumstance should the casual user employ token, seed, or distribution stocks, as these are validated, and lowest in passage number required to maintain the cell line.

1. Acquire a new cell line (e.g., Caco-2 BBe1). Only an experienced laboratory member should thaw and culture these cells as described in the aforementioned sections.
2. When this token stock is 80% confluent, use this culture to establish 3-5 additional stocks. To do this subculture the cells as described in the text above in 3-5 different sterile culture vessels.
3. When these 3-5 stocks are 80% confluent freeze the cell line, thaw one vial, and subsequently validate the cell line as described in the Freshney text before creating seed stocks.
4. To create seed stocks, thaw 1-2 token freeze stocks and generate 10-20 cryogenic ampules. Cryogenically preserve these ampoules.
5. Create distribution stocks by thawing seed stocks to generate 20-100 cryogenic ampules. One of these seed ampules must be thawed and subsequently validated before user stocks are generated.
6. One seed stock ampules is given to each user in the laboratory and it is the responsibility of the user to generate additional backups as user stocks. User stocks should be generated at 10-20 ampules, and only the user that made these ampules

should culture these cells. User ampules are discarded according to institutional biosafety protocols after the user has left the laboratory.

Cryogenically preserving Caco-2 BBe1 cells.

There are a number of reasons why cell lines should be cryogenically preserved. For starters, after cells have been in culture for 2 months (approximately 10 subcultures) there is the potential of genetic drift and clone variation. Furthermore, transformation, dedifferentiation, contamination/cross-contamination, and cost all corroborate the utility of maintaining cryopreserved stocks.

As a basic outline for the procedure described in the text below the investigator will grow the cells to late log phase in the desired culture vessel, trypsinize the cells and centrifuge, and resuspend the entire cell volume in cryopreservation medium. The cells are then immediately transferred to a cryogenic vial and heat is removed (i.e. the temperature is lowered) at 1°C per minute. The cells are subsequently transferred to liquid nitrogen for long-term storage.

1. Only generate at maximum 10 late log phase cultures via aseptic technique at a time, as manipulating additional culture vessels at the same time is difficult, and will lead to errors.

2. Cryopreservation medium should be prepared the same day the cells are frozen. Cryopreservation medium contains 80% complete culture medium supplemented with additional FBS at 10% and DMSO at 10%. Exercise caution as the addition of DMSO will result in an exothermic reaction, which raises the temperature beyond 37°C. This rise in temperature will result in reduced viability if the cells are exposed to this increased temperature. DMSO should be cell culture tested, and can be purchased from sources such as ATCC, Sigma Aldrich, etc.

3. Label the cryopreservation vials with a solvent-resistant marker and include the following information: The investigators name, the date, the cell line, the passage number, and the surface area or type of culture vessel used to grow the cells.

4. Wash the cultures with PBS, trypsinize the cells, centrifuge the cells, and aspirate the supernatant as detailed in steps 1-8 of protocol **2.1.** Proceed to the next step immediately.

5. Quickly resuspend the cell pellet(s) in cryopreservation medium, and transfer the contents of the centrifuge tube(s) to its own cryogenic ampule (Corning, 2028). Completely tighten the threading of the cryogenic ampule. Proceed to the next step immediately.

6. Quickly place the cryogenic ampule(s) into a Nalgene® Mr. Frosty unit (Thermo Scientific, 5100-0001), gently tighten the lid of the Mr. Frosty unit, and place the entire unit into a -70°C freezer.

7. After 12 hours the cryogenic ampules are transferred to canes labeled for quick identification, and stored in a liquid nitrogen dewer. After two days, thaw one cryogenic ampule and determine cellular viability by the trypan blue exclusion assay.

Growing Caco-2 BBe1 Epithelia for Morphometric Analysis of Brush Borders, and a Protocol for Specimen Preparation for Scanning Electron Microscopy

The following text provides a protocol to prepare Caco-2 BBe1 epithelia for scanning electron microscopy. In this text the investigators employ a critical point drier to convert liquid CO_2 to a gaseous state. It is advised that the critical point drier, in the case described below, a Balzer CPD 020, contains a stirring apparatus to promote exchange between acetone and liquid CO_2. If the investigator does not have a Balzer CPD 020, the optimal chamber pressure, solvent exchanges, and times may need to be determined empirically. It is equally important to grow the epithelium on a suitable

substrate. Non-compliant materials such as glass typically result in epithelia whose junctions appear non-continuous. Further, the extracellular matrix protein rat tail collagen I permits rapid cell adherence to the substrate, but other coating substrates (poly-D-lysine, fibronectin, etc) should be used with caution as Caco-2 BBe1 may not adhere to these proteins. During this procedure heat is removed from the specimen chamber adiabatically and the specimens are slowly infiltrated with liquid CO_2. During the drying process the liquid is vented and vaporizes to its gaseous state. Caution: This amount of CO_2 gas can result in asphyxiation if the surrounding area is not properly ventilated. It is advised that the critical point drier has adequate ventilation aided by an exhaust system.

1. Caco-2 BBe1 cells are seeded at $2.35x10^5$ cells/cm^2 on 6.5 mm (0.33 cm^2) Corning Transwell® inserts (Corning, 3495), and maintained for 17-21 days to promote differentiation of the epithelium (M. D. Peterson & Mooseker, 1993). This cell system permits optimal differentiation of the epithelium as both the apical and basal compartments are bathed with 300 μL and 1 mL of complete culture medium, respectively. The complete culture medium is replenished every 24-48 hours. Any indication that the pH of the medium has changed results in brush borders that appear unhealthy (e.g. limp microvilli, few in numbers, etc.).
2. Only after 17-21 days of culture are the epithelia cytologically fixed. The primary fixative of choice is electron microscopy grade glutaraldehyde (Electron Microscopy Sciences, 16020) made 2% in 100 mM sodium cacodylate buffer (pH 7.2). Specimens are fixed for 2 hours at room temperature. Proceed to the next step immediately.
3. The specimens are washed 10 times each for 10 minutes in 100 mM sodium cacodylate buffer (pH 7.2). Copious amounts of buffer should be used during each

incubation, and the specimens should be agitated gently at room temperature. Proceed to the next step immediately.

4. The epithelia are post-fixed in 1% OsO_4 in sodium cacodylate buffer (pH 6.4) for 60 minutes at room temperature. During this time the specimens are protected from light. Proceed to the next step immediately.

5. The specimens are washed 10 times each for 10 minutes in Nanopure® water (18.2 MΩ/cm) at room temperature with gentle agitation. Proceed to the next step immediately.

6. The epithelia are dehydrated carefully by passing the specimens through an increasing graded ethanol series, and subsequently transitioning the specimens to acetone. It is advisable to use 100% acetone that has been dried with molecular sieves for at least 2 days. Proceed to the next step immediately.

7. The only method that should be employed for drying specimens is with a critical point drier (e.g., Balzer CPD020), as all other methods will impart a number of structural artifacts. Fill the CDP chamber with enough anhydrous acetone to cover the specimens. The specimens are contained in a compartmentalized mesh basket, or solvent resistant container that permits infiltration of liquid CO_2 in exchange for acetone. Seal the chamber. Proceed to the next step immediately.

8. Cool the chamber to 4-6°C by turning on the non-filtered liquid CO_2 cylinder to pass through the chamber walls. Proceed to the next step immediately.

9. Slowly begin to fill the chamber with filtered liquid CO_2. The investigator will note a rise in the chamber pressure. Rapidly adding liquid CO_2 will artifactually fracture intracellular junctions as shown elsewhere (Passey et al., 2007), and as a consequence, the epithelium will appear disrupted when viewed with a scanning electron microscope. Under no circumstance should the pressure exceed 50 bars when changing the liquid

CO_2 as intercellular junctions will fracture. Turn on the stirring apparatus to mix the acetone and liquid CO_2. Wait 5 minutes for the acetone and the liquid CO_2 to mix. Proceed to the next step immediately.

10. Slowly vent the specimen chamber until the volume of the liquid mixture is just above the specimens. Proceed to the next step immediately.

11. Slowly fill the chamber with liquid CO_2. Once the chamber is filled, allow 5 minutes to mix the liquids. As indicated in step 9 the chamber pressure should not rapidly fluctuate. Proceed to the next step immediately.

12. Repeat step 11 for a total of 9 times. Proceed to the next step immediately.

13. Turn off the cooling and filling liquid CO_2 cylinders, the stirring apparatus, and change the temperature controller to 45°C. It takes about 5-7 minutes (Balzer CPD 020) for the specimen chamber to approach the critical pressure and temperature of CO_2 as the temperature rises. Proceed to the next step immediately.

14. After the specimens have transitioned through the critical point of CO_2, and the temperature is above 42°C, slowly begin to outgas (vent) the gaseous CO_2. This should take approximately 5-10 minutes at a rate of 5-10 bars of pressure released per minute. Proceed to the next step immediately.

15. Mount the specimens on an aluminum stub, and sputter coat the specimens with approximately 5 nm of vaporized metal (e.g., Pd/Au). After the specimens have been coated with metal they are stable for years when stored appropriately. The stubs can be housed in a small stub holder, and this entire box is stored desiccated in a vacuum sealed chamber.

Conclusions

At present there is a paucity of data regarding our understanding of the events that mediate disruption of the brush border *in vitro*. Several putative targets exist at a

mechanistic level, and these clues pave the way to identify a potentially unifying mechanism that accounts for the disruption of the brush border after exposure to engineered nanomaterials. Since this nanotoxicity research paradigm is in its infancy it behooves investigators to adopt standardized cell models appropriate to the study of NP-induced brush border disruption. Indeed, accurate data that can be compared across laboratories encourages forward progress in the field.

How can engineered NPs whose elemental composition is different result in morphologically similar changes (disruption) to the brush border? Such a universal event after exposure to NPs suggests that a cellular response, and not necessarily an inherent physico-chemical property of the nanomaterial, may account for brush border disruption. It was proposed by Zhang and coworkers (2010) that adsorption of NPs to the cell surface resulted in disruption of the brush border. If this is the case it could be predicted that sedimentation of agglomerated NPs onto the cell surface exacerbates disruption of the brush border. However, this hypothesis remains to be examined. The next mechanistic clue is derived from scanning electron microscopy and microarray data; both published (Madhavi Kalive et al., 2012) and results shown in Chapter 5 indicate that iron oxide (α-Fe_2O_3) nanoparticle exposure results in disruption of the brush border in Caco-2 and the b30 clone of BeWo, the latter is a human brush border expressing placenta cell model. Further, at the mRNA level the gene responsible for the actin filament capping protein, CapZ is upregulated in both cell systems. CapZ is a component of the plus tips of microvilli whose role is to "cap" the addition end of F-actin such that the filament cannot elongate. Upregulation of *CapZ* might suggest that the protein acts to reabsorb microvilli since additional actin monomers necessary to maintain the elongated structure would be unable to nucleate at the plus ends. Finally, it is intriguing to speculate that alterations in the terminal web account for a NP-induced

brush border disruption, as microarray data indicates changes to adhering junctions, which are known to be intimately connected with the terminal web.

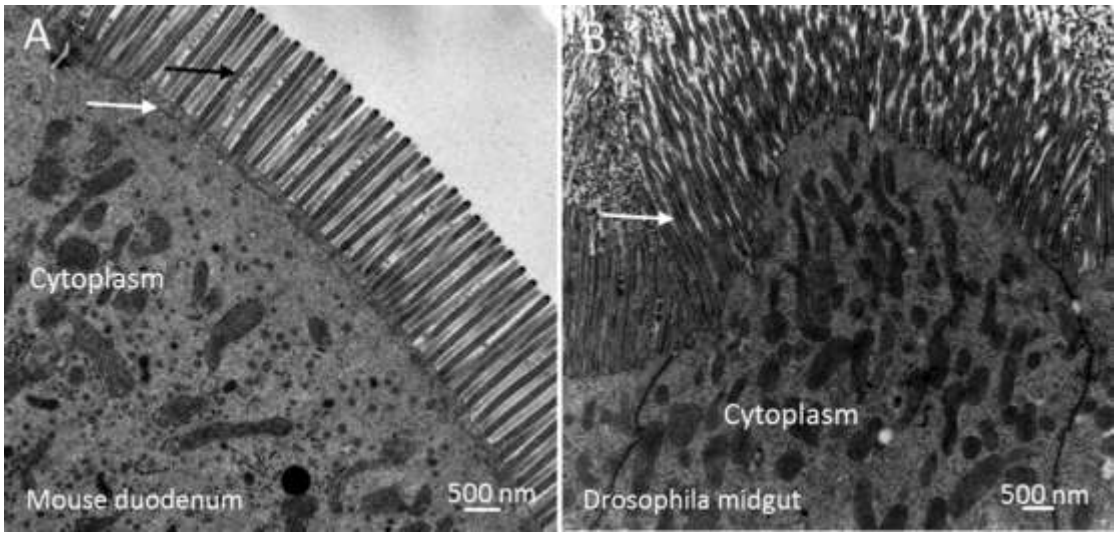

Figure 1. Transmission electron micrographs comparing the morphology of the brush border from intestinal cells of mouse and cells of the midgut from Drosophila. (A) The micrographs were transversely sectioned through the long axis of the polarized enterocyte. Note the robust number of microvilli, each containing an electron-dense region at the apical tip of the microvillus. Furthermore, the individual microvilli are of uniform length and diameter despite constant turnover of the proteins within each microvillus. This indicates a high degree of organization and control of this cell specialization. The black arrow points to the center of a single microvillus, while the white arrow points to the electron-dense terminal web region that supports the microvilli. The scale bar is 500 nm. (B) In comparison to the mouse model, Drosophila cells of the midgut have a rounded curvature since undulating folds (i.e., plicae) do not exists in this model. However, microvilli contain similar structural proteins within the microvillus indicating a somewhat universal blueprint across species. The arrow (white) points to a single microvillus. The scale bar is 500 nm.

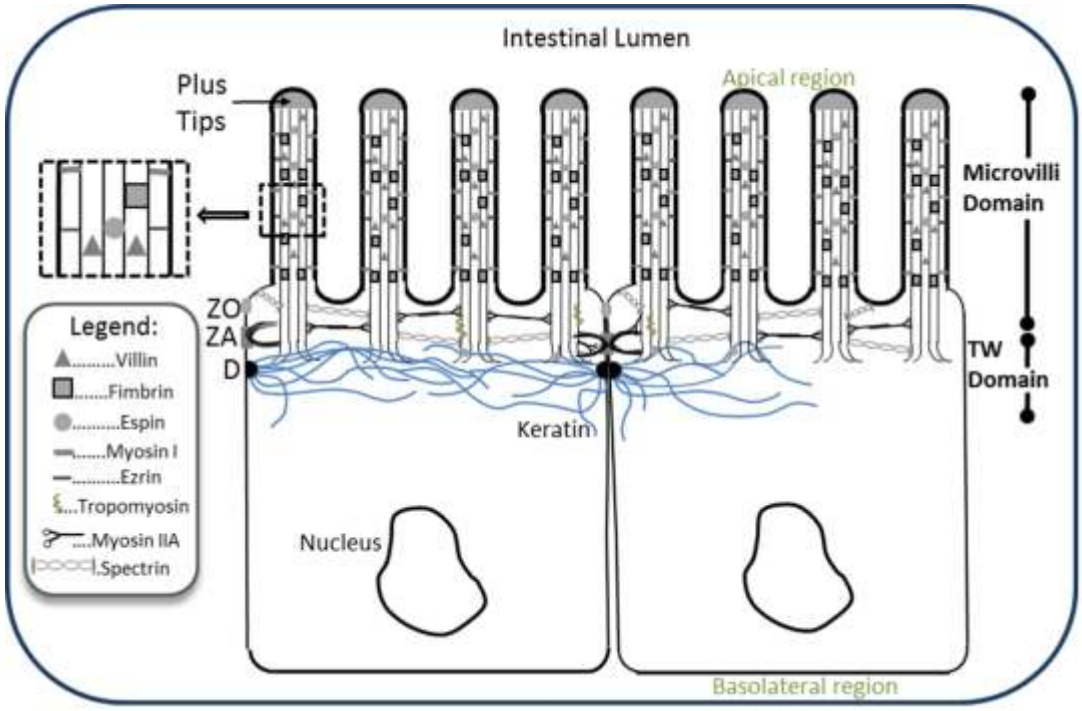

Figure 2. Graphical representation of the molecular components of the brush border. The diagram was adapted from many of the sources cited in the text, and does not account for scale/molar ratios of individual proteins.

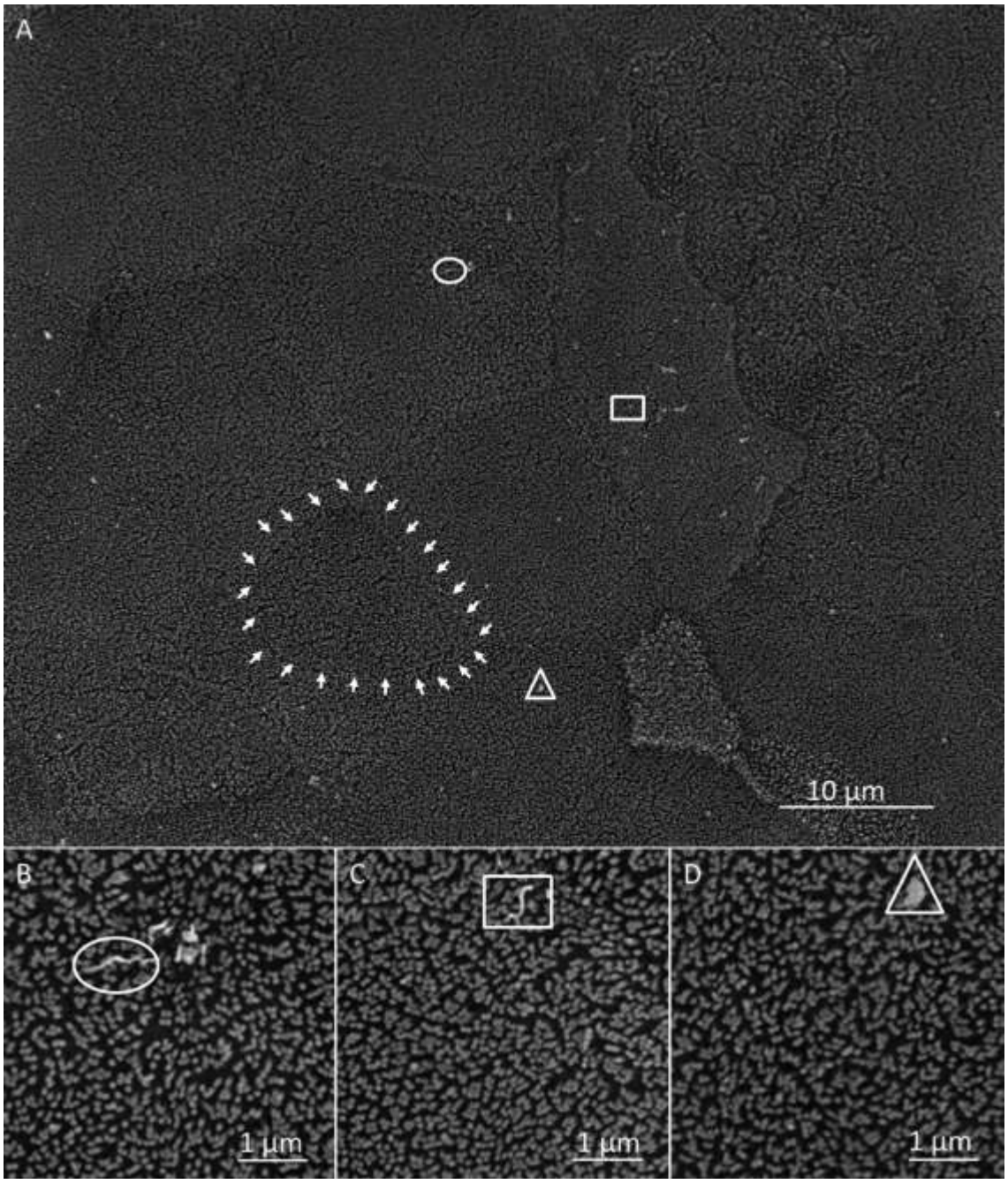

Figure 3. The differentiated Caco-2 BBe1 epithelium, shown as scanning electron micrographs demonstrates the classic archetypical organization of the brush border. (A) The low magnification view (originally captured at 1,500x) demonstrates a great number of cells with well defined brush borders. In this representative micrograph there are apparently 20+ cells within the field of view. The white arrows outline a single cell which was identified by the interdigitation of microvilli near the region of the intercellular junctions. The oval, rectangle and triangle serve as fiduciary markers for the high magnification views in B, C, and D. The scale bar is 10 µm. (B-D) Higher magnification

views of 3 randomly chosen regions within the epithelium. Note the consistency in number and structure of the brush borders from these regions. The scale bar is 1 μm.

CHAPTER 3

A FACILE METHOD FOR ISOLATING TITANIUM DIOXIDE NANOPARTICLES FROM FOOD AND PHARMACEUTICAL PRODUCTS: APPLICATION TO IN VITRO EXPOSURE ASSESSMENT

Introduction

Mixtures of micro- and nano-scale particles are added to consumer goods as color and texture modifiers (Weir et al., 2012), to control moisture (Maynard, 2014), or even as antimicrobial agents (Z. Zhang et al., 2012). In addition, human foodstuffs contain titanium dioxide (TiO_2) because of its brilliant white color, silicon dioxide (SiO_2) as an anticaking agent, and silver nanoparticles were found on fruit because of the antimicrobial properties of silver (Z. Zhang et al., 2012). Although a number of definitions for the word nanoparticle exist including size (Dunphy Guzman et al., 2006; Oberdörster et al., 2005), and definitions based on surface area, this study defines nanoparticle as particles below 100 nm and microparticles above 100 nm in diameter. Recent studies have indicated the pervasiveness of TiO_2 in human foodstuffs, and begun characterization of TiO_2 additives (Tiede et al., 2008; Weir et al., 2012). These studies have shown that TiO_2 additives have a variety of micro and nano components as determined by passing the material through 0.45 μm filters and depending on the food product tested (Weir et al., 2012). Although the intended use of the additive is benign, the fact that portions of these additives are nano-scale raises concern that this subset of nanomaterial in the additive could interact with the human gastrointestinal tract in fundamentally different ways compared to its micro counterpart. Moreover, it is known that as the lifecycle of the material changes, so do the material properties.

Consequently, there has been a paradigm shift in exposure assessment from employing material purchased as TiO_2 nanoparticles (Fisichella et al., 2012; Koeneman

et al., 2010), to employing TiO_2 that is designated as food grade (E171 coded), or even isolated directly from human foodstuffs (Athinarayanan et al., 2014; R.B. Reed et al., 2014). E171 is a European Union designation for pigment grade TiO_2 that is added to food. Furthermore, food grade TiO_2 (E171 coded) has been approved by the Food and Drug Administration with the stipulation that it have a high degree of purity and not exceed 1% by weight (Regulations, 2000). Although studies have revealed non-lethal effects of TiO_2 additives as micro- and nano-mixtures during *in vitro* exposure, they have ushered in the question: is the micro component of the additive, the nano component, or the mixture of micro and nanoparticles responsible for the observed effects?

As a means to this end, a number of analytical tools designed to separate particles based on defined criteria (e.g., size, charge, etc.) have been developed. The "gold-standard" method for particle separation is field flow fractionation (FFF), and this technique has been used in order to characterize the presence of nanoparticles in a number of human foods (Tiede et al., 2008). Although FFF is potentially the best way to separate micro and nanoparticles, the method requires equipment that can be costly, may not be readily available, and requires a degree of technical skill associated with its operation. An alternative method to separate micro from nanoparticles is filtration. The advantage of filters is that they are cost effective, and easy to use. However, filter pores are easily obstructed by particles, and collecting the micro fraction can be technically challenging. For these reasons, this investigation defines a simple alternative methodology for separating micro and nanoparticles from mixtures of TiO_2 additives intended for human ingestion based on sucrose step-gradient coupled with centrifugation.

Materials and Methods

Titanium dioxide isolation.

Titanium dioxide was isolated from the following consumer products that are intended for human ingestion: gum products that had a candy coating, name brand and generic pills marketed as headache relief, name brand and generic pills marketed to relieve allergies. TiO_2 was isolated according to the protocol described by Weir et al., (2012) with slight modification. For gum candy coatings, 2.5 servings were suspended in 10 mL of sterile Nanopure™ water with gentle agitation for 10 minutes at room temperature. The liquid containing TiO_2 (hereafter referred to as total TiO_2) was decanted into a separate 15 mL centrifuge tube, and the tube containing the gum base was discarded according to institutional guidelines. Endotoxin/nuclease-free microcentrifuge tubes (VWR, 16466-030) were filled with 1.5 mL of total TiO_2 isolate and centrifuged with a fixed-angle microcentrifuge (Ficher Scientific, Micro 14) at 14,000 g for 10 minutes. This extensive centrifugation was necessary because of the sugars that were solubilized from the candy coating. The translucent supernatant containing sugars, but devoid of TiO_2 was decanted and the tube was brought to volume with sterile Nanopure™ water. The pellet containing the TiO_2 was re-suspended by sonication with a microprobe sonicator (Fisher Scientific, Sonic Dismembrator Model 100) for 10 seconds at maximum output (29 watts RMS). The liquid containing TiO_2 was subsequently centrifuged at 14,000 g for 3 minutes to produce a TiO_2 pellet. The wash liquid was decanted, and the re-suspension step via sonication was repeated. This washing process, starting with re-suspending the TiO_2 pellet in sterile Nanopure™ water, and ending with centrifugation at 14,000 g for 3 minutes was repeated for a total of 5 times. Immediately following water washes, the TiO_2 was washed with non-denatured absolute ethanol via the aforementioned wash procedure for a total of 5 times. After the

final pelleting step, the ethanol was decanted and the microcentrifuge tube containing pellet was incubated in a drying oven at 68°C overnight to thoroughly dry the sample.

Concerning the samples with more complex components (i.e., over-the- counter drugs in the form of pills); 5 pills were applied to a 15 mL centrifuge tube containing 10 mL of sterile Nanopure™ water and incubated for 1 hour with gentle agitation at 25°C. The liquid slurry was sonicated for 30 seconds at maximum output. The slurry was centrifuged for 3 minutes at 125 g in order to remove the large debris. The supernatant was collected, and 1.5 mL of supernatant was added to endotoxin/nuclease-free microcentrifuge tubes (VWR, 16466-030). The entire wash and drying procedure described in the preceding paragraph for the total TiO_2 isolate was conducted.

Isolation of nano/micro enriched TiO_2 fractions.

Ultrapure sucrose (Sigma Aldrich, S7903) solutions (50% m/v and a saturated solution) were made by overnight incubation at room temperature in sterile Nanopure™ water. Sucrose step gradients were created by applying 250 µL of saturated sucrose to the bottom of a microcentrifuge tube (VWR, 16466-030) and carefully layering 500 µL of 50% sucrose on top. Immediately before use, dried TiO_2 pellets were re-suspended in 500 µL of sterile Nanopure™ water, and sonication with a microprobe sonicator (Fisher Scientific, Sonic Dismembrator Model 100) for 10 seconds at maximum output (29 watts RMS). The 500 µL of TiO_2 was carefully layered on top of the 50% sucrose solution, and the entire step gradient was centrifuged at 25°C for 3 minutes at 12,000 g. After this centrifugation process, the centrifuge tube had a pellet and a turbid appearance in all sucrose and water layer(s). The top 2 layers (water through 50% sucrose) were carefully collected (1 mL total) and placed in a new microcentrifuge tube. This new microcentrifuge tube is hereafter referred to as the nano tube. The microcentrifuge tube containing the pellet in saturated sucrose was set aside and hereafter referred to as the

micro tube. Additional water (500 µL) was added to the nano tube, the tube was vortexed, and subsequently centrifuged at 14,000 g for 10 minutes at 25°C. The washing and drying procedures described in the Titanium dioxide isolation section were conducted in order to obtain a nano-enriched fraction for later use.

The micro-enriched fraction was procured by gently inverting the micro tube to decant the saturated sucrose containing TiO_2, and gently washing the sides of the micro tube, while remaining inverted, with sterile Nanopure™ water. The pellet was washed and dried according to the procedure described in the Titanium dioxide isolation section in order to obtain a micro-enriched fraction for later use.

Transmission electron microscopy and primary particle analysis.

Total, micro, and nano isolates were re-suspended in sterile Nanopure™ water at a concentration of 10 ppm (i.e., 10 µg/mL) and drop-casted onto formvar-coated slot grids (Electron Microscopy Sciences, FF-2010-Cu). The grids were air dried overnight and imaged with a Philips CM-12 TEM fitted with a Gatan 791 sidemount CCD at an accelerating voltage of 80 kV. At least 10 images were collected per sample. Images were analyzed with ImageJ (Rasband, 2008), and primary particle diameters were calculated by measuring the x,y diameter from each particle in the field of view. The x,y diameters were averaged for each single particle in order to obtain an average particle diameter. The sample primary particle diameter was determined by averaging 300 to 750 particle averages.

Cell culture and scanning electron microscopy of Caco-2BBe1 epithelia.

The human brush border expressing cell line (Caco-2 BBe1; obtained from ATCC at passage number 47; CRL-2102) was maintained as described elsewhere (Koeneman et al., 2010; R. B. Reed et al., 2014). Briefly, cells were grown for 19-21 days in order to

form a confluent epithelium. The cell culture medium is DMEM (Cellgro, 10-013-CM) supplemented with 10 μg/mL of human transferrin (Invitrogen, 30124SA), 1% antibiotics (Cellgro, 30-004-CI), and 10% fetal bovine serum (Atlanta Biological, S-11150). Preliminary experiments were conducted in order to determine the minimum amount of time required for micro-enriched TiO_2 isolate to settle and subsequently adhere to the epithelium as determined by scanning electron microscopy. This time point (7 minutes) was used as a baseline for the remainder of the studies. Epithelia were cultured in the inverted position by adding the epithelia growing on a substrate to the bottom of a 15 mL centrifuge tube. Since the epithelium grows only on one side of the substrate, the epithelium can be inverted by tilting the centrifuge tube 90° while monitoring which side the epithelium is facing. The centrifuge tube cap was fastened half way to permit gas exchange and returned to the cell culture incubator immediately after applying medium containing nano or micro TiO_2 fractions.

Epithelia were washed once with phosphate-buffered saline (Cellgro, 21-030) in the inverted position, and cytologically fixed for 1 hour at 25°C. The primary fixative is composed of the following reagents: 2% electron microscopy grade glutaraldehyde (Electron Microscopy Sciences, 16020), 1% electron microscopy grade formaldehyde (Electron Microscopy Sciences, 15712), 5 mM ethylene glycol tetraacetic acid (Sigma Aldrich, E0316), 5 mM $MgCl_2$ (Sigma Aldrich, M2393), 100 mM KCl (Sigma Aldrich, P5405), and 20 mM 4-(2-hydroxyethyl)-1-piperazineethanesulfonic acid (Sigma Aldrich, H3784), pH 7.2. Only after the primary fixation step were the epithelia maintained in the upright position. Immediately following primary fixation, the epithelia were washed 10 times for 15 minutes each in copious amount of intracellular buffer (ICB). ICB contains 5 mM ethylene glycol tetraacetic acid, 5 mM $MgCl_2$, 100 mM KCl, and 20 mM 4-(2-hydroxyethyl)-1-piperazineethanesulfonic acid (pH 6.8). The secondary fixative,

which was necessary to preserve the membranes in these biological samples, was electron microscopy grade osmium tetroxide (OsO_4; Electron Microscopy Sciences, 19150). OsO_4 was diluted in sterile Nanopure™ water to a final working concentration of 1%. The secondary fixative was applied immediately to the epithelia after the final ICB wash. The epithelia were post fixed with 1% OsO_4 for 45 minutes at 25°C in a well-ventilated chemical hood. Epithelia were washed with copious volumes of sterile Nanopure™ water 10 times for 15 minutes each. Dehydration of the specimens, which is necessary to critical point dry the specimens was accomplished with a graded acetone series. The specimens were dried through the CO_2 critical point, and sputter coated with palladium/gold. Scanning electron micrographs were collected on a JOEL JSM6300. Upright samples were conducted in parallel with no change in the orientation of the epithelia as described by Faust and coworkers (Chapter 4). Neither air drying, nor drying with solvents circumvented artifacts associated with surface tension (Appendix, Supplemental Figure 1).

Results

Isolation and primary particle analysis of TiO_2 from food grade (E171), chewing gum, and over-the-counter medicine.

Due to the fact that a number of consumer goods contain TiO_2, and further, their particle diameters and physico-chemical parameters remain ill-defined this investigation isolated TiO_2 from two categories of consumer goods that are intended to be ingested by humans. This preliminary analysis of "total" TiO_2 additive was necessary because studies have shown mixtures of micro- and nanoparticles in consumer goods intended for ingestion (Weir et al., 2012). First, name-brand chewing gum that contained candy coatings was purchased from two independent grocery stores in the Phoenix area. Second, two types of over-the-counter medicine were purchased from two independent

grocery stores in the Phoenix area. Both generic and name brand medicine were purchased. The first product claimed to relieve headache and pain, while the second medicine claimed to relieve symptoms associated with allergies. All of the aforementioned consumer goods (i.e., gum and over-the-counter medicine) listed TiO_2 as an ingredient on the packaging label.

Immediately following the procedure described in detail in the materials and methods and supplement protocol 1, TiO_2 was analyzed via TEM in order to determine primary particle diameters (Figure 4). These primary particle diameters isolated from raw material are hereafter referred to as "total TiO_2." As a control, this study analyzed one source of TiO_2 purchased as food grade (E171 coded). Food grade TiO_2 appeared spherical, but contained also a number of particles with amorphous geometries (Figure 4 A). Food grade TiO_2 had diameters from as small as 38 nm to as large as 239 nm. The average primary particle diameter for food grade (E171) TiO_2 was 103 ± 40 nm (mean ± SD). TiO_2 isolated from name-brand gum appeared spherical and of amorphous geometries (Figure 4 B), and had diameters from 21 nm to 295 nm. The mean diameter after analyzing 493 particles was 122 ± 49 nm (Table 1). The averageTiO_2 isolated from name-brand medicine that was intended to treat allergies appeared spherical and contained a subset of particles of amorphous geometries (Figure 4 C). These particles were as small as 39 nm and as large as 175 nm. The average primary particle diameter determined from analyzing 344 particles was 94 ± 25 nm (Table 1). Generic allergy relief medicine appeared spherical with a subset of particles of amorphous geometries (Figure 4 D), and had diameters from 33 nm to 261 nm. The average primary particle diameter determined from analyzing 365 particles was 99 ± 40 nm (Table 1). TEM analysis of TiO_2 isolated from name-brand medicine that was marketed to relieve headache and pain appeared spherical, but contained also a fraction of particles with amorphous

geometries (Figure 4 E). The isolate had particle diameters from 44 nm to 259 nm. The average primary particle diameter was 119 ± 39 nm (from 414 particles; Table 1). TEM analysis of TiO_2 isolated from generic medicine marketed to relieve headache and pain appeared spherical, but contained also a number of particles with amorphous geometries (Figure 4 F). The particle diameters were as small as 46 nm and as large as 281 nm. The average primary particle diameter was 109 ± 39 nm (Table 1). Together, these data suggest that consumer goods intended for human ingestion contain polydispersed primary particle diameters composed of both micro and nano TiO_2 components. This mixture of small and large primary particle diameters (i.e., micro and nanoparticles) may have different physico-chemical parameters or alternatively might interact with cell systems differently.

Separation of nano- and micro-enriched TiO_2 fractions from select consumer goods intended for human ingestion.

Previous studies have begun characterization of TiO_2 in consumer goods (Weir et al., 2012), and have further investigated the effects of isolated TiO_2 from consumer goods (Chapter 4). However, one central barrier that remains to be decoupled is what, if any, differences exist when nano and micro fractions of total TiO_2 are separated and subsequently employed in downstream analysis. In order to separate nano and micro components of total TiO_2 isolated from consumer goods, this study first assessed the utility of filters with defined pore sizes. Preliminary experiments employing 100 nm and 200 nm pore sizes proved unsuccessful; The pores frequently blocked due to a barricade effect as has been noted elsewhere (Tiede et al., 2008). Moreover, and although it was possible to obtain a dilute nano isolation, micro isolation proved unsuccessful as it was contaminated with many nanoparticles. Therefore, this study employed a sucrose step-gradient in order to fractionate total TiO_2 into nano- and micro-enriched components

(described in detail in the material and methods). This was possible because primary particle mass is dependent on particle diameter (i.e., size). Small particles were slowed by the difference in density over the short term, whereas larger particles with a greater mass were less affected by changes in density over the short term.

In order to identify potential differences in particles diameters as a result of the aforementioned sucrose step-gradient procedure, primary particles were imaged via TEM and diameters were subsequently analyzed (Figure 5). As a control, this study first employed one source of TiO_2 purchased as food grade (E171 coded). The micrograph (Figure 5 A) illustrates the geometry and diameters of micro-enriched fraction. The particles appeared to be enriched with large (> 100 nm) particles that appeared similar in geometry as total E171 isolated. More importantly, the primary particle diameter determined by analyzing 522 particles shifted to 122 ± 38 nm (Table 2). The smallest particle was 38 nm and the largest was 264 nm in diameter. The image shown as Figure 5 B represents the nano-enriched fraction. The particles appeared much smaller than the micro enriched fraction, and analysis of primary particle diameters indicated a shift to 77 ± 22 nm (571 particles analyzed; Table 2). The smallest particle diameter was 24 nm, whereas the largest particle was 186 nm. These data suggest that this method may be applicable for enrichment of nano and micro TiO_2 fractions isolated from consumer goods.

In order to determine whether this method is applicable to TiO_2 isolated from consumer goods, this study employed the aforementioned sucrose step-gradient for TiO_2 isolated from gum, and two sources of TiO_2 isolated from over-the-counter medicine marketed to relieve allergies. Figure 5 C shows the morphology and diameters of the micro-enriched fraction isolated from chewing gum. The average primary particle diameter determined from analyzing 472 particles was 146 ± 48 nm (Table 2). The

smallest diameter was 49 nm, whereas the largest was 345 nm. Analysis of nano-enriched fractions via TEM indicated that the particles appeared similar in morphology, but diameters were smaller (Figure 2 D). Furthermore, the average primary particle diameter (622 particles analyzed) was 95 ± 28 nm (Table 2). The smallest particle was 31 nm and the largest particle was 143 nm.

One question that remains unanswered for studies employing total TiO_2 isolated from products intended for human ingestion (i.e., chewing gum) is whether the effects observed after exposure are due to the small diameter nanoparticles or alternatively from larger micro particles (Chapter 4). One way to address this was to employ two different orientations with regard to gravity during exposure to the nano and micro-enriched fractions of TiO_2 isolated from E171. Then to monitor the time necessary for nano and micro-enriched fractions as parallel replicate samples to adhere to the surface of cells grown as epithelia in these 2 orientations. The first orientation is upright whereas the second is inverted as described elsewhere (Cho, Zhang, & Xia, 2011). In the upright configuration, and after preparing the samples for SEM, micro-enriched particles were found adhered to the surface of the epithelia after 7 minutes of exposure (Figure 6 A). The micrographs shows regions decorated with particles (pointed to by white arrows). However, exposure to the nano-enriched TiO_2 as a parallel replicate resulted in fewer particles adhered to the cell surface (Figure 6 B).

An alternative epithelial orientation has been employed in order to mitigate the effects of sedimentation (Cho et al., 2011). In order to investigate the contribution of TiO_2 settling and subsequently adhering to the cell surface, the epithelia were inverted and exposed to nano- and micro-enriched fractions as replicate samples for 7 minutes. Under these conditions, relatively few particles from the micro-enriched fraction adhered to the cell surface (Figure 6 C). However, when replicate samples were exposed

to the nano-enriched fraction, the surface appeared to contain many more adherent nanoparticles (pointed to by white arrows; Figure 6 D). These data suggest that nano and micro particles may interact differently with cells over the short term, and further validate this method as a suitable separation protocol. Attachment of TiO_2 has been shown to be the first step involved in disruption of the intestinal brush border *in vitro* (Koeneman et al., 2010; R. B. Reed et al., 2014), and thus suggest that brush border disruption *in vitro* may be a consequence of the size of the TiO_2 employed.

Discussion

The major finding in the present investigation was that it was possible to separate micro (>100 nm in diameter) from nanoparticles (<100 nm in diameter) in polydispersed sources of TiO_2 to produce micro- or nano-enriched fractions. This was first demonstrated for TiO_2 purchased as food grade (E171 coded), and subsequently confirmed for TiO_2 isolated directly from consumer goods intended to be ingested by humans (i.e., the candy coating of chewing gum, and over-the-counter medicine). Although a number of techniques exist to separate nano and micro components from consumer goods and foodstuffs (Kammer, Legros, Hofmann, Larsen, & Loeschner, 2011; Singh, Stephan, Westerhoff, Carlander, & Duncan, 2014; Tiede et al., 2008), many of these techniques are contingent upon equipment that may not be readily available to the investigator. Therefore, this study utilized equipment and reagents that are readily available in most scientific laboratories. The crux of this method was separation due to differences in TiO_2 particle sedimentation as particles passed through a sucrose step-gradient during centrifugation.

This study chose to use sugar (sucrose) to impede the rate of travel of small compared to larger particle during centrifugation because the candy coating of chewing gum consists largely of sugar and TiO2. Since it is known that the physico-chemical

parameters of particles change depending on the solutions they are in, it might be necessary in future studies to identify "natural" solutions employed for the step-gradient based on the product the particles are isolated from. For example, it is known that TiO_2 is added to milk in order to improve color (Hallagan, Allen, & Borzelleca, 1995). It is a fact that one major component of milk is protein. Therefore, the investigator might establish a density gradient with the protein casein or albumin in order to permit a more "natural" separation. This is further exemplified by the fact that the electric double layer of the particles attracts components from its surrounding environment via van der Waals forces. For solutions rich in proteins, as is the case for many *in vitro* toxicity studies, particles become decorated by these proteins to make a corona (Monopoli et al., 2011). The corona can subsequently assign biological identity to the particles (Monopoli et al., 2012), and thus underscore the importance of employing the correct solution for the step-gradient for *in vitro* toxicity studies.

The physico-chemical differences between micro and nano components of the total isolated TiO_2 were not the only differences that were shown in this study. In this study we employed identical mass concentration as a dosemetric to illustrate the difference in particle adhesion when the cells in the epithelia were exposed to nano- or micro-enriched TiO_2 in the upright configuration and compared these results to the inverted configuration (Figure 6). This study showed apparently a greater concentration of micro-enriched particles decorating the surface of the epithelium in the upright, but not the inverted configuration, after as early as 7 minutes of exposure (Figure 6 A C). Exactly the opposite trend was observed for epithelia exposed to the nano-enriched TiO_2 (Figure 6 B D). Previous studies have shown that the density of the material can drastically affect the actual concentration the cells are exposed to (Cho et al., 2011). Further, recent studies have shed light on a non-lethal, but important effect of exposure

to food grade TiO_2 or supplements containing a variety of nanoparticles in a human *in vitro* model of the intestinal epithelium (R.B. Reed et al., 2014). That is, exposure to TiO_2 purchased as food grade (E171 coded) or isolated from chewing gum resulted in a loss of microvilli from the surface of the cells in both the upright and inverted configuration and during conditions of microgravity (Chapter 4). This suggested that the loss of microvilli was not absolutely dependent on sedimentation of the material, which is in agreement with the present findings. Collectively, these data suggest that this method offers a simple tool that can be used in order to identify changes in physico-chemical parameters or toxicity assessment from TiO_2 particles isolated from consumer goods.

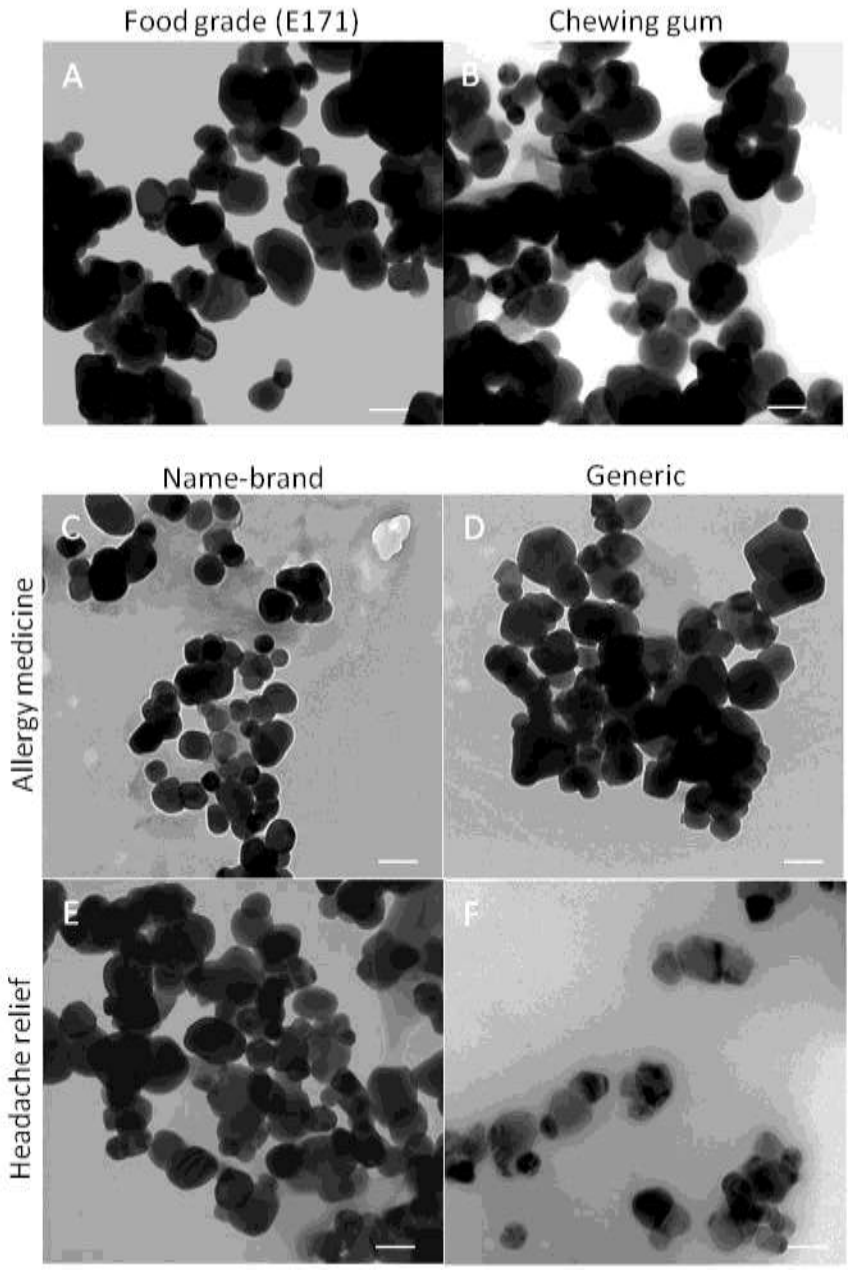

Figure 4. Primary particle analysis from a variety of TiO_2 isolated from products intended for ingestion reveal heterogeneous mixtures of micro and nanoparticles. (A) TiO_2 purchased as food grade (E171 coded) has a mixture of particles sizes. (B) TiO_2 isolated from gum similarly has a heterogeneous mixture of primary particles. (C-D) TiO_2 isolated from name-brand and generic allergy medicine has a variety of primary particles in the bulk and nano-scale. (E-F) TiO_2 isolated from name-brand and generic headache medicine has a variety of primary particles in the micro- and nano-scale. The scale bar in the lower right corner of each micrograph is 100 nm. All of the images were originally captured at 60,000x magnification.

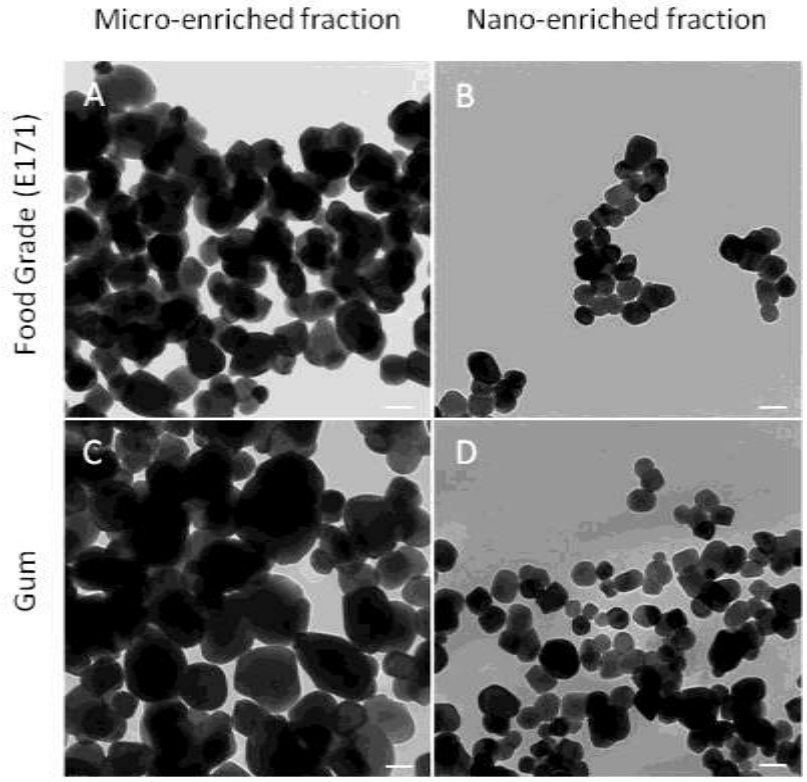

Figure 5. Primary particle analysis via TEM reveals a difference in size between nano- and micro-enriched fractions after the sucrose step-gradient centrifugation procedure. (A) Micro-enriched food grade TiO_2 purchased as E171 appear large compared to (B) the nano-enriched fraction. (C) Utilizing the same procedure on TiO_2 isolated from gum revealed a large, micro-enriched fraction, and (D) a small, nano-enriched fraction. The scale bar in the lower right corner of each micrograph is 100 nm. All of the images were originally captured at 60,000x magnification.

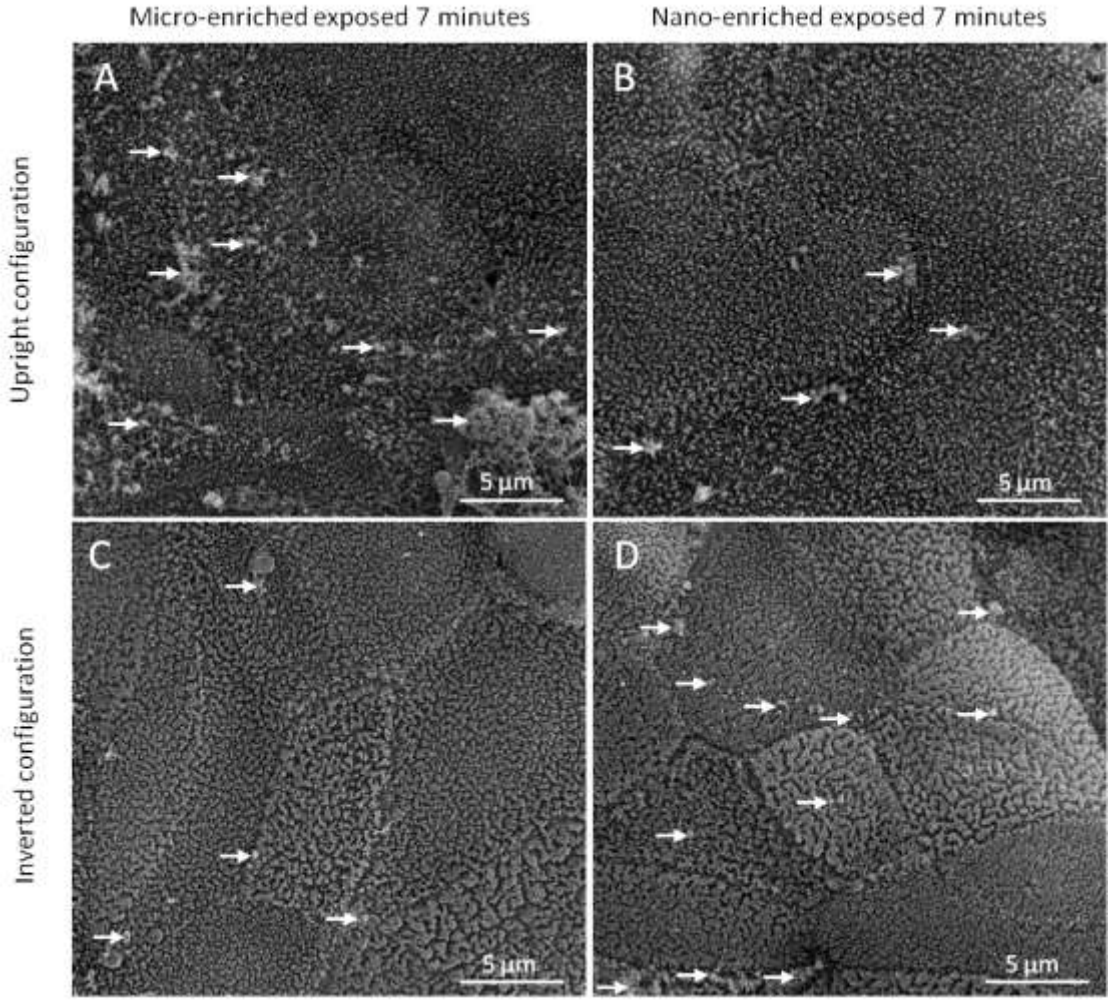

Figure 6. Exposure to nano- or micro-enriched fractions of TiO_2 prepared from E171 results in changes in particle adhesion after exposure to an *in vitro* cell model of the human intestine. (A) Epithelia exposed to 1 µg/mL of micro-enriched TiO2 in the upright configuration resulted in a large number of particles (white arrows) decorating the surface of the epithelium after 7 minutes of exposure. (B) However, exposing replicate samples to the nano-enriched TiO_2 fraction at a concentration of 1 µg/mL for 7 minutes in the upright configuration resulted in few particles adhered to the epithelial surface. (C) Inverting the epithelium and subsequently exposing the cells to micro-enriched TiO_2 fraction at 1 µg/mL for 7 minutes resulted in few particles adhered to the epithelial surface. (D) However, exposing replicate samples in the inverted configuration to nano-enriched TiO_2 fraction at 1 µg/mL for 7 minutes resulted in relatively more particles adhered to the epithelial surface.

TiO_2 Sample	Avg. primary particle diameter	Percent nano
Food grade (E171)	103 ± 40 nm	54%
Gum-TiO_2	122 ± 49 nm	35%
Name-brand allergy	94 ± 25 nm	32%
Generic allergy	99 ± 40 nm	58%
Name-brand headache	119 ± 39 nm	36%
Generic headache	109 ± 39 nm	49%

Table 1. Primary particle analysis of total TiO_2 isolated from a number of sources. The table indicates thatTiO_2 additives isolated from products intended for ingestion are mixtures of micro- and nanoparticles.

TiO_2 Sample	AVG Primary Particle Diameter	% Nano	% Micro
E171 micro-enriched	122 ± 22 nm	31%	69%
E171 nano-enriched	77 ± 22 nm	87%	13%
Gum micro-enriched	146 ± 48 nm	15%	85%
Gum nano-enriched	95 ± 28 nm	60%	40%

Table 2. Primary particle analysis from two sources of TiO_2 demonstrates that this procedure can produce nano- and micro-enriched fractions.

CHAPTER 4
FOOD GRADE TITANIUM DIOXIDE DISRUPTS INTESTINAL BRUSH BORDER MICROVILLI IN VITRO INDEPENDENT OF SEDIMENTATION

Introduction

TiO_2 has found use as a color additive in human food products because of its brilliant white color, and as a texture modifier in foods, which is used in a wide variety of confectionary foods, toothpastes and other ingestible products. "E" numbers are codes for substances that can be used as food additives in the European Union, and similar coding exists in other countries; food grade TiO_2 is coded as E171. In the United States, the Food and Drug Administration approved the use of TiO_2 in 1966 as a human food additive with the stipulation that TiO_2 is not to exceed 1% by weight (Regulations, 2000). While TiO_2 has been approved, the study by Weir et al., (2012) showed that approximately 38% of TiO_2 in one food grade (E171 coded) source had at least one external dimension that was < 100 nm, which was consistent with the size distribution observed in several food samples containing TiO_2, including confectionary products (e.g., chewing gum) or toothpastes (Weir et al., 2012). These data indicate that a subset of TiO_2 approved as additives in human food products is within the accepted definition of nanomaterial (Dunphy Guzman et al., 2006), yet little information on the toxicity of food grade TiO_2 has been published since these definitions for nanotechnology have been established.

Although there is clearly a beneficial niche for the use of TiO_2 as a food additive, it is coming to the attention of investigators that although not immediately damaging to an epithelium, TiO_2 NPs elicit subtle effects on cells within an epithelium (Koeneman et al., 2010). An epithelium has a barrier function that partitions parts of the body and even separates the body from the external environment. The study by Koeneman and

coworkers (2010) indicated that exposure to a 70/30 percent mixture of rutile/anatase TiO_2 NPs result in what appeared to be a dose-dependent disruption of the brush border, an anatomical feature that exists on the epithelial surface of absorptive cells of the intestine. These data have been corroborated by a number of brush border expressing cell models with another widely employed model NP, α-Fe_2O_3 (M. Kalive et al., 2012; W. Zhang et al., 2010). Although the entire picture has yet to be painted, the role of many molecular components of the brush border composed of individual microvilli have been elucidated (Mooseker, 1985). Briefly, the brush border has been partitioned into two regions that make up the apical portion of the enterocyte in the epithelium: The microvilli and terminal web domains. Within the microvilli domain, the single microvillus has 20-30 actin filaments organized as parallel bundles in a hexagonal array (Bretscher, 1983a). Each actin filament is fastened to the other by fimbrin, villin, and espin (Bretscher & Weber, 1980a, 1980b; Grimm-Günter et al., 2009). The entire microvillus core is laterally tethered in a helical arrangement to the overlying plasma membrane by brush border myosin I (Howe & Mooseker, 1983). The microvilli are rooted in the terminal web which is composed of a number of intermediate filaments and structural proteins (Hirokawa et al., 1983; Hirokawa & Heuser, 1981).

The study by Zhang and colleagues (2010) postulated that adsorption of NPs to the cell surface results in disruption of the brush border. In line with this view, at least one criticism of the *in vitro* culture model is the fact that as NPs agglomerate over time sedimentation ensues and effectively increases the concentration of NPs at the bottom of the culture dish that the cells would otherwise not be exposed to (Cho et al., 2011). This increase in NP concentration at the apical surface of the cell could result in artifactual disruption of the brush border. Therefore, the current study was conducted in order to determine if exposure to food grade TiO_2 (labeled as E171 compliant by the distributor)

as well as TiO_2 isolated from the candy coating of gum (hereafter referred to as gum-TiO_2) resulted in brush border disruption, and if this disruption was a result of sedimentation. In this study it was hypothesized that brush border disruption occurs as a result of exposure to food grade TiO_2 and that brush border disruption is an event independent of sedimentation. If TiO_2 disrupts the brush border, then changes will occur as a result of exposure to food grade TiO_2 as measured by an alteration in the archetypical organization of the brush border as well as a reduction in the total number of microvilli. Furthermore if brush border disruption is independent of sedimentation then removing the effects of sedimentation due to gravity should result in disruption of the brush border as measured by an alteration in the archetypical organization of the brush border as well as a reduction in the total number of microvilli.

Materials and Methods

TiO_2 isolated from candy coatings, and preparation of culture medium containing TiO_2.

E171 is a European Union designation for a white food color additive that is known elsewhere by other designations (CI 77891, Pigment White 6). For this research, a sample was obtained from a large commercial supplier in China which listed the material as complying with E171 requirements (referred to in this study as food grade TiO_2). Food grade TiO_2 was suspended in sterile Nanopure™ water (Barnstead; 18.2 MΩ) at a concentration of 1 mg/mL. TiO_2 were also isolated from gum (referred to in this study as gum-TiO_2) as described by Weir et al., (2012). Briefly, 3 servings of gum were added to 5 mL of sterile Nanopure™ water (Barnstead; 18.2 MΩ) and allowed to dissolve for 10 minutes. In order to determine the total Ti content in food grade TiO_2 and gum-TiO_2, approximately 0.03g of each was digested in HNO_3 and HF (4:1 v/v) using microwave digestion according to Standard Method 3030G (APHA et al., 2005). Element

concentrations including Ti, P, Si, and Al were measured using XSERIE-2 ICP-MS (Thermo Scientific, USA). The total amount of Ti from this stock concentration was determined by ICP-MS before the samples were used in any other experiment. Before the TiO_2 was resuspended in cell culture medium, the TiO_2 was sonicated with a Fisher Scientific model 100 probe sonic dismembrator at the maximum setting of 28 watts (RMS) for no less than 2 minutes. The TiO_2 was diluted to the final working concentration and sonicated a second time with a Fisher Scientific model 100 probe sonic dismembrator at the maximum setting of 28 watts (RMS) for no less than 2 minutes. In this study, concentrations are shown as mass/mL. It should be noted, however, that the cell culture device has a growth surface area of 3.5 cm^2 and the epithelium forms a confluent layer across this growth area. Consequently, when 1 mL of culture medium containing 350 ng TiO_2 is placed above this growth area the concentration is 350 ng/mL which is equal to 100 ng/cm^2 of TiO_2 available to the epithelia.

XPS.

Surface elemental composition and chemical state were analyzed using X-ray photoelectron spectroscopy (XPS) performed on an ESCALAB 220i-XL (Vacuum Generators, USA) with a monochromatic Al Kα source at hν = 1486 eV, a base pressure = 7×10^{-10} mbar, and a spot analysis size of 500 μm. Food grade TiO_2 was prepared by pressing the powder into a disk on clean indium foil. Gum-TiO_2 was prepared by drop casting the isolated suspension onto SiO_2. Peak fit was done manually using CasaXPS on the basis of the theoretical atomic percentages calculated from the wide scan. The estimated depth of analysis is approximately 2.87 nm as determined from the inelastic mean free path of electron scattering for TiO_2 (Tanuma, Powell, & Penn, 1994). The adventitious carbon peak was used for calibration.

XRD.

The crystal structure was determined using powder X-ray diffraction (XRD) on a D5000 (Siemens, USA) with a CuK_{α} source and an aluminum holder. Each sample was scanned from $2\theta = 20°$ to 60° to detect the characteristic TiO_2 peaks. The XRD spectrum was used to calculate the lower bound of the crystallites using Scherrer's Equation (Patterson, 1939). Surface elemental composition and chemical state were analyzed using X-ray photoelectron spectroscopy (XPS) performed on a ESCALAB 220i-XL (Vacuum Generators, USA) with a monochromatic Al Kα source at h = 1486 eV and a base pressure = 7×10^{-10} mbar. XPS spectra were calibrated using the O 1s peak for TiO_2 at 530.1 eV.

TEM and primary particle diameter analysis.

Food grade- and gum-TiO_2 samples were diluted to 1 μg/mL in Nanopure™ water (Barnstead; 18.2 MΩ) and sonicated with a Fisher Scientific model 100 probe sonic dismembrator at the maximum setting of 28 watts (RMS) for no less than 2 minutes. Small (10 μL) drops containing the titanium dioxide were placed on Parafilm. Formvar-coated copper grids were inverted and immediately placed on top of the drops for 10 seconds. The excess liquid was wicked away with Whatman No. 5 filter paper, and the grids were placed in a grid holder over night to dry before imaging with a Philips CM-12 TEM. Images were captured by randomly focusing on 5 different squares within the mesh of 3 different grids. Each of the micrographs (15 in total) were analyzed with ImageJ by measuring the x and y axis of the TiO_2 and averaging the diameter from every particle within the field of view. In total 100 particles were averaged, and the data was found to be consistent with those results reported elsewhere (Weir et al., 2012).

Dynamic Light Scattering.

Samples were prepared for phase analysis light scattering (ZetaPALS, Brookhaven Instruments Corporation, U.S.) to determine the hydrolyzed diameters of particles by application of 10 mg/L TiO_2 samples in Nanopure™ water and bath sonicating for 30 minutes. The aforementioned protocol was employed also to analyze particles in the presence of cell culture medium containing serum. Preliminary experiments indicated that there was no significant change in hydrodynamic diameter for either of the sonication methods employed in the present investigation (i.e., bath sonication for 30 min compared to probe sonication for no less than 3 min).

Zeta Potential Analysis.

In order to determine the zeta potential, the electrode was stabilized in 100 mM potassium nitrate at room temperature 24 hours prior to measurement. The samples were prepared by adding 0.03 g of food grade TiO_2 or gum-TiO_2 to 50 mL of 10 mM potassium nitrate (Sigma-Aldrich, U.S.) solution, which was mixed for 24 hrs. After this time period, the samples were bath sonicated for 30 min immediately before zeta potential measurements.

Cell culture.

This study exploits the use of the extensively characterized Caco-2_{BBe1} human derived cell system. When grown appropriately, this cell system exhibits a faithful representation of the *in vivo* structural characteristics (M. Peterson & Mooseker, 1992), and mirror differentiation of the brush border at the molecular level (M. D. Peterson & Mooseker, 1993). Furthermore, Caco-2 has been recommended by the International Life Sciences Institute Research/Risk Science Institute (Oberdörster et al., 2005). The human, brush border expressing cell line, Caco-2_{BBe1}, was cultured according to the protocol established elsewhere (M. Peterson & Mooseker, 1992). Briefly, Caco-2_{BBe1} cells

were purchased from ATCC (Manassas, VA; CRL-2102) at passage number 47 and discarded at passage 67. The cell culture medium is Dulbecco's modification of Eagle's medium (DMEM; Cellgro; 10-017-CM) supplemented with 10 μg/mL of human transferrin (Invitrogen; 0030124SA), 10,000 I.U./mL penicillin, 10,000 μg/mL streptomycin and 25 μg/mL amphotericin (Cellgro; 30-004-CI), as well as 10% fetal bovine serum (Biosera; FBS2000). The cell culture medium was replenished every 48 hours, and culture vessels containing the cells were housed in a humified incubator calibrated to maintain an atmosphere of 5% CO_2 at 37°C. The experiments were conducted only after the cells were aseptically maintained as confluent epithelia for 19-21 days (M. D. Peterson & Mooseker, 1993), where replicate samples had an electrical resistance of at least 250 Ω/cm^2 and ZO-1 is apically localized.

Electron microscopy.

Preparation of Caco-2_{BBe1} epithelia for electron microscopy was conducted according to a detailed protocol presented in Chapter 2. Briefly, specimens were grown for 19-21 days, the experiment conducted, and the specimens were fixed for 1 hour at room temperature in 2% glutaraldehyde made in 100 mM sodium cacodylate buffer (pH 7.2). The specimens were washed and post-fixed for 1 hour at room temperature in 1% OsO_4 made in 100 mM sodium cacodylate buffer (pH 7.2). The specimens were dehydrated, and either critical point dried and sputter coated, or infiltrated with Spurr's resin. Images were procured with either an XL-30 ESEM coupled with EDX analytical software, or a JOEL JSM-6300 equipped with an IXRF digital imaging system. TEM micrographs were procured with a Phillips CM-12 fitted with a Gatan 791 CCD camera. The images shown are representative micrographs from 5 randomly chosen cells of 3 independent experiments.

Procedure for the inversion of specimens to remove the effects of sedimentation of TiO_2 on the surface of the epithelium.

The human, brush border expressing cell line, Caco-2_{BBe1}, was cultured according to the protocol described the in the Cell culture section. After the 19-21 days necessary to permit differentiation of the epithelia the epithelia were transferred to 15 mL conical centrifuge tubes (VWR; 89039-664) containing no culture medium, the side facing the epithelia were labeled, and 5 mL of medium was added to the centrifuge tubes while the epithelia remained inverted. The specimens were returned to the cell culture incubator with the cap of the 15 mL centrifuge tube tightened half way to permit exchange of gas. At the indicated time points the specimens were removed and maintained in the inverted position, the cell culture medium was aspirated with the epithelia remaining inverted, and the cytological fixative was added while the specimens were inverted. Only after 1 hour of fixation were the specimens handled in any other orientation.

Videomicroscopy.

Caco-2_{BBe1} epithelia were cultured on μ-Dish$^{35\ mm,\ high}$ glass bottom Grid-50 dishes (Ibidi; 81148) according to the aforementioned cell culture protocol. Prior to examination, medium containing the food grade TiO_2 was prepared according to the method of Koeneman and coworkers (2010). Briefly, concentrated, TiO_2 stocks (no less than 500 mg/L) were thoroughly sonicated with a Fisher Scientific model 100 probe sonic dismembrator at the maximum setting of 28 watts (RMS) for no less than 2 minutes. This TiO_2 suspension was subsequently dosed at a working concentration of 1 μg/cm^2 of surface area (i.e., 3.5 μg/mL), sonicated a second time, and bath applied to the epithelia. Immediately following exposure to this TiO_2 -containing medium the cells were images with a Nikon Eclipse TE300 inverted microscope equipped with a stage warmer and a Hamamatsu Orca CCD camera. For experiments conducted without cells,

the TiO_2 were applied at a 1 μg/cm² (3.5 μg/mL) concentration to a gridded glass bottom dish that contained 50 μg/cm² collagen I. The TiO_2 were visualized by micropipetting the appropriate stock TiO_2 volume corresponding to 1 μg/cm² to the center of the field of view while imaging live. The cell culture medium was washed 2 times with Nanopure™ water (Barnstead; 18.2 MΩ), a still frame corresponding to the same region was captured, and the water was decanted and allowed to air dry overnight. The following day (12 hours later) the surrounding region that was imaged live was scored with a diamond-tipped glass cutter, immobilized on an aluminum stub, and sputter coated with gold. The same region that was imaged with the phase contrast microscope live was imaged with an FEI XL-30 ESEM equipped with EDX elemental analysis.

Procedure for culturing Caco-2_{BBe1} epithelia under conditions of microgravity.

The human, brush border expressing cell line, Caco-2_{BBe1}, was cultured according to the protocol described the in the Cell culture section. The epithelia were cultured 19-21 days to permit differentiation of the epithelia and subsequently transferred to disposable rotary cell culture vessels (Synthecon; D-410), and microgravity was engaged through the use of a microgravity bioreactor (Synthecon; RCCS-4) with the controller set to 24.3 RPM. After microgravity was obtained, as evidenced by "floating" epithelia in the center of the disc, the NP-containing medium was perfused into the chamber and permitted culture for 24 hours in a cell culture incubator. The specimens were fixed while maintaining microgravity for 1 hour at room temperature prior to removing the epithelia from the disc.

Data analysis.

In this manuscript an experiment is defined as at least replicate samples for each treatment with the respective controls conducted on three different days (i.e. at least

technical duplicate with 3 biological replicates). The number of microvilli and the organization of the brush border were analyzed by randomly imaging at least 3 micrographs from each replicate sample. Random 1 μm^2 squares were generated through the use of Powerpoint and the number of microvilli within the 1 μm^2 squares were counted from at least 3 random squares in a single micrograph. The three to five regions were averaged, and the data from the three experiments were compiled to generate an average. Error was determined with Excel and shown as standard error of the means. Multiple comparisons were accomplished via one-way ANOVA with either Dunn's or Tukey posttests. Data were considered significant if $P<0.05$. If untreated specimens appeared in poor health, the entire experiment, including those epithelia exposed to the TiO_2 was culled from analysis.

Results

Material characterization.

Thorough characterization of the two TiO_2 samples was conducted to provide information on their size, morphology, and chemical composition, for which little information exists in open peer-reviewed literature on food grade TiO_2. TEM analysis revealed that food grade- and gum-TiO_2 are colloidal-scale and have spherical to a slightly longer aspect ratio geometry (Figures 7 A and B). The primary particle diameters for food grade- and gum-TiO_2 were 122 ± 48 and 141 ± 56 nm in any external dimension, respectively. There were a range of primary particle diameters (longest dimension) from 51- to 290 nm, and 48.5- to 305 nm for food grade- and gum-TiO_2, respectively. The food grade- and gum-TiO_2 samples contained 23% and 23% of nano-scale particles upon the size distributions with a confidence level of 95%, respectively, based on counting 100 particles sampled from a total of 10,000 particles. Separate phase analysis light scattering for food grade TiO_2 and gum-TiO_2 conducted on an ultrapure water solution

containing TiO_2 at a concentration of 10 mg/L indicated the mean (± standard deviation) hydrodynamic diameter was 220±9 nm (polydispersity = 0.130±0.013) and 250±10 (polydispersity = 0.165±0.014), respectively. In additional, light scanning for food grade $TiO_2$and gum-TiO_2 was conducted in serum-containing cell culture medium. When the samples were bath sonicated for 30 minutes prior to measurements the hydrodynamic diameters were 336 ± 6nm (polydispersity = 0.164±0.0058), and 365 ± 5 nm (polydispersity = 0.162±0.0048) for food grade TiO_2 and gum-TiO_2, respectively. These results suggest that many of the primary TiO_2 particles were aggregated together, although primary particles < 100 nm were clearly present.

Figure 8 shows the XRD spectra for food grade- and gum-TiO_2. Food grade- and the gum-TiO_2 consisted of anatase crystal structure only and not rutile or brookite. For the gum-TiO_2, there is a reflection not associated with anatase at 44.6° that is presumably from the 200 reflection from the aluminum sample holder (theoretically at 44.8°). XRD spectra indicated that the lower bound of the food grade TiO_2 and gum-TiO_2 size was 36 and 26 nm, respectively, which is in good agreement with the TEM results (i.e., Figure 7).

Figure 9 shows the XPS spectrum for the O 1s spectral line for (a) food grade- and (b) the gum-TiO_2. For food grade TiO_2, the O 1s (532 eV) was shifted negatively, indicating O bonding on the surface. The large peak (2) was TiO_2 (530.1 eV) and the smaller peak (1) was presumably phosphate on the basis of the K 2p spectra (i.e., Appendix, Supplemental Figure 2) and the wide scan (i.e., Appendix, Supplemental Figure 3). For the K 2p spectra, the K $2p_{3/2}$ line (294 eV) was shifted negatively to 293 eV, which is in agreement with referenced K_3PO_4 binding energies (Shih, Yung, & Chin, 1998). For the wide scan, K is present and if it is assumed that the phosphate was in the

form of K_3PO_4, then there would theoretically be an atomic percentage of K of 9.6%, which was in good agreement with the measured K amount of 10.8%.

For the gum-TiO_2, the O 1s was also shifted negatively, indicating bond formation. Similar to food grade TiO_2, there is a peak at 529.8 (peak 5) for TiO_2 and at 530.3 eV (peak 4), which was presumably a calcium phosphate compound on the basis of reference binding energies (Demri & Muster, 1995) and the wide scan (i.e., Appendix, Supplemental Figure 4) that showed the presence of Ca. Assuming the compound was $Ca_3(PO_4)_2$, the theoretical atomic percentage of Ca would be 1.2%, which was in good agreement with the measured value of 1.8% in the wide scan. Peak 1 at 533.4 eV, Peak 2 at 532.7 eV, and Peak 3 at 531.4 eV are carboxyl (COOH; Weng et al., 1995), phenol (C-O; Jouan et al., 1993), and carbonyl groups (C=O; Gardner, Singamsetty, Booth, He, & Pittman, 1995), respectively, as confirmed by referenced data and the C 1s spectra (Appendix, Supplemental Figure 5). The C 1s spectra has four peaks that correspond to (1) carboxyl (289.4 eV; Clark & Thomas, 1978), (2) carbonyl (288.1 eV; Delpeux et al., 1998), (3) phenol (286.3 eV; Delpeux et al., 1998), and (4) sp^2 C-C (284.8 eV; Bachman & Vasile, 1989). These bonds and their atomic ratios matched those found in the O 1s spectra, thus confirming the identification of the surface contamination remaining on the TiO_2 gum coating.

In order to provide information on the surface charge characteristics of the TiO_2 samples, zeta potential analysis (Figure 10) demonstrated that both the food grade TiO_2 and gum-TiO_2 samples had a negative surface charge above pH = 4. This was found to be a result of the phosphate and oxygenated functional groups found on the surface of the food grade TiO_2 and gum-TiO_2, respectively. For the food grade TiO_2, the iso-electric point (IEP) pH was at approximately 3.3. The gum TiO_2 pH_{IEP} was not observed at the

pH range examined (~3–8.5), and at neutral pH, its zeta potential was significantly more negative (-46 mV) compared to the food grade TiO_2 (-19 mV).

Food grade TiO_2 disrupts the normal arrangement of constituent microvilli of the Caco-2_{BBe1} brush border.

Under optimal conditions differentiated Caco-2_{BBe1} epithelia were shown to faithfully mimic the *in vivo* epithelium in the mucosal layer of the human enterocyte brush border (M. Peterson & Mooseker, 1992; M. D. Peterson, Bement, & Mooseker, 1993; M. D. Peterson & Mooseker, 1993) when grown in cell culture. The organization of the brush border microvilli gives the apical surface of these cells an archetypical structure (Heintzelman & Mooseker, 1992; Hirokawa et al., 1982; Mooseker, 1985; TM Mukherjee & Staehelin, 1971). Deviations from this archetypical structure can be easily detected in specimen exposed to experimental treatments when examined by scanning electron microscopy (SEM). This study exploits the archetypical structure of the brush border as an assay that is sensitive to changes in the normal organization of the brush border. Food grade TiO_2 could be applied to this cell system to test if the brush border is disrupted.

In order to test if food grade TiO_2 disrupt the normal arrangement of microvilli a SEM approach was employed. A representative, untreated Caco-2_{BBe1} cell in a differentiated epithelium is viewed from above the apical cell surface (Figure 11 A). At this magnification (imaged at 10,000x), used in order to permit adequate detail, one cell occupied the field of view (Figure 11 A-D are shown at the same magnification). This region represents the surface that would face the lumen of the gut and had initial interaction with the TiO_2. At the 10,000x magnification the structure observed are the tops of the many brush border microvilli. These microvilli stand straight off the surface of the cell, a condition referred to as erect (Figure 11 A; De Beauregard et al., 1995) and

had 43±7 microvilli/μm² (Figure 11 F). This number of microvilli in untreated specimens is so great that no relief (i.e. the plasma membrane between the bases of adjacent microvilli) can be seen. In contrast, gum-TiO_2 (white arrows) appeared to decorate the surface of the epithelium and resulted in disruption of the brush border (Figure 11 B – D). Indeed, it was found that exposing Caco-2_{BBe1} epithelia to 350 ng/mL (i.e., 100 ng/cm²) of gum-TiO_2 (white arrows) for 24 hours produced brush borders whose constituent microvilli appeared limp and fewer in number (Figure 11 B). Quantification of the number of microvilli shown in Figure 5 B indicated that the brush borders contained 25±6 microvilli/μm² (n=9; Figure 11 F). Exposure to 3.5 μg/mL (i.e., 1 μg/cm²) of gum-TiO_2 (white arrows) more clearly illustrated the limpness of the microvilli (Figure 11 C). These microvilli appeared to rest on one another to bolster the standing morphology of the microvilli (Figure 11 C). Quantification of the microvilli after exposure to this concentration indicated that the brush borders had 18±4 microvilli/μm² (n=9; $p < 0.001$; Figure 11 F). Exposure to 3.5 μg/mL (i.e. 10 μg/cm²) of gum-TiO_2 (white arrows) demonstrated brush borders whose apical surface appeared absent of microvilli in some regions, and whose apical membrane appeared decorated with membrane "blebs" (dotted white circles) of approximately 100 nm in diameter (Figure 11 D). Quantification of the number of microvilli shown in Figure 11 D indicated that the brush borders contained 12±5 microvilli/μm² (n=9; $p < 0.001$; Figure 11 F).

It is important to rule out the possibility that leeching of ions from the food grade or gum materials, or sequestration of serum components by the TiO_2, resulted in disruption of the brush border. In order to test this gum-TiO_2 at a concentration of 35 μg/mL (i.e., 10 μg/cm²) was applied to culture medium, the medium was sonicated, and the TiO_2 were allowed to settle through sedimentation to the bottom of a conical tube. Once the TiO_2 settled as evidenced by visual inspection the culture medium, the top 1/3

of the supernatant was employed as growth medium for epithelia and the following day the specimens were cytologically fixed and processed for SEM. Through the use of single particle ICP-MS it was found that approximately 99.99% titanium settled, while 0.01% remained in the supernatant, and when this medium was applied to the epithelium (shown as the inset in Figure 11 D) SEM analysis indicated that the brush borders appeared well ordered and densely packed identical to untreated control microvilli. Of note, the effect of the 350 ng/mL (i.e., 100 ng/cm^2) of gum-TiO_2 (white arrows) appeared to be a localized effect (Figure 11 E). That is only those areas that were found to be in intimate contact with the agglomerated NPs (white arrows) showed regions devoid of microvilli (imaged at 4,300x in Figure 11 E). Regions devoid of the TiO_2 (outlined by the alternating dashed lines) had an erect, dense array of microvilli on the apical surface of the cell whereas regions with gum-TiO_2 had limp and fewer microvilli surrounding the gum-TiO_2. The regions in Figure 5 pointed to by white arrows are presumed to be agglomerated gum-TiO_2 as SEM coupled with energy dispersive x-ray spectroscopy showed round, electron-dense aggregated material (Figure 12 A) with identifying peaks corresponding to titanium and oxygen (Figure 12 B). Analysis of particle diameters indicates that some TiO_2 were NPs as the smallest particle measured was 20 nm whereas the largest was 291 nm in diameter after sputter coating.

In light of the fact that the food grade- and gum-TiO_2 are of the same crystal structure (anatase), and food grade TiO_2 (E171 compliant) is a pigment for use in human foods, one might predict that exposure to food grade TiO_2 results in a similar disruption of the Caco-2_{BBe1} brush border. In order to test this possibility, a dose-response experiment was conducted. Consistent with the results of Figure 11, Figure 13 indicates effacement of the brush border after the 24 hour exposure window. It was found that untreated specimens had microvilli that appeared erect (Figure 13 A) with 43±7

microvilli/μm² (Figure 13 F). Similar to the results reported in Figure 11, exposure to 350 ng/mL (i.e., 100 ng/cm²) of food grade TiO_2 (white arrows) resulted in a slightly limp microvillar morphology (Figure 13 B) and brush borders contained 26±5 microvilli/μm² (Figure 13 F). Exposure to 3.5 μg/mL (i.e., 1 μg/cm²) of E171 TiO_2 (white arrows) produced brush border with individual microvilli apparently limp (Figure 13 C), and quantification of the number of microvilli indicated that there were 21±7 microvilli/μm² (Figure 7 F). After exposure to 35 μg/mL (i.e. 10 μg/cm²) of food grade TiO_2 (white arrows) microvilli appear tethered at the plus tips and laying perpendicular to the plasma membrane. This disrupted phenotype was prevented by permitting sedimentation of the food grade TiO_2 to occur *in vitro* and subsequently culturing epithelia in the supernatant largely removed of the TiO_2 (inset in Figure 13 D) as was done early with the gum-TiO_2. Finally, incubating 350 ng/mL (i.e., 100 ng/cm²) of food grade TiO_2 (white arrows) appeared only to locally affect the normal arrangement of the microvilli (originally imaged at 4,300x), as those cells with agglomerated colloids at the cell surface showed a mildly limp/clustered morphology (Figure 13 E).

Agglomerated TiO_2 do not remain stationary at the surface of the epithelium.

The presence of agglomerated TiO_2 on the cell surface presents the possibility of a direct interaction between the agglomerates and the brush border. In order to determine if there is a direct interaction between the agglomerates and the brush border a time-lapsed video microscopy approach was employed. This was possible because the agglomerated colloids were within the limit of resolution of light microscopy , but a large subset of the material maintained at least one or more external dimension < 100 nm in diameter as a characteristic of a NP (Dunphy Guzman et al., 2006). When viewed with phase-contrast microscopy untreated specimens showed a typical honeycomb

arrangement of cells within the epithelium (Figure 14 A). Upon careful inspection of those epithelia exposed to 3.5 μg/mL (i.e., 1 μg/cm²) food grade TiO_2 there appeared to be phase-dense, granular material at the cell surface. More importantly, Figure 14 B showed agglomerates (white arrows) decorated the apical surface of the epithelium and these agglomerates apparently moved position with respect to time (Figure 14 B); The black rectangle in Figure 14 B surrounds one such agglomerate collected as 4 still frames every 10 seconds. The white arrow head points to the TiO_2 agglomerate midpoint, and a white line was inscribed from the midpoint of the arrowhead to the fixed end of the micrograph. Under these conditions the length of the fixed end of the micrograph to the midpoint of the arrowhead changed (shown in arbitrary units *; the scale bar is 20 μ in A – B**)** indicating movement of the putative TiO_2 agglomerates**.**

In order to assess if these phase-dense, granular material might be the TiO_2 agglomerates the TiO_2 was applied to a glass bottom dish at 3.5 μg/mL (i.e., 1 μg/cm²) in the presence of cell culture medium, but devoid of cells. This positive control for the agglomerated TiO_2 demonstrated phase-dense, granular material moving at the bottom of the culture dish. The white oval in Figure 14 C showed that the position of the agglomerated TiO_2 changed with time. Furthermore, and similar to the result described in Figure 14 B, the measuring device indicated that the length of the inscribed white line changed over time (Figure 14 C; shown in arbitrary units *; the scale bar in the still frames is 8 μm). The same region shown in Figure 14 C was washed to remove any unbound TiO_2 and a correlated light and SEM approach was employed in order to show the material in high magnification, as well as to conduct elemental analysis (Figure 14 D). From left to right, the first micrograph indicated that some TiO_2 adhered to the collagen after washing the dish 3 times with deionized water. The white arrow in each image points to the top portion of the “L” that was employed as a feducial marker. The second

image showed that the specimen remained largely unchanged after processing the slide for SEM. The third image is a higher magnification of the top portion of the "L" (white arrow). The fourth image showed a high magnification view of the top of the "L" etched in the glass. The white dashed box was the region used to determine elemental composition (data not shown). It was found that this region contained peaks corresponding to titanium and oxygen as expected for TiO_2. What follows from these results is that after sedimentation the agglomerated TiO_2 moved, potentially through Brownian motion (Cho et al., 2011). Coupled the effects of sedimentation and movement might depress the microvilli and permit adsorption/effacement of the brush border.

Disruption of the brush border is independent of sedimentation due to gravity.

The clue that agglomerated TiO_2 oscillated on the surface of the epithelium and that food grade TiO_2 result in disruption of the brush border suggested that sedimentation due to gravity and consequently the mass of the agglomerated TiO_2 may account for brush border disruption. In order to test this prediction two alternative approaches to remove the effects of gravity and consequently the mass of the nanomaterial were employed; first by inverting the configuration of the epithelia during exposure to TiO_2 illustrated in the cartoon, and second by culturing the epithelia in a microgravity bioreactor (Figure 15 A-B). During inverted culture of untreated Caco-2_{BBe1} epithelia the morphology and density of the microvilli was not found to be different than untreated specimens in the upright configuration (Figure 16 A). However, exposure to 350 ng/mL (i.e., 100 ng/cm^2) of food grade TiO_2 (white arrows) while the epithelium was in the inverted configuration appeared to disrupt both the erect morphology of the microvilli and the total number of microvilli; SEM analysis indicated that the microvilli were limp (Figure 16 B) and quantification of the number of microvilli indicated that

there was a significant reduction to a value of 23±6 microvilli/μm^2. Furthermore, the brush border effacement was confirmed during inverted exposure to food grade TiO_2 at a concentration of 350 ng/mL (i.e., 100 ng/cm^2; Figure 16 C, D). That is, the microvilli appeared limp in regions decorated with agglomerated TiO_2 (white arrows), and the number of the microvilli was significantly reduced to 27±8 microvilli/μm^2. The black arrows point to TiO_2 settled at the inverted bottom of the centrifuge tube (Figure 15 B). No statistical difference in the number of microvilli was found after exposure to neither gum- TiO_2 nor food grade TiO_2 at any concentration or epithelial orientation. These data were confirmed employing the microgravity bioreactor (Figure 15 C). The white arrow in Figure 15 C points to the cell monolayer in microgravity at the center of the culture disc and this is the proper location for the cells to be exposed to microgravity (Schwarz and Wolf, 1991).

Food grade TiO_2 is internalized by cells of the $Caco2_{BBe1}$ human intestinal model.

Several lines of evidence indicate that internalization of NPs could play a role in actin remodeling at the apical surface of the cell (Madhavi Kalive et al., 2012; Koeneman et al., 2010; W. Zhang et al., 2010). Remodeling of the actin cytoskeleton at the apical surface (i.e. the brush border) could result in disruption of the brush border, since microvilli would not exist if remodeling occurred. In order to test if food grade TiO_2 was internalized by the Caco-2_{BBe1} epithelia, a TEM approach was employed. Under optimal conditions the brush border of differentiated Caco-2_{BBe1} epithelia demonstrated polarity with numerous brush border microvilli at the apical surface as an untreated control (Figure 17 A). After a 24 hour treatment with either 350 ng/mL (i.e., 100 ng/cm^2) of gum-TiO_2 or 350 ng/mL food grade TiO_2 (black arrows) two populations of nanomaterial existed (Figure 17 B - D). There was a subset of agglomerated TiO_2 enclosed by electron

dense vesicles as internalized material, and another fraction remained in an electron-dense granular material "tangled" in the brush border at the cellular apex (Figure 17 B - D). Analysis of the individual particle diameters within each of the micrographs indicated a range of sizes from as small as 58 nm to as large as 286 nm, indicating that a subset of the internalized particles were NPs.

Discussion

In the present investigation, it was found that food grade TiO_2 disrupted the brush border after exposure to an *in vitro* model of the human intestine. A significant fraction of this food grade TiO_2 had dimensions of primary particles < 100 nm in its longest-axis length. Specifically we addressed the hypothesis that exposure to food grade TiO_2 results in brush border disruption and disruption due to TiO_2 is an event independent of sedimentation *in vitro*. The study by Cho et al., (2011) indicated that large and/or dense metal NPs have the potential to rest on top of the cells at the bottom of the culture dish, which could be due to the effects of NP agglomeration and subsequently sedimentation. This settling out of solution after agglomeration could increase the concentration of NPs that the epithelium would otherwise not be exposed to. In the present investigation it was found that TiO_2 purchased as food grade (E171 coded) as well as TiO_2 isolated from the candy coating of gum were of similar physico-chemical characteristics. These particles exposed to the epithelia at the lowest concentration of 350 ng/mL (i.e., 100 ng/cm^2) that elicited a cellular response when grown upright, also resulted in brush border disruption after removing the effects of TiO_2 settling due to sedimentation. This effect was first demonstrated when the substrate with the epithelium was inverted and exposed to TiO_2 at a concentration of 350 ng/mL. Under these conditions there was no statistical difference between those exposed to TiO_2 in neither the upright nor the inverted configurations. This result was confirmed by an

independent approach where epithelia were exposed to TiO_2 under conditions of microgravity, indicating that sedimentation of agglomerated TiO_2 does not account for disruption of the brush border. Furthermore, results from control experiments indicate that it is unlikely that leeching of ions, or adsorption of serum components from/to TiO_2 resulted in brush border disruption as exposure to cell culture medium removed of the TiO_2 resulted in brush borders that appeared healthy and morphologically similar to unexposed (control) brush borders.

Studies have shown that exposure to α-Fe_2O_3 NPs at a concentration of 100 μg/mL elicited an upregulation of the gene (*CapZ*) that encoded the actin capping protein CapZ in the Caco-2 cell model (Madhavi Kalive et al., 2012) and in a brush border expressing model of the human placenta Chapter 5. As indicated in the Introduction, it is well known that elongation of filamentous actin (F-actin) coupled with the addition of actin bundling proteins to the core fine filaments permits the normal morphology of the microvillus. Studies have also shown that polymerization of actin occurs at the most distal point of the microvillus tip in a region referred to as plus tips (Begg et al., 1978; Hirokawa & Heuser, 1981; Ishikawa et al., 1969; Tilney & Mooseker, 1971). Further, the addition of actin monomers to F-actin is known to be a dynamic and continuous process (Stidwill et al., 1984). In the event that the actin capping protein, CapZ is translated from upregulated messenger RNA, CapZ could inhibit F-actin polymerization at the plus tips. This hypothesis is corroborated by the constant turnover of the structural proteins, and addition of monomers at the plus tips; Should CapZ protein cap F-actin plus tips there would be no regulated addition of monomers necessary to maintain the microvilli length.

In vitro analysis necessitates the use of a physiological milieu containing serum proteins. Commonly, investigators use serum at a 10% concentration in a liquid medium

formulated with the necessary salts, vitamins, minerals, etc., as a surrogate for a chemically defined culture medium in order to propagate cells in a culture dish. When materials such as metal nanoparticles are applied to this medium, the proteins from the medium adsorb to the material surface. Since some nanoparticles have a large surface-area-to-volume ratio and consequently high surface free-energy a large number of proteins have been shown to decorate the material surface based on material surface chemistry (Lundqvist et al., 2008). These decorated proteins bind with different affinities and are referred to as the "hard" and "soft" coronas (Milani, Baldelli Bombelli, Pitek, Dawson, & Rädler, 2012). Studies employing non-functionalized (i.e., pristine) silica nanoparticles clearly showed the effects of the NP corona (Lesniak et al., 2012). In the study by Lesniak and coworkers (2012) pristine silica nanoparticles (50 nm in diameter) were exposed to A549 lung epithelia in serum free conditions for 1 hour and were found decorated with a variety of proteins after recovery of the nanomaterial from the cells. Of note, the proteins spectrin and α-actinin had high spectral counts during mass spectrometry analysis, indicating a large number of these proteins were part of the NP corona (Lesniak et al., 2012). Although purely speculative, one could hypothesize that a similar process may result in brush border disruption as was shown to be independent of sedimentation in the present investigation. Both spectrin and α-actinin are necessary for the structural integrity of the terminal web and inter-microvillar rootlets. If spectrin and α-actinin adsorbed to the NP corona with a higher affinity than serum components and/or the proteins that directly bind spectrin and α-actinin in the terminal web it could be predicted that particles, such as the TiO_2 employed in the present investigation, sequester these structural components. Sequestration of structural proteins necessary to maintain the erect morphology of microvilli could transiently disrupt the brush border since, as indicated in the preceding paragraph,

many of the proteins in the microvilli are constantly turned over, and retrograde actin flux coupled with monomer addition at the plus tips maintains the length of microvilli in a highly controlled manner. Therefore, at present the possibility that the biological corona is in part responsible for brush border disruption cannot be excluded from the putative list of causal agents.

To date a number of studies using TiO_2 NPs have been conducted in order to determine whole organism (*in vivo*) toxicity as a result of exposure to TiO_2 and not the "subtle" effect of brush border disruption as a consequence of exposure to TiO_2 from human food products as was found in the present investigation. Studies conducted in the mouse model indicate a wide range of effects after intragastric administration of anatase TiO_2 NPs (Duan et al., 2010). The authors, employing concentrations of 0, 62.5, 125 and 250 mg/kg body weight every other day, found significant loss in body weight at concentrations of 125, and 250 mg/kg TiO_2 NPs exposure (Duan et al., 2010). One possible explanation for the significant loss of body weight between control groups and those exposed to 125, and 250 mg/kg body weight of anatase TiO_2 NPs is a disruption manifested as a retraction of the brush border. If brush borders were disrupted in this system, there would be a net loss of surface area by which food stuffs could be absorbed. The decrease in surface area of the small intestine could result in malnutrition and decreased body weight. However, when mice were dosed once by oral galvage according to the OECD protocol, acute toxicity was observed and resulted in an increase in body weight (J. Wang et al., 2007). Further, studies employing the rat model indicate no change in body weight. In the study (Warheit et al., 2007), the authors applied 175, 550, and 1750 mg/kg of ultrafine mixtures of TiO_2 NPs (79% rutile 21% anatase) once to a single fasted female (n=1) and investigated the effects 14 days after dosing according to the OECD protocol (Oecd, 1994). Of note the authors dosed 3 rats as a single experiment

at concentrations of 5 g/kg body weight with the same material and found no change in body weight after 14 days (Warheit et al., 2007). However, many of the *in vivo* studies have not directly addressed the "subtle," non-lethal phenomenon of brush border disruption. Therefore, at present there is evidence for and against *in vivo* brush border disruption, which appear to be dose- and species dependent.

There are several *in vivo* studies indicating that TiO_2 can translocate to the liver, kidney, and brain in rodents (Duan et al., 2010; Fröhlich & Roblegg, 2012; Hu et al., 2010; Powell, Faria, Thomas-McKay, & Pele, 2010; J. Wang et al., 2007). This fact implies that TiO_2 was able to pass several of the physiological barriers that could otherwise sequester the material from direct interaction with the epithelium. Perhaps the greatest physiological barrier that exists in mammals including rodents, but not the *in vitro* cell model employed in the present investigation, is mucus. Mucus is secreted by Goblet cells that are interspersed within the *in vivo* mucosal layer. Of their many functions, Goblet cells largely serve to lubricate and "protect" the enterocytes/brush borders from abrasion. Furthermore, it is widely accepted that the entire mucosal layer is turned over every 4-5 days in mammals including rodents (van der Flier & Clevers, 2009). Therefore, if brush border disruption occurred in these systems, evidence for this event would be found shortly after administration of the TiO_2 and is liable to present itself as a retraction/shortening of the microvilli. Disruption of the brush border *in vivo* could appear as a retraction for a number of reasons; In an attempt to investigate proteins necessary to maintain the archetypical structure of the microvillus, investigators have developed several knockout models for a number of structurally important brush border proteins in rodents (Ferrary et al., 1999; Grimm-Günter et al., 2009). In spite of triple knockdown models, microvilli still appeared on the apical cell surface (Revenu et al., 2012). These data potentially indicate that there is functional redundancy within the

in vivo system in rodents to maintain the erect microvilli morphology that may not exist in the Caco-2_{BBe1} human cell model since this cell system appears amenable to experimental manipulations that result in changes in the brush border (De Beauregard et al., 1995; M. D. Peterson & Mooseker, 1993).

These data indicate that food grade TiO_2 apparently elicits a *bona fide* biological response and not simply a physical artifact as a consequence of *in vitro* exposure. Estimates based on *in vitro* exposure suggest that approximately 42% of microvilli are lost after exposure to food grade TiO_2 at the lowest concentration of 350 ng/mL (i.e., 100 ng/cm^2), together these data indicate a need to: 1) identify the aforementioned putative effects of food grade TiO_2 with the correct *in vivo* models that capture cells in their complex social context; 2) identify which physico-chemical parameters influence brush border disruption as the food grade TiO_2 employed in this study were both anatase, and; 3) identify biological mechanisms by which TiO_2 disrupt the brush border since the loss of microvilli results in a decrease in the total surface area of the gut.

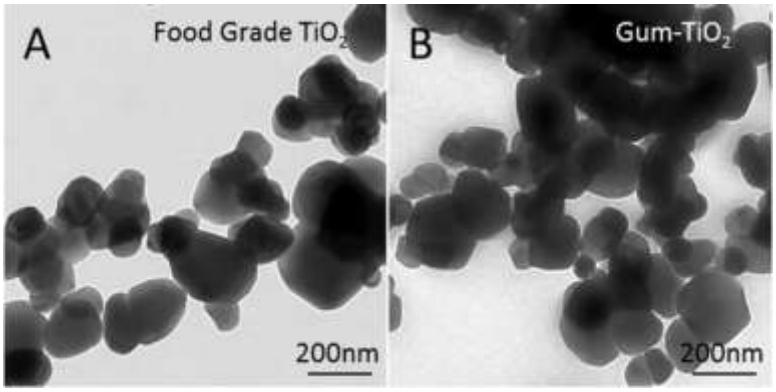

Figure 7. Transmission electron micrographs of food grade TiO2 (A; identified as E171 compliant) and, (B) gum-TiO2. The scale bar in the lower left corner of the micrographs is 200 nm.

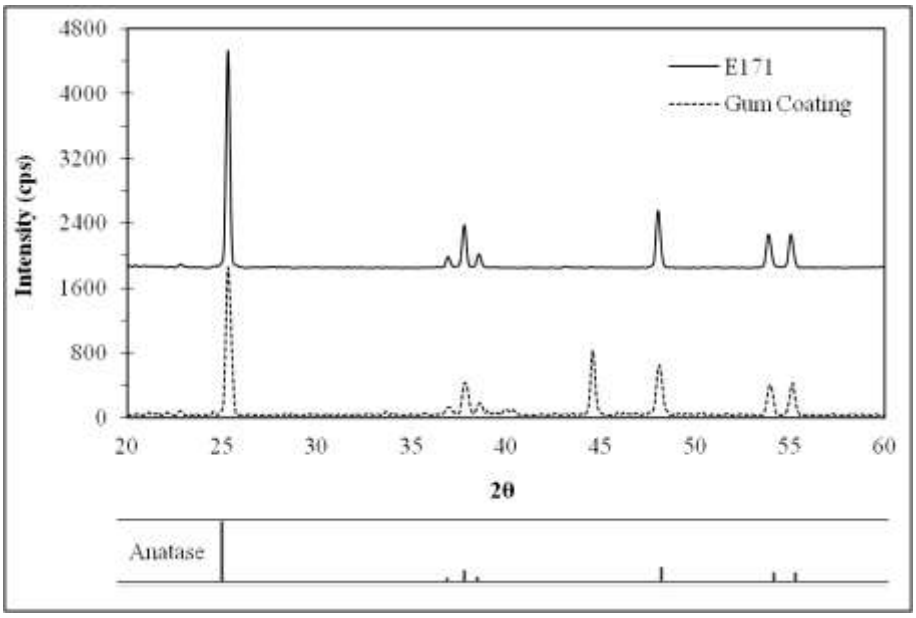

Figure 8. XRD specta for food grade TiO_2 (solid line) and gum-TiO_2 (dashed line) samples, plus standard reflections for anatase (bottom).

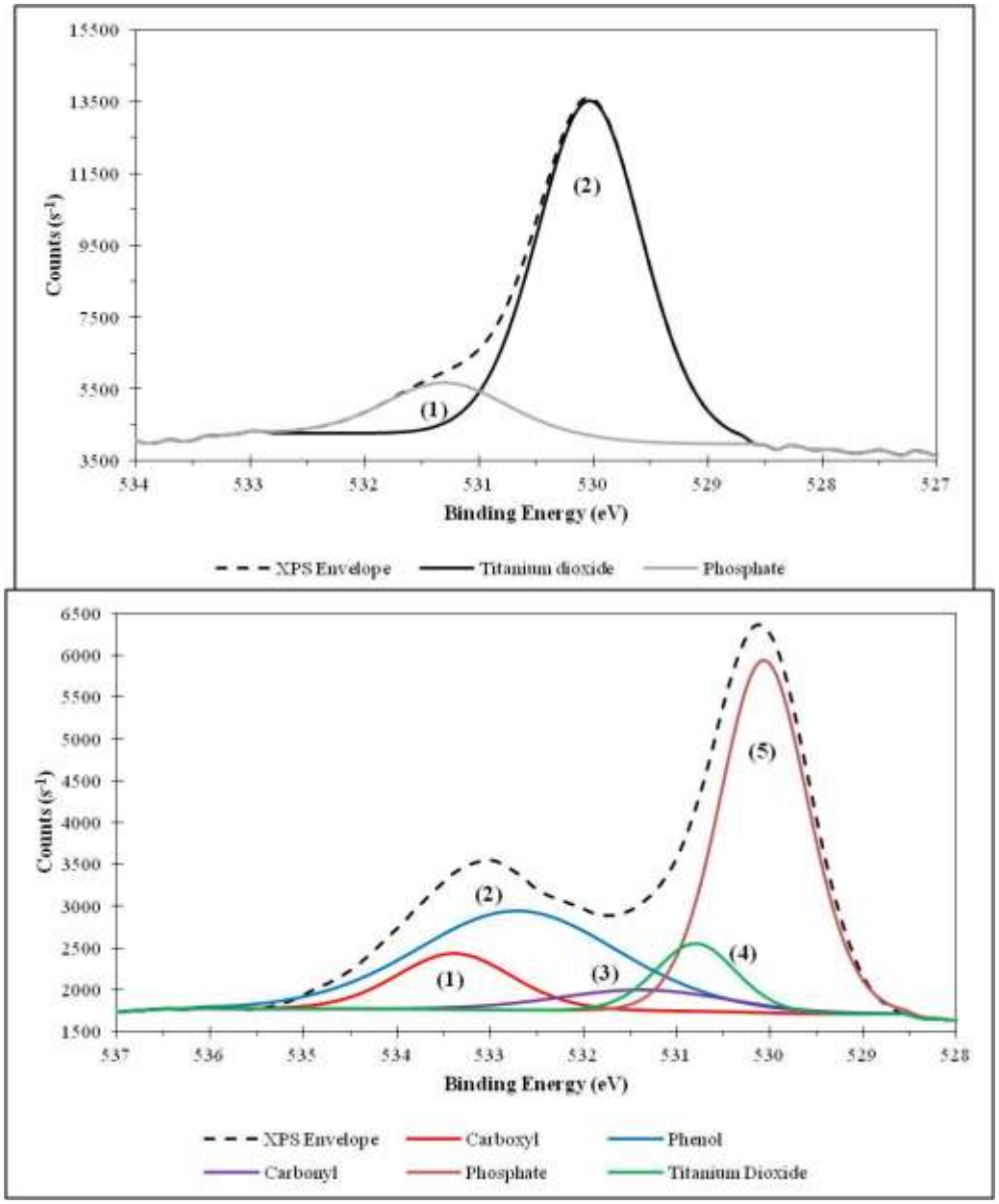

Figure 9. XPS O 1s spectra of (A) food grade and (B) gum-TiO_2. The inset table in (B) shows the theoretical atomic concentration taken from the XPS wide-scan (i.e., Supplemental Figure 3) and calculated with the assumption of $Ca_3(PO_4)_2$ presence, and the fitted atomic concentration that is based on the O 1s XPS fittings shown in this figure (i.e., peaks 1, 2, 3, 4, and 5).

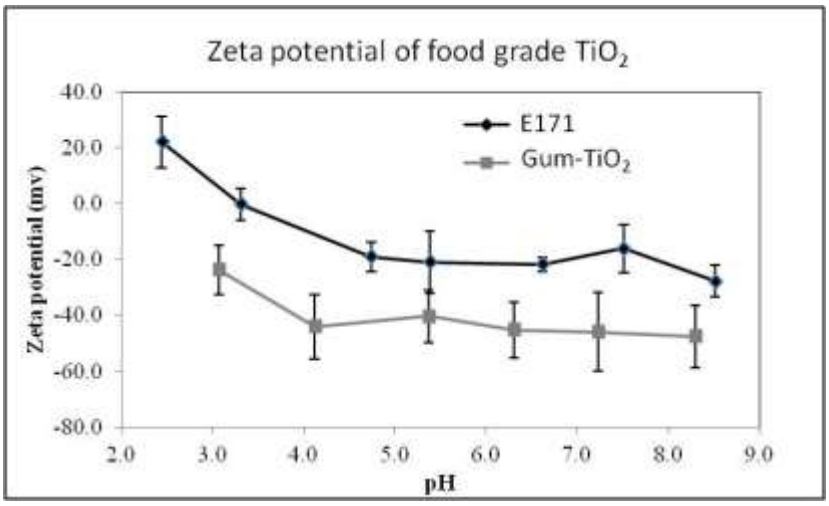

Figure 10. Zeta potential analysis for food grade TiO_2 and gum-TiO_2. TiO_2 samples were measured with respect to pH. Both food grade TiO_2 and gum-TiO_2 have negative zeta potentials. Note that the zeta potential of food grade TiO_2 is less negative and consequently agglomerates faster in solution compared to the gum-TiO_2 samples employed in this investigation.

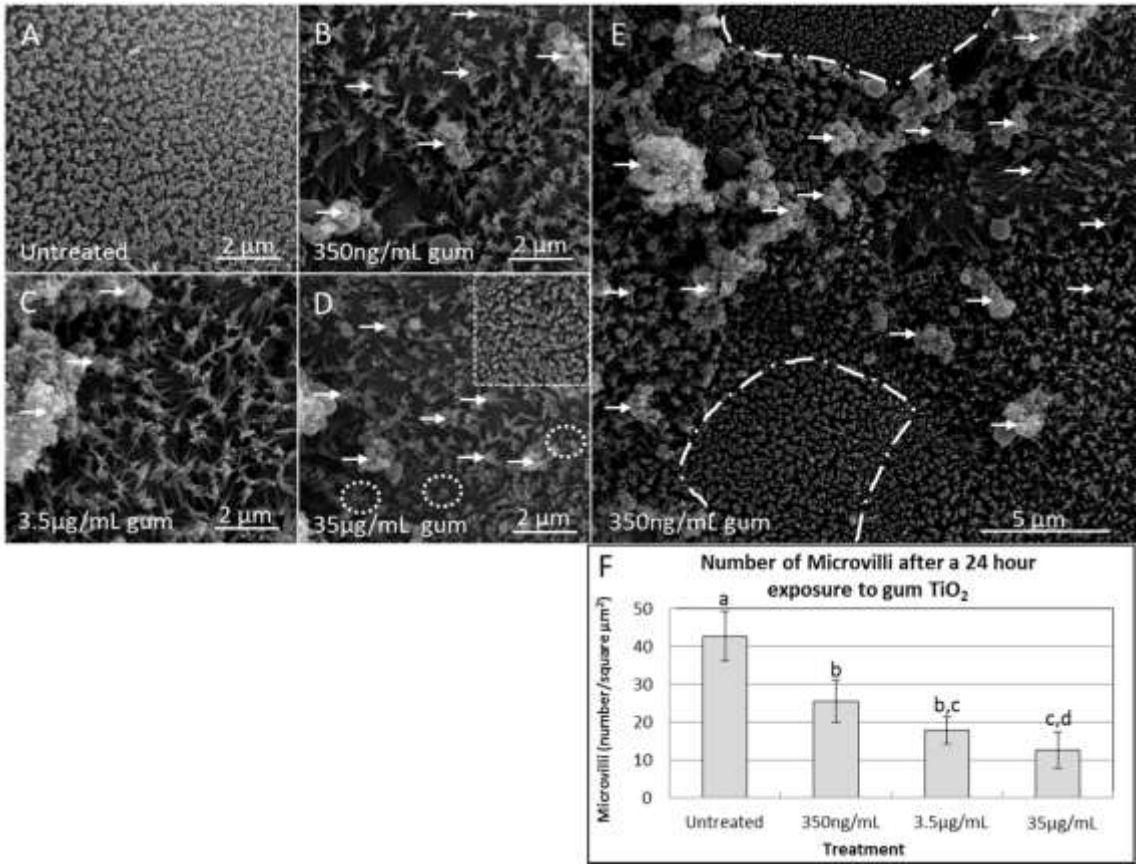

Figure 11. Exposure to food grade TiO_2 isolated from name-brand gum resulted in disruption of the brush border as evidenced by SEM. (A) Untreated, control specimens appeared well-organized and densely-packed with many brush border microvilli. (B) Exposure to 350 ng/mL gum-TiO_2 for 24 hours reduced the number of standing microvilli. The white arrows point to the TiO_2. (C) Exposure to 3.5 µg/mL gum-TiO_2 for 24 hours apparently caused the microvilli to go limp. (D) Exposure to 35 µg/mL gum-TiO_2 for 24 hours resulted in brush border microvilli that appeared retracted, and contained almost no erect microvilli. The inset in D is a control specimen, whereby the TiO_2 was applied to complete culture medium at a concentration of 35 µg/mL, the TiO_2 was allowed to settle, and the top fraction was used to feed the epithelia. This control specimen appeared identical to the untreated control. (E) The low magnification micrograph showed that the effect of exposure to 350 ng/mL gum-TiO_2 for 24 hours was localized to those cells that were in intimate contact with the TiO_2. Some regions within the micrograph showed signs of microvilli that may have been depressed by TiO_2. The alternating dashed line surrounds cells that had no material on the cell surface and consequently a developed brush border. The white arrows point to gum-TiO_2. (F) The histogram shows the number of microvilli after the dose response experiment. The data is shown as mean ± SEM, and significance ($P < 0.05$) was determined based on a one-way ANOVA followed by Dunn's posttest. Characters represent significance where redundant characters indicate non-statistical differences.

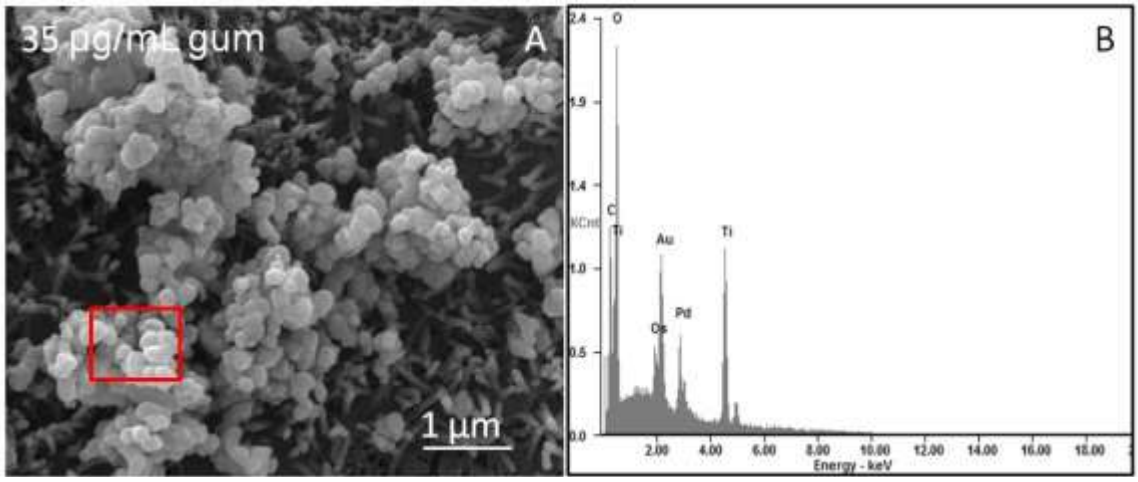

Figure 12. The material on the surface of the epithelia was TiO_2 as determined by EDX analysis. (A) The micrograph shows a high magnification view of the material that decorated the epithelia. The morphology of the material appears similar to the TEM micrographs shown in Figure 7. The red box is the region of interest for EDX analysis. (B) EDX analysis indicated that the material was composed of titanium and oxygen. The osmium peak was apparently due to the secondary fixative (OsO_4) used for the underlying biological specimens (i.e., the brush border), and the Pd/Au was the material used to sputter coat the specimens.

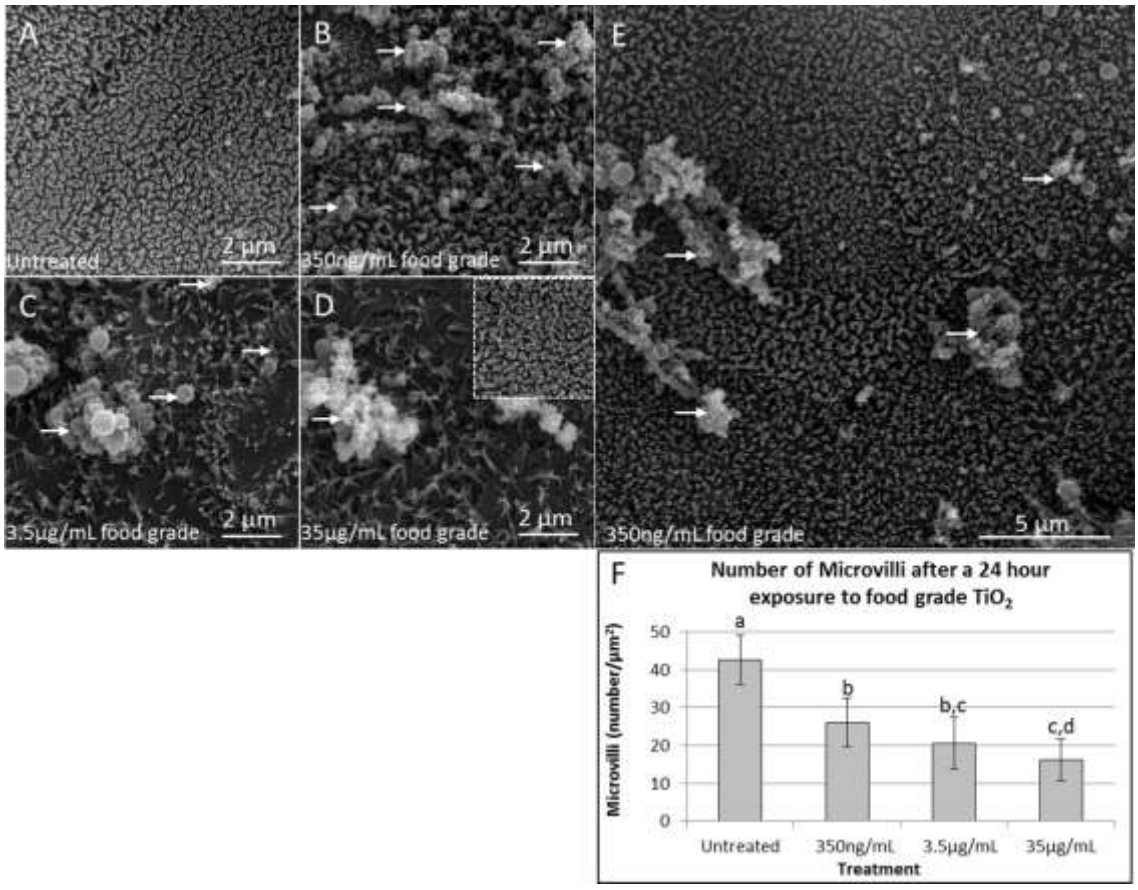

Figure 13. SEM analysis indicates that food grade (E171 compliant) TiO_2 disrupted the brush border microvilli. (A) Untreated, control specimens retained a well-developed brush border after sustained culture. Note that at least 2 edges of individual cells can be seen as identified by the slight interdigitation of microvilli between adjacent cells. (B) Exposure to 350 ng/mL food grade TiO_2 for 24 hours reduced the number of standing microvilli. The white arrows point to the TiO_2. (C) Exposure to 3.5 µg/mL food grade TiO_2 for 24 hours apparently caused the microvilli to go limp. The white arrows point to the TiO_2. (D) Exposure to 35 µg/mL food grade TiO_2 for 24 hours resulted in brush border microvilli that appeared limp/disorganized, and the plasma membrane of the cell was easily seen indicating a significant loss of microvilli. The arrows point to the TiO_2. The inset in D is a control specimen, whereby the TiO_2 was applied to complete culture medium at a concentration of 35 µg/mL, the TiO_2 was allowed to settle, and the top fraction was used to feed the epithelia. This control specimen appeared identical to the untreated control. (E) The low magnification micrograph showed that the effect of exposure to 350 ng/mL food grade TiO_2 for 24 hours was localized to those cells that were in intimate contact with the TiO_2. The white arrows point to the TiO_2. (F) The histogram shows the number of microvilli after the food grade TiO_2 dose response experiment. The data is shown as mean ± SEM. Significance ($P < 0.05$) was determined by a one-way ANOVA followed by Tukey posttest. Characters represent significance where redundant characters indicate non-statistical differences.

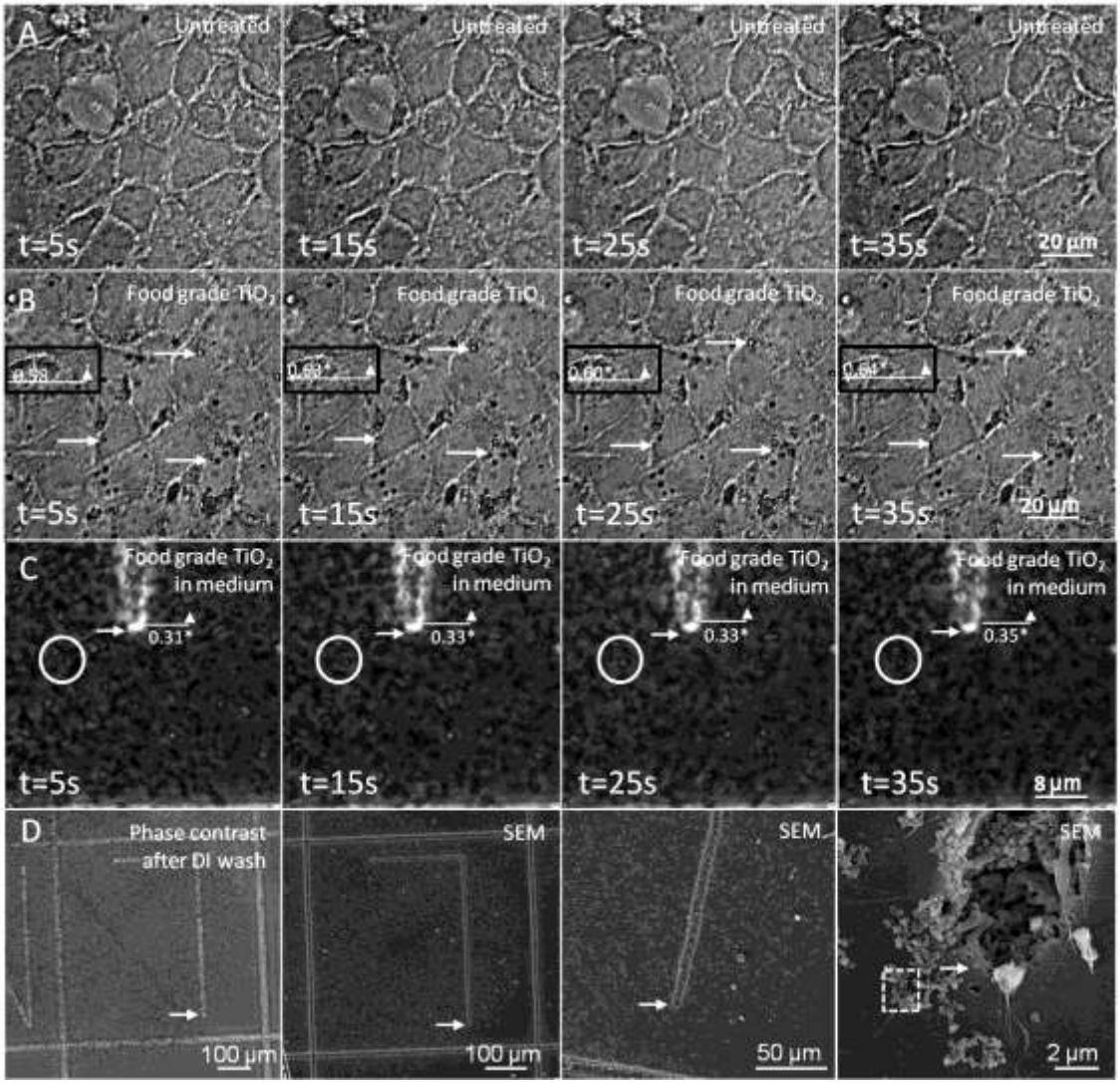

Figure 14. Live cell imaging indicates that agglomerated TiO_2 settles and moves with respect to time. (A) Untreated, control specimens show the typical honeycomb arrangement of phase-light junctions between cells. No granular material is evident in the complete culture medium, or at the cell surface. (B) Application of 3.5 µg/mL food grade TiO_2 resulted in granular material, pointed to by white arrows that appeared to oscillate on the surface of the epithelia. The white circle shows one such event; (C) The center of the putative TiO_2 agglomerate changed position over time indicate by a change in arbitrary units from a fixed point at the edge of the micrograph. Applying food grade TiO_2 to a gridded Ibidi dish in the absence of cells indicated that the granular material shown in B was agglomerated TiO_2. (D) The data shown in C were confirmed to be TiO_2 through the use of SEM coupled with EDX analysis. From left to right, the top of the "L" (white arrow) was employed as a feducial marker. The first image corresponds to the TiO_2 that adhered to the collagen after washing with deionized water to remove salts. The second image is the same "L," but imaged with a SEM. The third image is a higher magnification of the second. The fourth image is further magnified and shows agglomerated TiO_2. The white arrow in each micrograph of C and D points to the top portion of the "L." The white dashed box is the region of interested employed for EDX

analysis. EDX indicated that these regions contained peaks corresponding to titanium and oxygen.

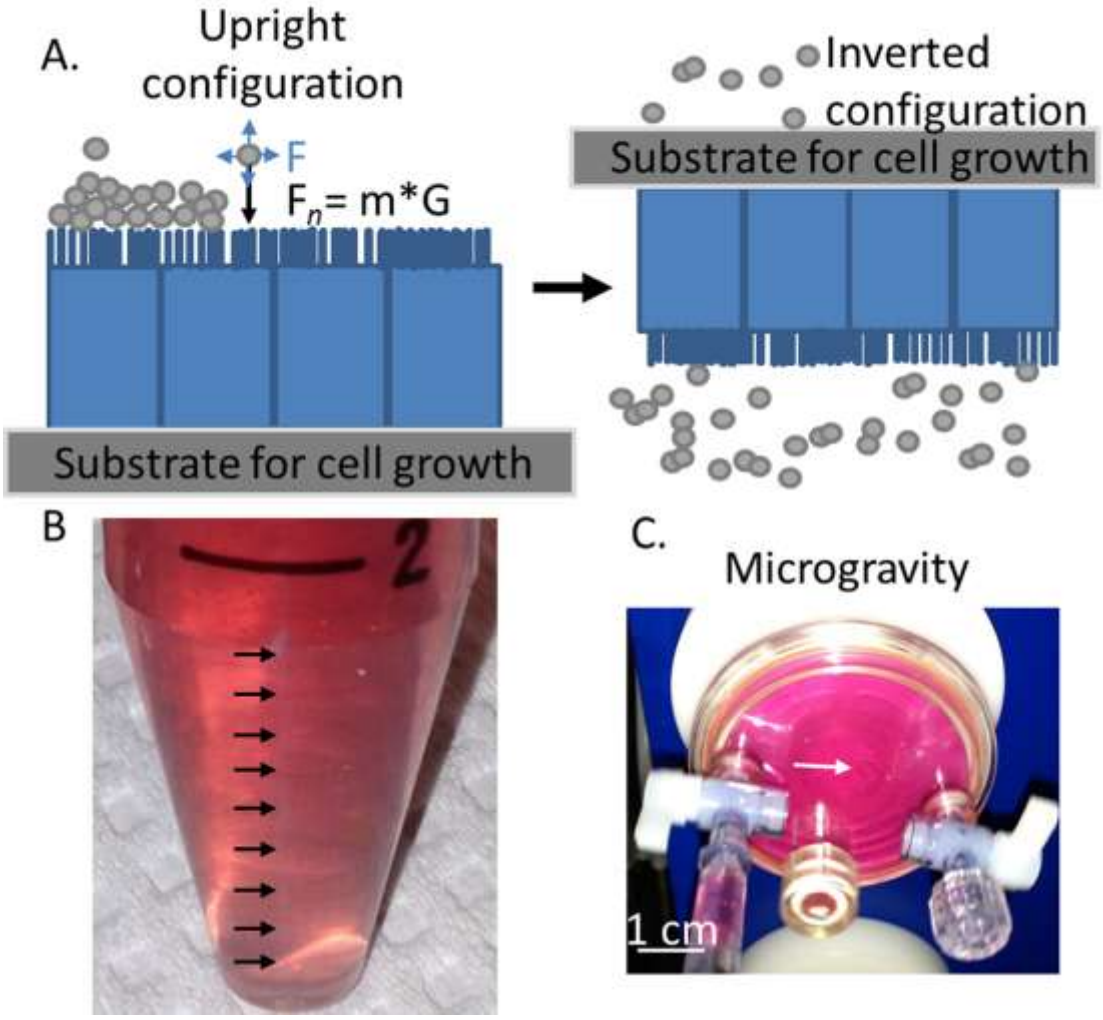

Figure 15. The cartoon and images illustrate the experimental design to remove the effects of sedimentation. (A) During exposure to TiO_2 in the upright condition could permit sedimentation of the TiO_2. However, an alternative scenario exists whereby the epithelia are inverted and the TiO_2 can no longer settle at the cell surface. (B) After culturing epithelia in the inverted position a thin, white line appeared at the bottom of the tube that housed the specimens. The arrows point to the TiO_2 that settled. (C) The microgravity bioreactor permitted conditions of microgravity thereby eliminating settling of the TiO_2. The white arrow points to an epithelium whose collagen-coated, PTFE membrane was excised from the plastic housing. The central position of the substrate containing the epithelium indicates that it is in a state of microgravity.

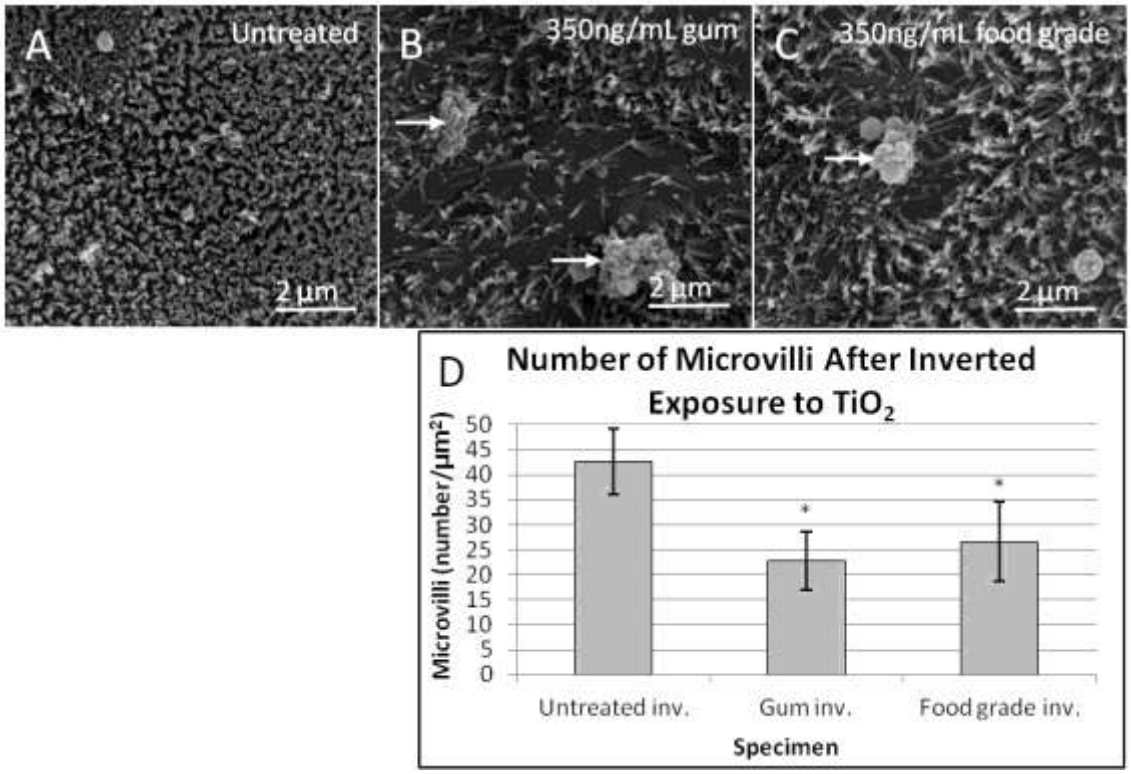

Figure 16. Inverting the specimens to remove the effects of TiO_2 settling indicate that sedimentation does not account for brush border disruption. (A) Untreated specimens, when grown upside-down retain a well developed, and densely packed brush border. (B) Exposing the specimens to a concentration of 350 ng/mL gum-TiO_2 while inverted resulted in disruption similar to that found during right side up culture. The white arrows point to gum-TiO_2. (C) Exposing the specimens to a concentration of 350 ng/mL food grade TiO_2 while inverted resulted in disruption similar to that found during upright culture. The white arrows point to gum-TiO_2. (D) The histogram indicates that there is a significant reduction in the number of microvilli between untreated, and TiO_2 treated specimens. No statistical difference was observed between inverted and upright exposure to TiO_2. Characters represent significance where redundant characters indicate non-statistical differences.

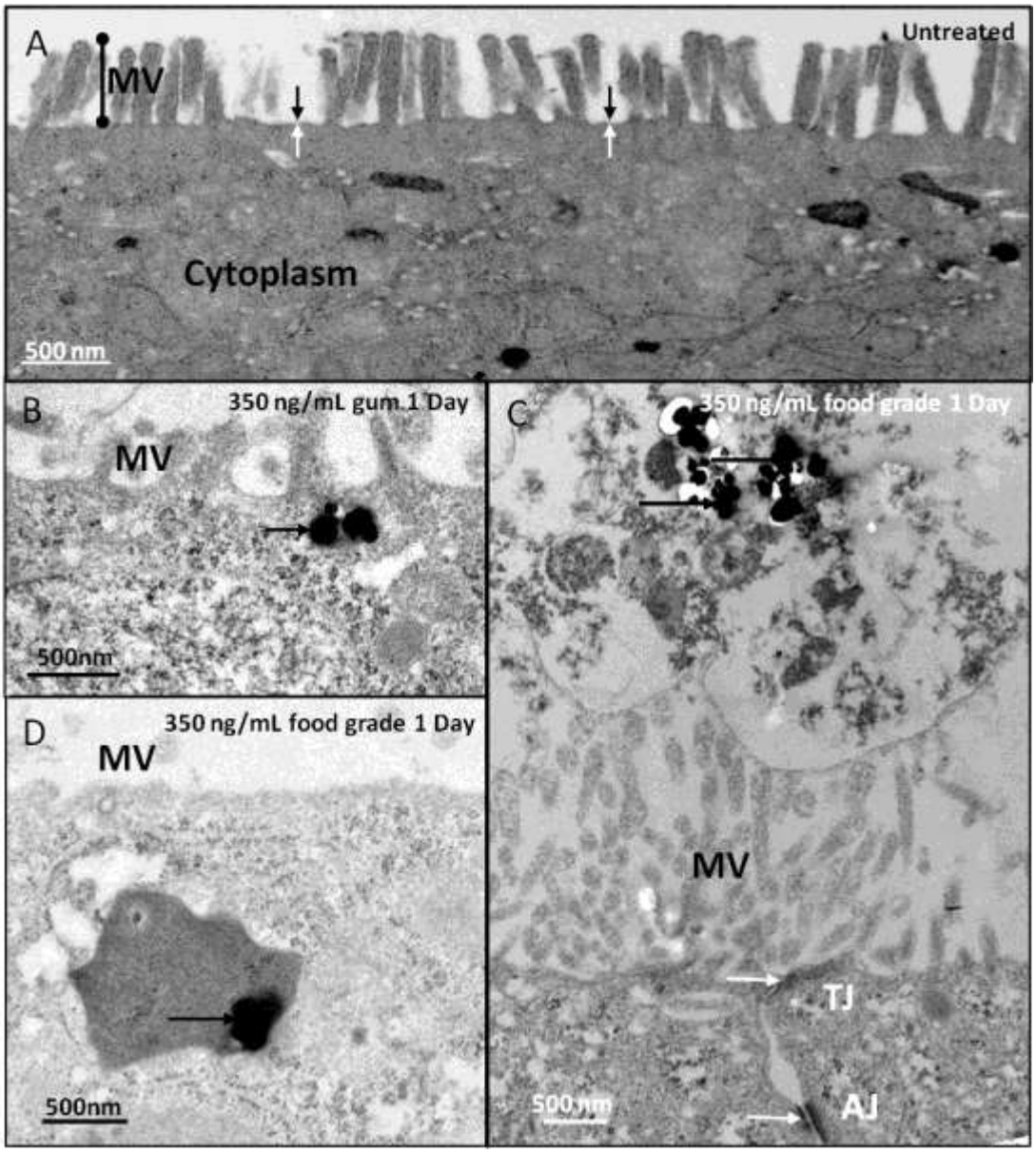

Figure 17. TEM analysis indicates that the TiO_2 was internalized as early as 1 day after exposure to 350 ng/mL of TiO_2. (A) Untreated, control specimens showed apical differentiations (i.e., brush borders), an electron-dense terminal web region, and an organelle-free zone. The microvilli appear numerous and well-ordered. The black and white arrows point to the plasma membrane of the cell. (B) Exposure to 350 ng/mL gum-TiO_2 after 1 day resulted in internalization of the TiO_2, and limp microvilli. The black arrow points to the electron-dense TiO_2. (C) Exposure to 350 ng/mL food grade TiO_2 after 1 day resulted in a subset of TiO_2 found enmeshed within an amorphous network at the tops of some cells. The microvilli were disorganized. However, tight- and adherens junctions were seen (pointed to by the white arrows). (D) Exposure to 350 ng/mL food grade TiO_2 after 1 day also showed that the TiO_2 was internalized. The black arrow points to the TiO_2.

CHAPTER 5
ALPHA-FE2O3 ELICITS DIAMETER-DEPENDENT EFFECTS DURING EXPOSURE TO AN IN VITRO MODEL OF THE HUMAN PLACENTA

Introduction

Ferric oxide nanoparticles (NPs) stand at the cornerstone of molecular imaging (Amstad, Textor, & Reimhult, 2011; Kievit & Zhang, 2011) water remediation (Guo, Stüben, & Berner, 2007; Westerhoff, Zhang, Crittenden, & Chen, 2008), and industry (Wu, Yin, Zhu, OuYang, & Xie, 2006; Zhou, Kotru, & Pandey, 2002) due to the unique physico-chemical properties on the nanoscale (10^{-9} m) compared to their bulk forms. In this work NP is defined on the basis of material diameter. Iron oxide NPs are commonly synthesized as crystals of α-Fe_2O_3, γ-Fe_2O_3, or Fe_3O_4 depending on their intended use. Furthermore, synthesis of small (e.g., <20nm in diameter) iron oxide NPs such as γ-Fe_2O_3 result in production of superparamagnetic NPs, whereas those diameters synthesized >20nm are antiferromagnetic (Ajay Kumar Gupta & Gupta, 2005; A. K. Gupta, Naregalkar, Vaidya, & Gupta, 2007; Kievit & Zhang, 2011; Wahajuddin, 2012). This transition in diameter concomitant to a change in magnetism is underscored by the fact that these small diameters can be employed as a contrast agent during magnetic resonance imaging. In water systems, α-Fe_2O_3 NPs serve as sorbents for groundwater remediation (Blowes, Ptacek, & Jambor, 1997). Furthermore, in these water systems α-Fe_2O_3 NPs were shown to be stable (He, Wan, & Tokunaga, 2008; W. Zhang, Crittenden, Li, & Chen, 2012; Y. Zhang, Chen, Westerhoff, Hristovski, & Crittenden, 2008). This investigation employed a model iron oxide NP, α-Fe_2O_3, whose physico-chemical parameters are well defined in the literature (He et al., 2008), and whose primary particle diameter can be controlled during synthesis (W. Zhang, Hughes, & Chen, 2012; W. Zhang et al., 2010). Previous studies conducted in the Caco-2 cell model indicate that

adsorption of α-Fe_2O_3 NPs is diameter-dependent (W. Zhang et al., 2010). For these reasons the effects of exposure to α-Fe_2O_3 were subsequently assessed after exposure to an *in vitro* model of human cytotrophoblasts, the cell barrier that interfaces maternal and fetal circulation in the placenta.

In eutherian mammals including humans, development of the fetus occurs inside the uterus of the mother. After fertilization the embryo hatches from a glycoprotein rich matrix known as the zona pellucida and implants into the endometrial stroma of the mother (Aplin, 1996). The first primitive epithelium of the embryo is known as the trophectoderm and later differentiation of the tissues takes place to form a placenta. The placenta parasitizes the circulatory system of the mother to supply the fetus with nutrients (Pijnenborg, 1990). In humans the direct interface of the maternal blood supply with the embryo is a cell layer of cytotrophoblasts referred to as a syncytiotrophoblast. This single cell layer is underlain by cytotrophoblasts, basement membrane, and fetal capillaries which provide for a number of essential functions required for normal pregnancy including: nutrient and metabolite transport, immune function, gas exchange, and clearance of fetal waste and toxins (B. F. King, 1992).

Due to the ethical limitations surrounding the use of, and availability of human tissues, investigators have relied on immortalized cell lines in order to study *in vitro* events such as implantation (Denker, 1993; Grummer, Hohn, Mareel, & Denker, 1994; Hannan, Paiva, Dimitriadis, & Salamonsen, 2010; John, Linke, & Denker, 1993; Mardon, Grewal, & Mills, 2007), syncytialization (Wice, Menton, Geuze, & Schwartz, 1990), drug, nutrient, oxygen (Bode et al., 2006; Morck et al., 2010; Rytting & Audus, 2005, 2007), and NP transport (Cartwright et al., 2012; Kulvietis, Zalgeviciene, Didziapetriene, & Rotomskis, 2011). The BeWo b30 cell line can be employed for these tasks and was subcloned from the parental cell line (b30 is hereafter referred to as BeWo; Pattillo &

Gey, 1968) to more closely resemble that of an *in vivo* trophoblast cell (van der Ende, du Maine, Schwartz, & Strous, 1990; van der Ende, du Maine, Simmons, Schwartz, & Strous, 1987). While a number of studies have employed the BeWo model to assess the toxicity and transport of a variety of NPs, to our knowledge there has yet to be a study assessing the potential effects of α-Fe_2O_3 NPs and a model for the human placenta (Menezes, Malek, & A Keelan, 2011; Pietroiusti, Campagnolo, & Fadeel, 2012; Saunders, 2009). Furthermore, the body of literature related to NP transport and toxicity during early fetal development remains ill-defined.

In a seminal study by Semmler-Behnke, et al., (2007) it was shown that gold NPs can cross the placental barrier in rats after maternal intravenous or intratracheal administration and these NPs were found in fetal target organs (Semmler-Behnke et al., 2007; Semmler‐Behnke et al., 2008). Studies conducted employing the mouse model through the combined use of inductively coupled plasma-mass spectroscopy (ICP-MS) and transmission electron microscopy (TEM) clearly demonstrated that NPs are found in the placenta, liver, and brain of developing pups after NP (SiO_2/TiO_2) administration through the maternal tail vein (Yamashita et al., 2011). Subcutaneous injection of TiO_2 NPs has been shown to cross the placenta and damage the genital and nervous system of developing pups (Takeda et al., 2009). Furthermore, studies employing the BeWo cell model demonstrated that fluorescent polystyrene NPs cross the placenta in a diameter-dependent fashion (Cartwright et al., 2012), NPs were able to induce DNA damage across BeWo epithelial barrier (Bhabra et al., 2009), and this was subsequently found to be dependent on the barrier thickness (Huppertz, 2011; Sood et al., 2011). For these reasons this study assessed the effects of a well characterized NP, α-Fe_2O_3, in the BeWo cell model in order to define the potential toxicity of these NPs in an *in vitro* model of the human placenta.

In this study it was hypothesized that α-Fe_2O_3 NPs would have diameter-dependent effects upon *in vitro* exposure to a model human placental epithelium. If α-Fe_2O_3 NPs have diameter-dependent effects on the epithelium, then a number of predictions follow; 1) Transepithelial electrical resistance (TEER) as a monitor of epithelia intactness will report differences in epithelial integrity after exposure to NPs of different diameters; 2) Cellular viability as measured by Live/Dead® analysis and reactive oxygen species production will be directly influenced by the diameter of the NPs; 3) Junctional integrity of the epithelium will be directly influenced by the diameter of the NPs; 4) Morphological differences will accrue as a result of the diameter of the NP employed; 5) Genotoxicity will be influenced by the NP diameter.

Materials and Methods

Synthesis of α-Fe_2O_3 NPs.

All α-Fe_2O_3 NPs were synthesized by Dr. Wen Zhang in the laboratory of Dr. Chen at Georgia Institute of Technology according to the method of Penners and Koopal (1986). Briefly, 20 mM $FeCl_3$ in 4 mM HCl solution was incubated at 100 ± 0.1°C in a forced-convection oven. Different diameters of α-Fe_2O_3 NPs were obtained at different incubation times of approximately 30 min, 5 hrs, and 8 hrs for the three sizes (15, 50, and 78 nm) used in this study. The suspension was centrifuged (Eppendorf centrifuge 5430R, Germany) at 5000×g for 30 min, and the supernatant was discarded. The concentrated α-Fe_2O_3 NPs were stored in deionized (DI) water (Millipore, >18.2 MΩ) at pH 4 ± 0.1 adjusted by hydrochloride acid.

The morphology and particle diameters were examined with a Philips CM-12 TEM operating at an accelerating voltage of 80 kV. Hydrodynamic diameters of α-Fe_2O_3 NPs dispersed in DI water or culture media were determined by a dynamic light scattering (DLS) instrument (Malvern Instruments, Zetasizer Nano, ZS instrument). The

concentration of α-Fe_2O_3 NPs in suspension was determined by an Induced Coupled Plasma-Optical Emission Spectrometry (ICP-OES, Thermo iCAP 6300, USA). The concentration of α-Fe_2O_3 NPs was expressed mg/L of ferric ion.

Cell Culture.

BeWo (b30) cells were obtained from Dr. Erik Rytting (UTMB, Galveston, TX), and used with permission from Dr. Alan Schwartz. Cells were maintained in T-75 flasks (Corning, Manassas, VA) coated with 50 μg/mL human placenta collagen (Sigma Aldrich, St. Louis, MO) as described elsewhere (Bode et al., 2006). Briefly, culture medium was replenished daily with DMEM:F-12 containing 1% antibiotics (10,000 IU/mL penicillin/ 10,000 μg/mL streptomycin/ 25 μg/mL amphotericin B; Cellgro, Manassas, VA), and 15% fetal bovine serum (Atlanta Biological, Lawrenceville, GA), and incubated in a humidified chamber of 5% CO_2 in air at 37°C. Upon 80% confluence, the cells were subcultured at a 1:10 dilution. Subculturing was accomplished by briefly incubating the cells in Ca^{2+}/Mg^{2+}-free phosphate buffered saline (PBS), followed by a 5 minute incubation in 0.25% trypsin/2.21 mM EDTA in Hanks Balanced Salt Solution (Cellgro, Manassas, VA) until the cells were no longer adherent to the culture plastic as assessed by phase contrast microscopy. The trypsin was neutralized, removed, and the cells were resuspended to the appropriate cell dilution.

NP-containing medium was prepared as described by Koeneman and coworkers (Koeneman et al., 2010). Briefly, water-soluble α-Fe_2O_3 at a stock concentration of no less than 2000 mg/L was sonicated with a Fisher Scientific model 100 probe sonic dismembrator at the maximum setting of 28 watts (RMS) for no less than 2 minutes. After applying the NPs to the appropriate volume of medium required to obtain the final working concentration, a second round of sonication, prior to exposure to epithelia was performed according to the aforementioned settings. All NP concentrations used in this

study were calibrated to equal the concentration employed during TEER analysis depending on the area of the culture vessel (i.e. 33 μg/mm² = 100 μg/mL in a Transwell® insert).

Transepithelial electrical resistance.

Cells were grown on collagen-coated, 0.4 μm pore, 6.5 mm Transwell® Inserts (Corning, Manassas, VA) and allowed to grow until an intact monolayer formed as described elsewhere (Cartwright et al., 2012). Typically the monolayer, and TEER is established 3 days post-seeding (Cartwright et al., 2012) and this timepoint was used in all experiments reported in this study as "day 0," and the values obtained were in agreement with recent reports (Li, van Ravenzwaay, Rietjens, & Louisse, 2013). Before measurements were taken, the 24-well plate was set in the dark on an air curtain for 15 minutes to equilibrate to room temperature. A thermometer was placed in blank well containing 1.5 mL of medium, and only after the medium was room temperature were the measurements taken. Measurements were consistently taken in order. Three different measurements were taken from each insert and averaged. TEER measurements were conducted with an EVOM (World Precision Instruments, Inc., Sarasota, FL) and TPX2 "chopstick" electrodes (World Precision Instruments Inc., Sarasota, FL). Resistance was assessed only after the electrode was calibrated with a CaliCell (World Precision Instruments, Inc., Sarasota, FL) to ensure accurate readings. Background resistance was measured by employing a blank inserts (n=3) with medium only and no cells. TEER is calculated from the following equation:

$$R_{\text{TEER}} = [R_C - R_B] \text{ X } A \quad (1)$$

Where R_{TEER} is the transepithelial electrical resistance represented in Ω cm²; R_C is the resistance of the cells in Ω; R_B is the resistance of the blank (Ω); and A is the surface area of the membrane insert (cm²). There were several populations of "blanks" depending on

the experiment; however, control blanks are defined as inserts containing no cells bathed in 300 μL of medium in the apical chamber and 1 mL of medium in the basal chamber. For experiments assessing TEER for NP-treated epithelia, the blank is redefined as an insert containing no cells, but incubated with medium containing the total working concentration of the nanomaterial at a consistent volume in the apical chamber as described earlier in the text (i.e. 300 μL at x μg/mL NPs), and with 1 mL of medium containing no NPs in the basal chamber. In each case, no fewer than 3 blank inserts were averaged to obtain the "blank" resistance required to calculate TEER values. All TEER values were normalized to percent TEER based on the average percent of the epithelia for 3 consecutive days prior to NP application. NP containing medium was applied once at day 0 to the apical chamber alone. Each insert received the same amount of medium; The apical chamber contained 300 uL and the basal chamber contained 1 mL of culture medium. Cell culture medium was replenished every 24 hours. Each experiment was repeated at least 3 times where (n=3).

ROS analysis.

BeWo cells were seeded on human placenta collagen-coated glass bottom dishes (Sigma Aldrich, St. Louis, MO; MatTek, Ashland, MA) and grown for 3 days corresponding to the maximal TEER as described in the sections in the above text (i.e. the "day 0" timepoint). The cell permeate reactive oxygen species indicator, H_2DCFDA (Molecular Probes; D-399) with aid from 0.02% Pluronic F-127, was bath-applied to the epithelia. Once the reduced fluorescein derivative enters the cell, esterases can cleave acetate groups and the probe can be oxidized by ROS. Upon oxidation H_2DCFDA is converted to 2',7'-dicholorofluorescein and exhibits a bright green fluorescence. This cocktail was applied to epithelia for 30 minutes in a humified incubator, subsequently washed several times in pre-equilibrated Ca^{2+}/Mg^{2+}-containing PBS (37°C), and imaged

as detailed in the preceding text. A positive control for reactive oxygen species was employed by applying 5 μM H_2O_2 in standard cell culture medium overnight (8 hrs) and later assessing fluorescent cells. No fewer than 5 randomly chosen fields of view were imaged and the entire field of view scored for fluorescence in each specimen. Each experiment was repeated 3 times where (n=3).

Live/dead analysis.

The live/dead cytotoxicity assay (Molecular Probes; L-3224) was used to identify dead cells. Briefly, the red-fluorescent ethidium homodimer-1 is excluded by intact cells indicative of cell viability. However, when membrane integrity is compromised during cellular death, ethidium binds to nuclear DNA and undergoes an increase in intensity (40-fold increase in fluorescence; Gaugain et al., 1978). Thus, cells that are dead have intense nuclear fluorescence. To indentify dead cells in the epithelium, BeWo cells were seeded on human placenta collagen-coated glass bottom dishes (MatTek, Ashland, MA) until confluence. Ethidium was made 10 μM in standard culture medium and the cells were incubated for 40 minutes in a humified chamber at 37°C. The cells were subsequently washed in Ca^{2+}/Mg^{2+}-containing PBS to remove any unbound ethidium, standard culture medium was replaced, and the plates were immediately imaged in the dark on a Nikon Eclipse TE300 inverted microscope equipped with a stage warmer and a Hamamatsu Orca CCD camera. Each experiment was repeated 3 times where (n=3).

Transmission electron microscopy.

All reagents and materials were purchased from Electron Microscopy Sciences (Hatfield, PA) unless otherwise indicated. In all cases describing cytological fixation, EM grade formaldehyde and glutaraldehyde were opened and used fresh from vials stored under N_2 gas. Cells were seeded on collagen-coated aclar and cultured as described in the preceding text. To obtain resin-embedded monolayers, the cells were cytologically fixed

for 2 hours in sodium cacodylate buffer (pH 7.2) made 2% with formaldehyde/2% glutaraldehyde. The specimens were washed extensively to remove the excess fixative and subsequently post-fixed in 1% OsO_4 for 1 hour in the dark at room temperature. After extensive washes in Nanopure™ water, the cells were incubated overnight in 0.5% uranyl acetate in Nanopure™ water at 4°C. Specimens were dehydrated in an increasing graded series of ethanol and infiltrated with Spur's embedding medium and polymerized overnight at 60°C. Seventy nanometer sections (corresponding to silver interference patterns) were cut on a Leica Ultracut E equipped with a diamond knife (Diatome, Hatfield, PA), and collected on formvar-coated, carbon-stabilized copper grids. The section-containing grids were stained with uranyl acetate and Sato's lead citrate, allowed to air dry overnight, and imaged on a Phillips CM-12 TEM fitted with a Gatan 791 CCD camera.

Scanning electron microscopy.

Poly-D-lysine -coated cover slips were purchased (BD Bioscience, San Jose, CA) and subsequently coated with human placenta collagen at 5 μg/cm^2. The cover slips were extensively washed in PBS and BeWo cells were seeded at 4x10^5 cells/mL. Epithelia were washed briefly with PBS and cytologically fixed for 30 minutes in 100 mM sodium cacodylate buffer (pH 7.2) made 2% formaldehyde/2% glutaraldehyde at room temperature. Specimens were washed through several changes of sodium cacodylate buffer (pH 7.2) and post-fixed in 1% OsO_4 for 60 minutes in the dark. Following post-fixation, the epithelia were washed with Nanopure™ water and dehydrated in an increasing graded ethanol series. Samples were dried through the critical point of CO_2 (Balzers), mounted on aluminum stubs, and sputter coated with approximately 5 nm of palladium-gold in a vacuum (Technicks Hummer II). Images were collected on a JOEL

JSM-6300 scanning electron microscopy equipped with an IXRF digital imaging system. Each experiment was repeated a minimum of 4 times (n=4)

Cytochalasin D treatment to prevent actin-mediated endocytosis.

Cytochalasin D binds to g-actin and prevents f-actin formation and subsequent actin-mediated endocytosis. Cytochalasin D was purchased from Sigma Aldrich and made 10 mM in cell culture tested dimethylsulfoxide (ATCC). This stock dilution was stored at -20°C in 10 μL aliquots and thawed just prior to use. Prior to NP treatment, a dose response analysis (unpublished data) for Cytochalasin D was conducted and it was found that application of 1 μM Cytochalasin D 30 minutes prior to, and during the duration of NP incubation (≥8 hours) resulted in a loss of f-actin, but maintained cellular viability. The final working concentration of 1 μM was employed in all subsequent studies.

Immunocytochemistry.

Unless otherwise stated, all reagents used for immunocytochemistry were purchased from Sigma Aldrich (St. Louis, MO). Confluent epithelia were treated and maintained as replicate samples at their respective time points. The epithelia were briefly washed in PBS equilibrated to 37°C, and subsequently cytologically fixed in 100mM PBS made 2% with formaldehyde prepared fresh from paraformaldehyde for 30 minutes at room temperature. Epithelia were permeabilized with an intracellular buffer (ICB) made 2% with formaldehyde and 0.1% Triton X-100 for 30 minutes at room temperature in the dark. ICB contains the following: 100 mM KCl, 5 mM $MgCl_2$, and 20 mM HEPES™ (pH 6.8). The epithelia were washed 3 times for 15 minutes per wash in ICB made 1% with bovine serum albumin (ICB-BSA) at room temperature. After this blocking step, the primary antibody (anti-ZO-1, Invitrogen ZO1-1A12; formerly from Zymed) was applied at a 1:500 dilution in an antibody dilution buffer (ICB modified to

contain 0.1% Tween-20 and 1% non-fat dry milk) and incubated overnight at 4°C. The following day the epithelia were washed 3 times for 15 minutes each in ICB-BSA. The fluorophore-conjugated secondary antibody used in this study, which permitted visualization of the primary antibody, was goat-anti-mouse Alexa-488. The secondary antibody was used at a 1:500 dilution in antibody dilution buffer and incubated overnight at 4°C. The following day the epithelia were washed 3 times for 15 minutes each in ICB. Visualization of the nuclei was accomplished by employing DAPI (Molecular Probes) diluted in ICB for 15 minutes. The cover slips were subsequently mounted on slides in drops of Vectashield (Vector Labs) and sealed with optically clear nail polish. Images were collected with a Leica SP5 laser scanning confocal microscope housed in the W.M. Keck Bioimaging Facility at Arizona State University. The images represent 0.4 μm optical Z-sections obtained through the entire volume of the cells for confocal analysis. Optical sections were reconstructed using Leica Imaging Software to represent a maximum projection image. The images shown are representative of 4 independent experiments where n=3.

Microarray analysis.

mRNA isolation.

All plastic cultureware employed during microarray analysis was certified as "Nuclease-free." Messenger RNA (message) was isolation by the Purelink® RNA method (Ambion) according to the manufacturer's instructions. Briefly, 3 confluent 60 mm^2 culture plates for each condition (i.e. untreated, 15 nm treated and 78 nm treated) for a total of 9 plates were washed in ice-cold PBS, scrapped, at the respective times, with a rubber policeman and collected in ice-cold PBS. PBS was removed, replaced with lysis buffer, and mechanically disrupted with 5 strokes of a Dounce homogenizer. Message

was subsequently isolated on membranes and eluted into collection tubes through the use of TE buffer. RNA was stored in a mechanical freezer at -80°C until use.

aRNA amplification and microarray analysis.

Messenger RNA was thawed on ice and analyzed for total RNA content with a Nanodrop™ spectrophotometer. RNA was aliquotted into non-stick PCR tubes at a total concentration of 1000 ng per tube. Reverse transcription "master mix" was prepared and DNA was transcribed in a hybridization oven at 42°C for 2 hours. Complementary DNA (cDNA) was subsequently prepared at 16°C for 2 hours. The cDNA was purified and transcribed into amino allyl RNA. The aRNA was purified and the yield was assessed. Depending on the specimen Alexa-fluor 555 or Alexa-fluor 647 was coupled to the aRNA, the former representing the untreated specimens, while the latter represents the NP-treated specimens. Dye-coupled aRNA was purified, fragmented and equal concentrations of untreated and treated aRNA was pooled. The samples were subsequently hybridized on Agilent Human 4x44K arrays at 60°C for 16 hours, scanned, and analyzed with GeneSpring (Agilent Technologies, Inc., Santa Clara, CA). Data represent biological replicates conducted on the same day.

Q-PRC analysis.

The same mRNA that was employed for microarray analysis was used to confirm relative fold-changes for the *CASP8* and *TNFR12A* genes. Reverse transcription was accomplished with the qScript cDNA synthesis kit according to the manufacturer's instructions (Quanta Biosciences, Gaithersburg, MD). This cDNA was used as a template for quantative PCR analysis through the use of Brilliant III CYBR® Green (Agilent Technologies, Inc., Santa Clara, CA). Briefly, equal amount of template were amplified and fluorescence was monitored and analyzed by the ΔΔCt method (Livak & Schmittgen 2001). The housekeeping gene, *TUBA1A*, which encodes the protein α-

tubulin, was used to normalize data. The *CASP8* amplicon was generated with primers corresponding to the forward: CAGTGAAGATCTGGCCTCCC and reverse: TGCGGAATGTAGTCCAGGCT sequences. The *TNFR12A* gene product was amplified with forward AAGGAACTGCAGCATTTGCA and reverse CCTCTAGGAAGGAGGGCACC primers according to the manufacturer's recommendations (Integrated DNA Technologies, San Diego, CA). Data represent biological replicates conducted on the same day. Error is shown as mean±SD.

Data analysis.

In this manuscript an independent experiment is defined as 3 or more technical replicates conducted on the same day. Unless otherwise stated, all data represent at least 3 independent experiments conducted on different days. Student's t-test was performed through the use of GraphPad software and a p value of ≤0.05 was considered statistically significant. Error was calculated in Excel and is shown as mean±SEM. In some cases error bars appear smaller than the data point marker. All comparisons are made between untreated and NP-treated epithelia at their respective time points unless otherwise indicated.

Microarray data was analyzed through the use of GeneSpring and the data appears as 3 biological replicates conducted on the same day. Only those genes that whose change represented p ≤0.05 were considered for subsequent analysis. Quantitative PCR analysis was conducted on the same day as 3 technical replicates. Both microarray and QPCR are shown as mean±SD.

Results

Large, but not small, non-functionalized α-Fe_2O_3 NPs disrupt BeWo epithelial integrity.

If a population of NPs exist that exhibit diameter-dependent effects, it is anticipated that gross alterations in epithelia integrity will occur after exposure to NPs of different diameters. In order to test this, three different mean diameters of α-Fe_2O_3 NPs (small NPs defined as 15, and the large diameter NPs as 50, and 78 nm) were synthesized and subsequently employed, and each group displayed a narrow hydrodynamic diameter (Table 3). Diameters were confirmed by transmission electron microscopy (TEM; Figure 18) each exhibiting a homogenous, colloidal NP population for each diameter tested. The physicochemical parameters of these particles have been extensively characterized elsewhere (He et al., 2008; Madhavi Kalive et al., 2012; W. Zhang, J. Hughes, et al., 2012; W. Zhang et al., 2010), but briefly, a change in ζ-potential from positive to net negative as a result of incubation in medium containing supplements (i.e., fetal bovine serum and antibiotics) was observed as might be expected due to NP adsorption of serum components and/or the ionic strength of the culture medium (Ehrenberg, Friedman, Finkelstein, Oberdörster, & McGrath, 2009; Kreuter, 1994; Maiorano et al., 2010).

As predicted, application of different NP populations (i.e., the small diameter of 15, and large diameters of 50, and 78 nm) resulted in significant changes in transepithelial electrical resistance (TEER) at a consistent mass concentration of 100 μg/mL (i.e. 33 μg/mm^2) for each diameter tested (Figure 19 A; see also Appendix, Supplemental Figure 1 A). The mass concentration of 100 μg/mL was employed as a starting point since data concerning human exposure is limited and the effects of iron oxide NPs on the placenta are heretofore undefined (Menezes et al., 2011; Saunders,

2009). Furthermore the concentration employed in this study is consistent with the concentrations employed in other studies (Buyukhatipoglu & Clyne, 2011; Madhavi Kalive et al., 2012), and during specialized imaging techniques (Mahmoudi et al., 2011; Mishra, Patel, & Tiwari, 2010). It was found that the initial disruption (i.e., drop in TEER) occurred at 24 hours after applying the NP-containing medium to the apical chamber of the Transwell® insert for large, but not small NPs. After 24 hours epithelia exposed to both large populations of NPs (i.e., 50, and 78 nm) continued to decrease in TEER until the 5 day endpoint. At the 5 day endpoint TEER was nearly half its original value for the epithelia exposed to large NPs. In contrast, it was found that both the untreated epithelia and those treated with 15 nm particles at a concentration of 100 μg/mL maintained a high TEER throughout the experiment. In order to determine if application of NPs results in a permanent decrease in TEER a wash experiment was performed and terminal data (5 day endpoint) were assessed. It was found that untreated specimens had a significant, albeit modest increase in TEER at the 5 day endpoint. In this study, untreated was defined as those epithelia not exposed to nanomaterials at any time. However, epithelia treated with 15- and 78-nm α-Fe_2O_3 NPs and washed before 12 hours resulted in no difference in TEER and a significant decrease in TEER, respectively (Figure 19 B). In the histogram the grey and white bars correspond to the 12 hour TEER value (grey bars) and the 5 day TEER endpoint value (white bars).

The dosimetry necessary to disrupt epithelial integrity for large NPs was subsequently assessed by titering down the concentration of 78 nm particles (Figure 19 C, D). It was found that exposure to 20-, but not 10 μg/mL concentrations of 78 nm NPs resulted in loss of TEER similar to the 100 μg/mL treated epithelia shown in Figure 19 A.

This no-loss in TEER scenario of exposure below a mass concentration of 10 μg/mL was confirmed for all other diameters of NPs (Figure 19 D; see also Supplemental Figure 1 B).

Large diameter nanoparticles evoke increased reactive oxygen species (ROS) and cell death.

In order to determine if the loss of epithelial integrity assessed as a change in TEER was due to cytotoxic mechanisms resulting in cell death, reactive oxygen species and subsequently cell death were investigated as a function of time. Under normal conditions (<10 cell per $1.4x10^5$ μm^2) BeWo epithelia contained very few cells positive for reactive oxygen species as measured over the $1.4x10^5$ μm^2 field of view in phase contrast, epifluorescent overlay micrographs (Figure 20 A, all micrographs are representative of $3.5x10^4$ μm^2). BeWo epithelia were stimulated to produce reactive oxygen by the addition of 5 μM H_2O_2 overnight (8 hrs) supplemented into culture medium (Figure 20 B). Under these conditions, as a positive control for ROS, approximately 150 cells were positive for reactive oxygen species as measured by fluorescence of 2',7'-dicholorofluorescein and this accounted for the majority of the total cells (220 cells per $1.4x10^5$ μm^2). At both 1- and 3-days post treatment, the small diameter NP population (Figure 20 C, D) was not found to elicit large numbers of cells positive for ROS. However, a statistically significant difference between untreated and the 15 nm, 100 μg/mL-treated epithelia 1 day after exposure was noted (Figure 20 I). Further, both 50- and 78-nm diameter NPs at a concentration of 100 μg/mL after 1- and 3-days in culture showed a significant increase in cells positive for ROS (Figure 20 E-I).

If large-diameter NPs result in an increase in ROS, it might be expected that cell death occurs subsequent to this event. Cellular viability was assessed through the use of ethidium homodimer-1. Ethidium is a cell-permeate probe, which upon nuclear-membrane disruption intercalates into DNA. Upon intercalation, ethidium undergoes a

40-fold increase in fluorescence, and this event can be monitored by an epifluorescent microscope. In this figure, $1.4x10^5$ μm^2 was analyzed per micrograph, whereas $3.5x10^4$ μm^2 was shown in order to permit adequate magnification. Under normal conditions, healthy BeWo epithelia at the 1 and 3 day time points analyzed as an area of $1.4x10^5$ μm^2 had very few dead cells (1±1, 10±3, respectively; Figure 21 A**,** all micrographs shown are representative of $3.5x10^4$ μm^2). Under conditions employed to assess maximal cell death, (a positive control for cellular death; saponin treatment), it was found that 217 ± 6 cells died (Figure 21 B). Notable differences were found between the small (15 nm) and large (50 and 78 nm) NP treatments at a concentration of 100 μg/mL; there appeared to be a diameter-dependent increase in cell death (Figure 21). After 1 and 3 days epithelia treated with 15 nm particles were not significantly different from untreated epithelia (Figure 21 C, I). However, at both the 1 and 3 day time points it was found that epithelia treated with 50 nm particles contained significantly more dead cells than untreated epithelia (Figure 21 E-F, I). Further, 78 nm treated epithelia also resulted in significantly more dead cells than untreated epithelia (Figure 21 G- I).

Large (78 nm) diameter α-Fe_2O_3 NPs disrupt intercellular tight junctions.

Epithelial leakiness, as evidenced by the decrease in TEER, suggested the possibility of disruption of intercellular junction integrity. In order to test the prediction that the tight junctions, that must exist to maintain TEER, were disrupted as a result of NP exposure, a laser-scanning confocal approach was employed. It is well accepted that the apical localization of the tight junction protein ZO-1 labels intercellular tight junctions as well as indicating terminal differentiation of the epithelium (Anderson et al., 1989; W. M. Bement, P. Forscher, & M. S. Mooseker, 1993; Matter, Aijaz, Tsapara, & Balda, 2005). Both the untreated and NP-treated specimens had a similar nuclear

organization as evidenced by emission of the nuclear probe 4',6-diamidino-2-phenylindole (DAPI; Figure 22 A, D). Analysis of the antibody to ZO-1 in untreated specimens demonstrated the conventional honeycomb arrangement of tight junctions surrounding each cell (Figure 22 B, C). However, after a 24 hour exposure to α-Fe_2O_3 at a concentration of 100 μg/mL ZO-1 was disrupted with breaks in the continuous distribution of ZO-1 surrounding each cell (Figure 22 E, F). In some areas indicated by the white arrows ZO-1 was found to be completely absent though underlying nuclei (blue) were seen (Figure 22 E, F). It was found that the 15 nm-treated specimens were similar to the untreated, normal distribution of ZO-1 (Appendix, Supplemental Figure 7).

The bulk of large (78nm) diameter α-Fe_2O_3 NPs internalize through actin-mediated endocytosis, and accumulate at different cellular planes of the z-axis as a function of time.

Epithelial leakiness, as evidenced by a decrease in TEER, suggested the possibility of disruption of intercellular junction integrity. In order to test this as well as to assess the intracellular NP localization a TEM approach was employed. Untreated BeWo epithelia contained moderately polarized cells. Each cell had an electron-dense cytoplasm with numerous membrane-bound vesicle and organelles (Figure 23 A). After 4 hours of incubation in NP-containing medium at a concentration of 100 μg/mL NPs were found internalizing apparently by a phagocytotic mechanism (Figure 23 B, C). Figure 23 B shows membrane invaginations (white arrows) engulfing agglomerated NPs, whereas Figure 23 C shows a similar event with NPs encapsulated in a vesicle (black arrows). Later, at the 8 hour time point (Figure 23 D, E) NPs appeared to sediment and collect at the plasma membrane interface (Figure 23 D). Further, at this time point NPs were found concentrated at the lateral margins between cells (Figure 23 E). At the 16 hour time point three distinct internalized populations of NPs were found (Figure 24);

That is, one population of large-diameter NPs was found enclosed within membrane bound vesicles (black arrows), another not membrane-bound (white arrows), and a third population seemed to be in a vesicle whose membrane appeared ruptured (white arrowheads; Figure 24).

If large-diameter NPs are internalized by an actin-based mechanism (i.e. phagocytosis, macropinocytosis), then inhibiting actin polymerization should result in loss or decrease of large-diameter NP internalization. To test this prediction the fungal toxin Cytochalasin D, which is known to inhibit actin-mediated endocytosis (Silverstein, Steinman, & Cohn, 1977) was employed during NP treatment. Figure 25 A illustrates a representative cell that was exposed to neither Cytochalasin D nor NPs. Electron dense membranes are distinguishable, and the actin based projections known as microvilli are seen. Figure 25 B indicated that NP agglomerates decorated the apical plasma membrane at 8 hours of NP incubation in combination with cytochalasin D incubation. However, after cytochalasin D inhibition there appeared to be a small amount of NPs inside the cell and it appeared as if these NPs were not surrounded by membrane (Figure 25 C, black arrows). At the 8 hour time point, and consistent with Figure 24 D, E, Figure 25 D shows a number of NPs internalized in cells not treated with Cytochalasin D.

Alpha-Fe_2O_3 NPs litter the apical brush-border and abolish the standing microvillar morphology.

TEM analysis demonstrated that these NPs sediment to the epithelial surface in bulk over time in cell culture medium at the 8 hour time point. If these large-diameter NPs result in effects that are deleterious to the cell, it might be expected that initial changes begin to occur at the cell-NP interface after NP touchdown. Thus, scanning electron microscopy (SEM) was employed to elucidate potential surface changes at this essential biological interface. In order to do this, a time-course experiment was

conducted with replicate samples at a concentration of 100 μg/mL using the 78 nm diameter as the model large NP. The scanning electron micrographs in Figure 26, A-C illustrate the untreated brush-border at the apical surface of BeWo cells at 1, 3, and 5 days respectively. Untreated, healthy BeWo cells had approximately 9 microvilli per square micrometer, and the number of microvilli appeared to extend to and remain at 11 microvilli per square micrometer over time (Figure 26 G). In contrast, micrographs of NP- treated epithelia (Figure 26, D-F) demonstrate a near complete effacement of the brush-border organization over the same time course. SEM analysis illustrated clusters of NPs littering the apical surface of BeWo epithelia (Figure 26, D-F, white arrow heads). After treatment with NPs, the total number of microvilli plummeted to fewer than 2 microvilli per square micrometer ($p<0.001$; Figure 26 G). Similar to the distribution of the untreated specimens, the number and morphology of the 15 nm treated specimens appeared to not be affected by exposure (Appendix, Supplemental Figure 8).

Large (78nm), but not small (15nm), α-Fe_2O_3 NPs elicit cellular changes at the level of the gene.

The experiments conducted in the aforementioned text indicate cellular changes as a result of NP exposure. In order to investigate the potential that α-Fe_2O_3 NPs evoke a response in gene expression a genome-wide DNA microarray approach was employed. Through the use of Agilent human 44K arrays, it was found that epithelia treated with 78 nm α-Fe_2O_3 at a mass concentration of 100 μg/mL for 72 hours resulted in statistically significant ($p\leq0.05$) changes in 799 genes. In contrast, epithelia treated with 15 nm α-Fe_2O_3 at a mass concentration of 100 μg/mL for 72 hours were found to have no statistically significant changes (Figure 27). In this study a fold-change cutoff of ±2.0 was selected consistent with other reports (Mutch, Berger, Mansourian, Rytz, & Roberts, 2002; Quackenbush, 2002). Concerning the 78 nm NP exposure, of the 799 genes that

were changed it was found that 589 genes were up regulated, and 210 genes were down regulated. Through the use of GeneSpring (Agilent) these numbers were narrowed and genes that potentially explain epithelial integrity were further interrogated. Down regulated genes (Table 4) included 2 broad categories: "Tight junctions," and "adherens junctions." It was found that claudin 19 was suppressed 4.82-fold, as well as a number of protocadherins which are known to be expressed during early development (Kokkinos, Murthi, Wafai, Thompson, & Newgreen, 2010; Rampon et al., 2008) had fold-changes ranged from -2 to -7. Up regulated genes (Table 5) included those involved in actin-binding (actin associated), the cytoskeleton, and apoptosis. It was found that the expression of α-actinin 1 and 3 were enhanced by 2.10 and 2.80, respectively. *CapZ* mRNA which encodes the actin filament capping protein was up regulated 5.80-fold. Three other actin associated genes were found up regulated from 3.65 – 4.62 and those include genes encoding dynamin, twinfilin, and tropomyosin. Gamma-actin was found up regulated 3.33-fold and Keratin 8 and 83 were 6.66 and 9.86-fold increased compared to untreated specimens, respectively. Twelve genes were found up regulated and associated with apoptosis and those include: Caspase 3 (2.80), caspase 8 (5.36), programmed cell death 6 (3.89), tumor necrosis factor (TNF) associated factor 2 (3.69), TNF receptor 5 (2.39), death associated protein (DAP; 4.59) TNF receptor 12A (2.88), foxo4 (4.16), heat shock protein 90 A (4.73) BCL2-like 1 (2.18) and death inducer-obliterator 1(3.06).

In keeping with the microarray analysis described in the preceding text, quantative-RT-PCR (QPCR) analysis demonstrated that *CASP8*, and *TNFRSF12A*, had similar expression (Figure 28).

Discussion

The principal finding in this study is that the diameter of a nanomaterial (α-Fe_2O_3) elicits differential effects ranging from lethal to almost no effect in an established model of the human placental epithelium based on the criteria described in the text below. This investigation showed that the large α-Fe_2O_3 NP diameters tested (50, and 78 nm) deleteriously affect this placental epithelium, while the small diameter NP (15 nm) exhibited relatively fewer effects in this model system within the context of points 1-4 described in the text below. This investigation clearly showed, through the use of four orthogonal techniques, that the epithelium was disrupted as a result of exposure to the large (78 nm), but not small (15 nm), α-Fe_2O_3 NP diameter: 1) TEER measurements as an indication of epithelial integrity (Claude, 1978; Hidalgo et al., 1989; Koeneman et al., 2009) indicated that large, but not small diameter α-Fe_2O_3 NPs disrupt the "intactness" of the epithelium; 2) At the protein level through the use of antibodies directed against ZO-1 it was shown that these α-Fe_2O_3 NPs disrupted the normal arrangement of ZO-1 for large, but not small α-Fe_2O_3 NPs; 3) The microarray analysis indicated gross changes in gene expression for large, but not small NPs; 4) Finally, ultrastructural and morphological changes were observed after exposure to large, but not small α-Fe_2O_3 NPs.

The trophoblast layer in eutherian mammals including humans forms the interface between the mother and the developing fetus (Saunders, 2009), and further acts as a selective physiological barrier (B. F. King, 1992). The data presented in this report suggest that there are two routes acting in concert to disrupt the barrier function of the epithelium. The first route of epithelial disruption can be attributed to a loss of the intercellular tight junctions. In this study it was shown that as early as 12 hours in culture, TEER begins to drop and this drop does not appear to be recoverable after exposure to large NPs. In addition, laser scanning confocal analysis demonstrated that

exposure to large, but not small NPs disrupted the normal arrangement of ZO-1, an established marker for tight junctions (Furuse et al., 1994; Stevenson, Siliciano, Mooseker, & Goodenough, 1986). Ultrastructural analysis indicated that NPs accumulate in the lateral margins between cells. Finally, at the mRNA level the claudin 19 gene whose protein product is known to bind ZO-1 and permit tight junction assembly (Lee et al., 2006), was down regulated ~5 fold. Debate has arisen within the scientific community as to the reliability of TEER measurements (Jovov, Wills, & Lewis, 1991; T. Mukherjee, Squillantea, Gillespieb, & Shao, 2004). In particular, a number of factors are known to affect TEER measurements. In this study, TEER was found to be similar in magnitude to those values reported elsewhere (Cartwright et al., 2012). Further, in this study the temperature was controlled for by equilibrating the epithelia to room temperature before conducting the measurements (see the TEER subheading in the Methods section for the experimental details). While much of this work was contingent on the interpretation of the TEER results, the orthogonal techniques of immunocytochemistry and TEM clearly supported these data. Indeed, during the initial drop in TEER ZO-1 localization as an indicator of tight junctions was found to be disrupted after exposure to the large diameter NP (78 nm; Figure 22). Furthermore, TEM analysis indicated that NP agglomerates (78 nm) were found distributed between the lateral margins of cells (Figure 23 D, E). Since TEER is effectively a measure of the integrity of the tight junctions (Blume, Denker, Gieseler, & Kunze, 2010), and the orthogonal techniques indicated a disruption of the tight junctions during the time there was a drop in TEER, these data are well supported.

An alternative route to disrupt the barrier function can be accredited to "holes" in the epithelium as a result of cell death. This study tested if the diameter of the α-Fe_2O_3 NP affects the viability of the epithelium and it was found that large, but not small α-

Fe_2O_3 NPs induced cell death as measured by ethidium-homodimer nuclear fluorescence at both 1 and 3 days of NP exposure. Cell death can be attributed to a number of mechanisms (Ellis, Yuan, & Horvitz, 1991), however evidence (described in the subsequent paragraph) was presented in this study to suggest that cell death is of the apoptosis variety. Concerning apoptosis two signaling mechanisms by which the cell can commit suicide exist (Fulda & Debatin, 2006; J. C. Reed, 2000; Thorburn, 2004). The extrinsic pathway can be stimulated by extracellular signaling ligands that bind to integral membrane death receptors (Nagata, 1997; Thorburn, 2004). This ligand-receptor interaction causes a conformational change in the protein and permits establishment of a molecular scaffold known as the death-inducing signaling complex (DISC; Thorburn, 2004). Caspase 8 is a molecular component of the DISC and upon its release from the DISC has the potential to activate the executioner caspase, caspase 3 (Fischer, Jänicke, & Schulze-Osthoff, 2003).

Genome-wide analysis through the use of DNA microarray employed during this study indicated that epithelia exposed to large diameter NPs (78nm) at the same concentration and exposure duration as the 15nm specimens elicited a statistically significant ($p \leq 0.05$; n=3) increase in the expression of these pro-apoptotic genes. Indeed, this study showed that those molecular components at the mRNA level are up regulated corresponding to the extrinsic pathway of cell induced apoptosis (Table 5). In addition, it was found that mRNA encoding two receptors of TNFα were up regulated as well as both caspase 8 and caspase 3. In contrast, it was found that there were no statistically significant changes in gene expression after exposure to the 15nm α-Fe_2O_3 NPs at a concentration of 100 μg/mL.

The data presented in this report shows that there are notable changes in the number of cells positive for reactive oxygen species after treatment with these NPs at

both 1 and 3 days post exposure. Moreover, it is a known phenomenon that NPs are able to "escape" endosomes (Verma & Stellacci, 2010). The transmission electron micrographs shown in this study appear to contain some agglomerated intracellular NPs that have no indication of electron-dense membranes surrounding the NPs. It is known that iron oxide NPs elicit the production of ROS and furthermore rupture of the lysosome as might be the case for the apparently non-membrane bound NPs found in this study (Buyukhatipoglu & Clyne, 2011). This increase in intracellular ROS could "jumpstart" a signaling cascade for apoptosis.

Apoptosis is not the only effect of NPs on cells. Subtle effects of NPs on the biology of the cells and tissues have also been reported. The first paper to describe what was then referred to as "subtle" effects of NP exposure demonstrated that NPs (a 70/30% mixture of rutile and anatase TiO_2) efface the brush-border of intestinal enterocytes *in vitro* in a dose-dependent manner (J. J. Faust et al., 2012; Koeneman et al., 2010). Subsequent studies employing α-Fe_2O_3 NPs by Zhang et al (2010) and later Kalive et al (2012) at concentrations ranging from 1-300 μg/mL showed a similar microvillar disruption as a result of NP exposure (Madhavi Kalive et al., 2012; W. Zhang et al., 2010). In the present study a number of structural proteins related to actin bundling (tropomyosin and α-actinin) were found to be upregulated after exposure to large NPs. Furthermore the actin capping protein CapZ, which is a known constituent of the apical region of the microvillus in placental cells (Heintzelman, Hasson, & Mooseker, 1994), was found to have a 5-fold increase in mRNA expression in the present study. This apical region referred to as the plus-tips of the microvillus appears in electron micrographs as an electron dense region and was shown to be the organization center from which microfilaments emanate during morphogenesis (Berryman, Gary, & Bretscher, 1995; Mooseker, 1985). These data indicate a change in the normal actin-

bundling properties of the trophoblast epithelium and suggest that at the mRNA level actin capping as a means to promote actin disassembly may be the mechanism driving the loss of microvilli in this cell system at the protein level.

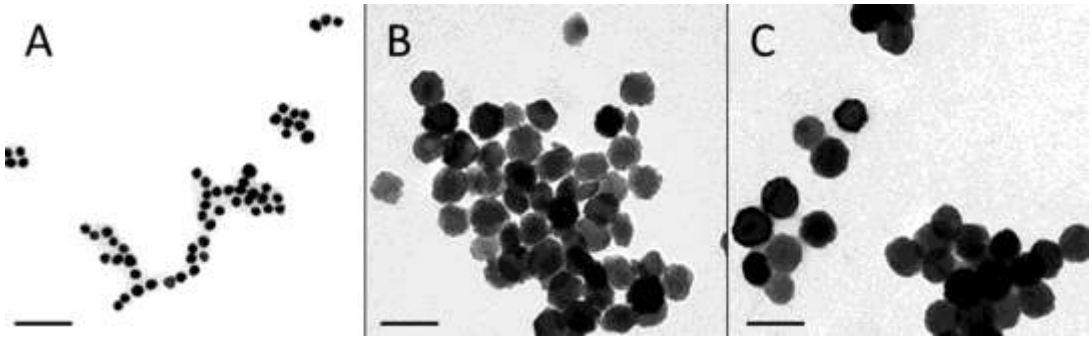

Figure 18. TEM analysis of α-Fe_2O_3 NPs. TEM demonstrates a narrow distribution of the primary particle diameter for the nanomaterial employed in this study. (A) is the 15 nm NPs. (B) is the 50nm diameter and (C) is the 78 nm diameter. The scale bar is 100 nm.

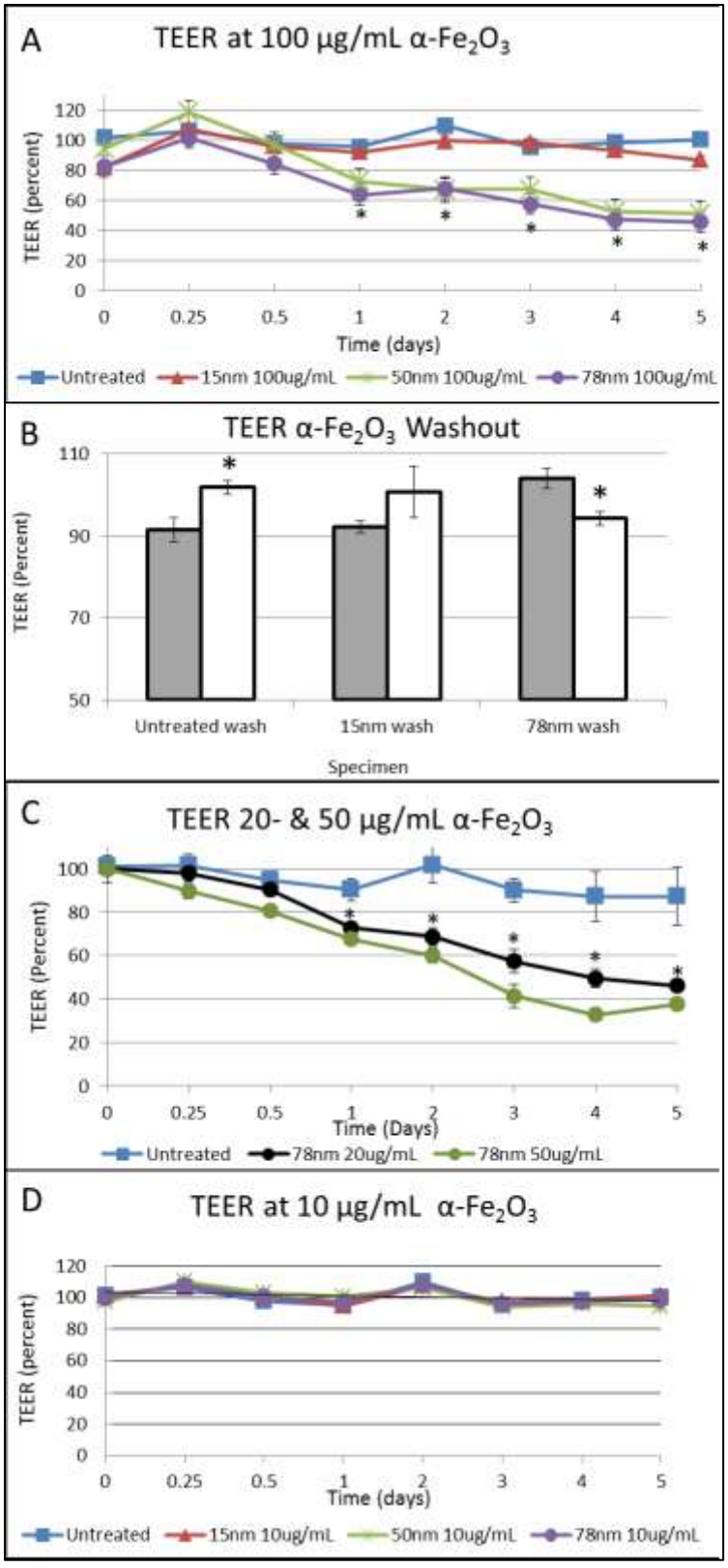
A
TEER at 100 µg/mL α-Fe2O3
TEER (percent)
Time (days)
Untreated
15nm 100ug/mL
50nm 100ug/mL
78nm 100ug/mL
B
TEER α-Fe2O3 Washout
TEER (Percent)
Untreated wash
15nm wash
78nm wash
Specimen
C
TEER 20- & 50 µg/mL α-Fe2O3
TEER (Percent)
Time (Days)
Untreated
78nm 20ug/mL
78nm 50ug/mL
D
TEER at 10 µg/mL α-Fe2O3
TEER (percent)
Time (days)
Untreated
15nm 10ug/mL
50nm 10ug/mL
78nm 10ug/mL

*Figure 19***.** TEER disruption is NP diameter- as well as concentration dependent. (A) The graph illustrates the change in TEER after application of different diameters of α-Fe_2O_3 at a concentration of 100 µg/mL. Both 50- and 78 nm NP treated epithelia follow the same trend, whereas the 15nm diameter exposure followed the trend of the untreated specimens. (B) Epithelial exposure to large-diameter NPs do not recover at the 5 day endpoint. The 12 hour TEER value is shown in grey and the 5 day endpoint value shown in white. (C) Application of 78 nm α-Fe_2O_3 at a mass concentration of 50- and 20 µg/mL appears to disrupt TEER. (D) Exposure to 10 µg/mL for all α-Fe_2O_3 diameters tested results in no change compared to the untreated specimens. As indicated in the Methods section, TEER levels off at its maximum value of 40 Ωcm^2 3 days after seeding BeWo cells. The NPs were applied after this 3 day culture period which is denoted as t=0 in the graphs. All experiments were conducted at least 3 independent times where n=3; error bars appear smaller than the data point marker for some points.

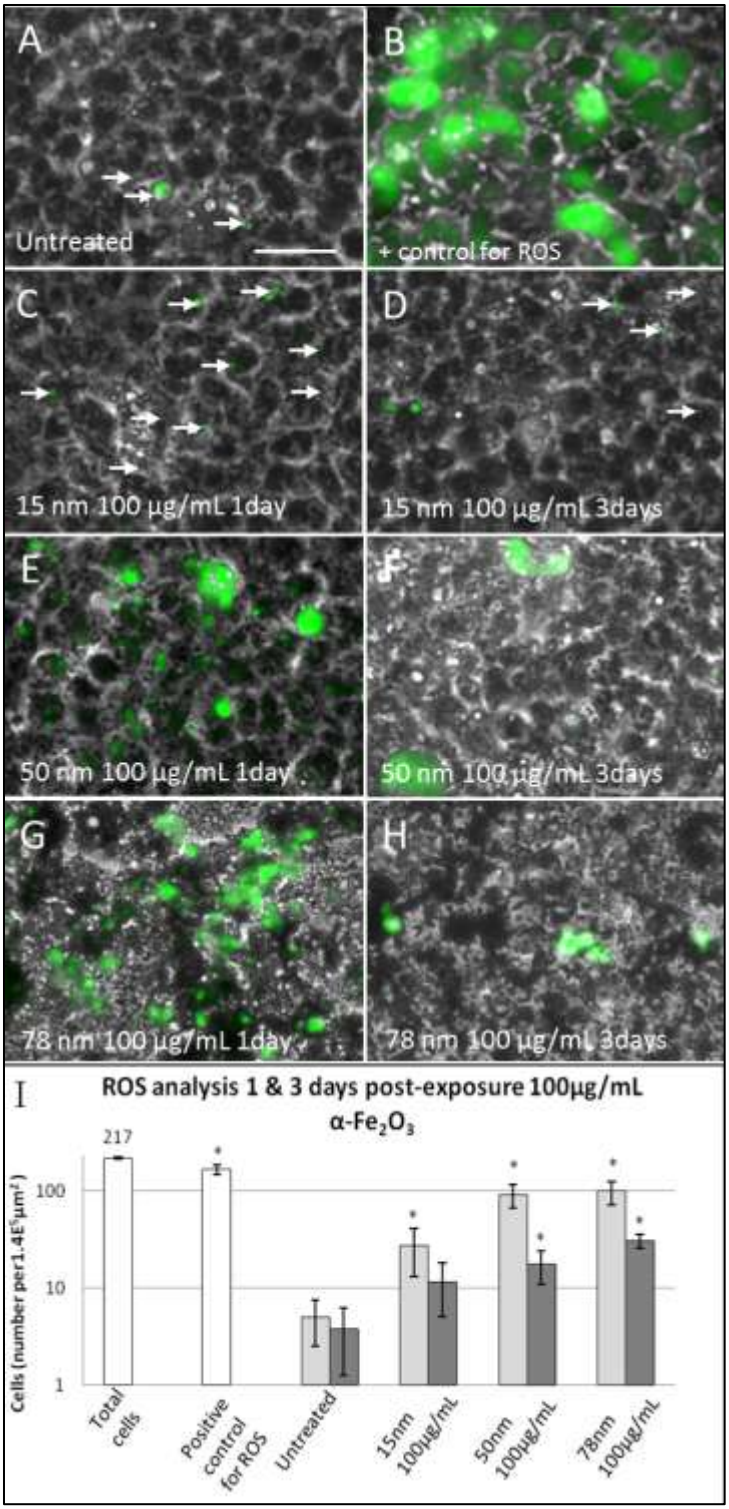

Figure 20. ROS analysis indicates that larger diameter α-Fe_2O_3 result in significant increases in ROS. At the one day time point the epithelia had few cells positive for ROS (*green*) for every 1.4x10^5 µm^2 field of view that was observed (A). A positive control for

ROS was conducted to illustrate high numbers of cells positive for reactive oxygen (B). After 1 day of exposure to the 15 nm NPs a statistically significant increase is ROS was observed (C) and this number of ROS positive cells appears to decrease at the 3 day endpoint (D). (E) After 1 day of exposure to the 50 nm NPs an increase in ROS was observed, and in contrast to the 15nm specimens, this statistically significant increase was observed after 3 days as well (F). This increase in ROS at both 1, and 3 days was also observed for the 78 nm treated specimens (G.H). (I) Quantification of the cells positive for ROS is shown in the histogram. In all cases data is shown as mean ± standard error and $p<0.05$ was considered significant. Note that the histogram is shown as log-fold change on the y-axis. The histogram represents $1.4x10^5$ μm^2 of epithelium while the micrographs are representative of $3.5x10^4$ μm^2 of the epithelium to permit adequate magnification. The scale bar is 50 µm. Light grey boxes indicate 1 day post-exposure, while dark grey boxes indicate 3 days post-exposure. The white arrows point to ROS puncta. All comparisons are made between untreated and NP-treated epithelia at their respective time points. All experiments were conducted at least 3 independent times.

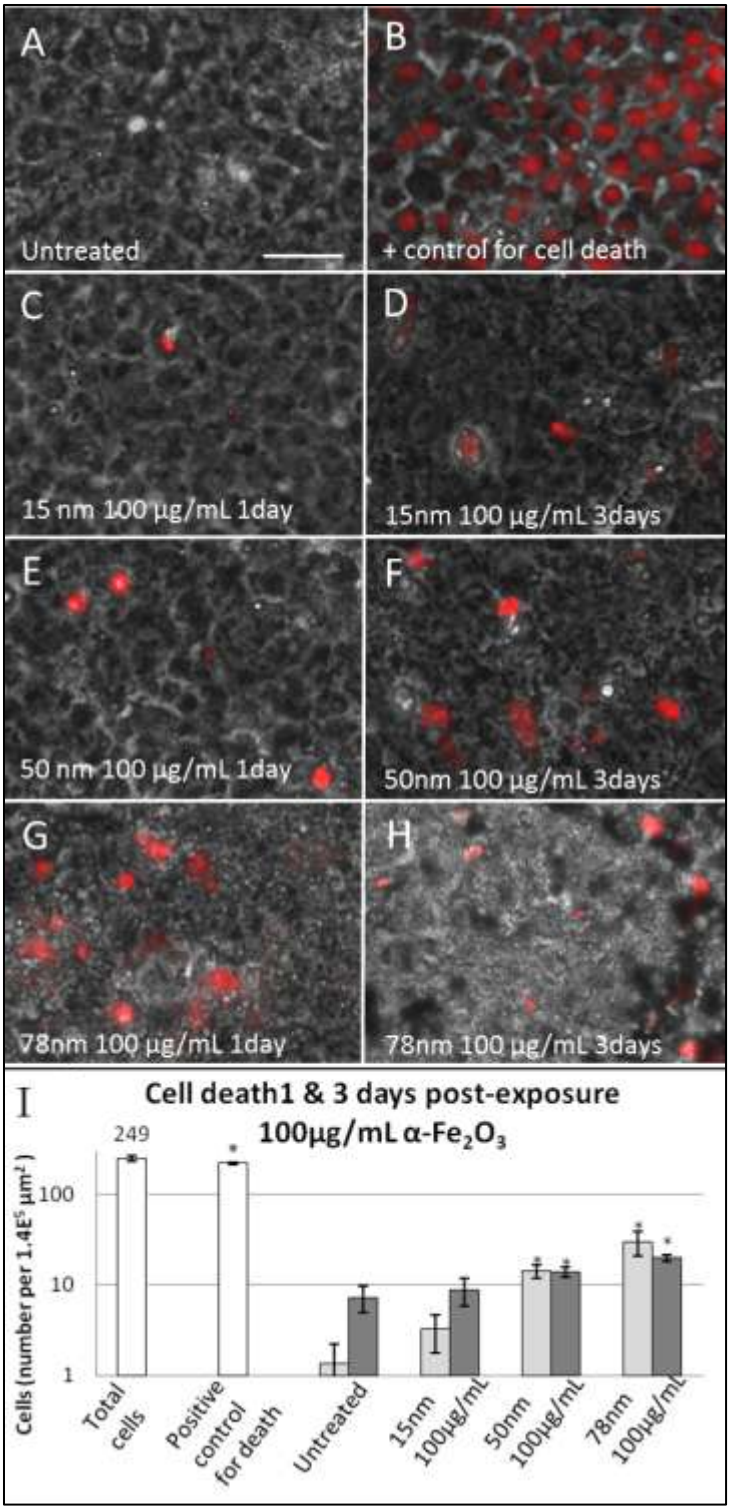

Figure 21. Live/dead analysis of BeWo epithelia as assessed by phase contrast, fluorescence overlay micrographs indicate cell death after exposure to large-diameter α-Fe_2O_3 NPs. At one day healthy epithelia have about 1 dead cell (*red*) per $1.4x10^5$ μm^2

field of view was observed in both control specimens (A). A positive control for cell death was conducted to illustrate eithidium fluorescence in the nuclear area of most cells in the epithelium (B). After 1 day and 3 days post-exposure to 15 nm NPs (C,D) there was no significant difference compared to controls (A). (E) After 1 day of exposure to the 50 nm NPs an increase in cell death was observed, and this number was consistent at the 3 day time point (F). Furthermore those epithelia exposed to the 78 nm diameter NPs had a high number of dead cells. (I) Quantification of cell death is shown in this histogram. In all cases data is shown as mean ± standard error and $p<0.05$ was considered significant. Note that the histogram is shown as log-fold change on the y-axis. The histogram represents $1.4x10^5$ μm^2 of epithelium while the micrographs are representative of $3.5x10^4$ μm^2 of the epithelium to permit adequate magnification. The scale bar is 50 µm. Light grey boxes indicate 1 day post-exposure, while dark grey boxes indicate 3 days post-exposure. All comparisons are made between untreated and NP-treated epithelia at their respective time points. All experiments were conducted at least 3 independent times.

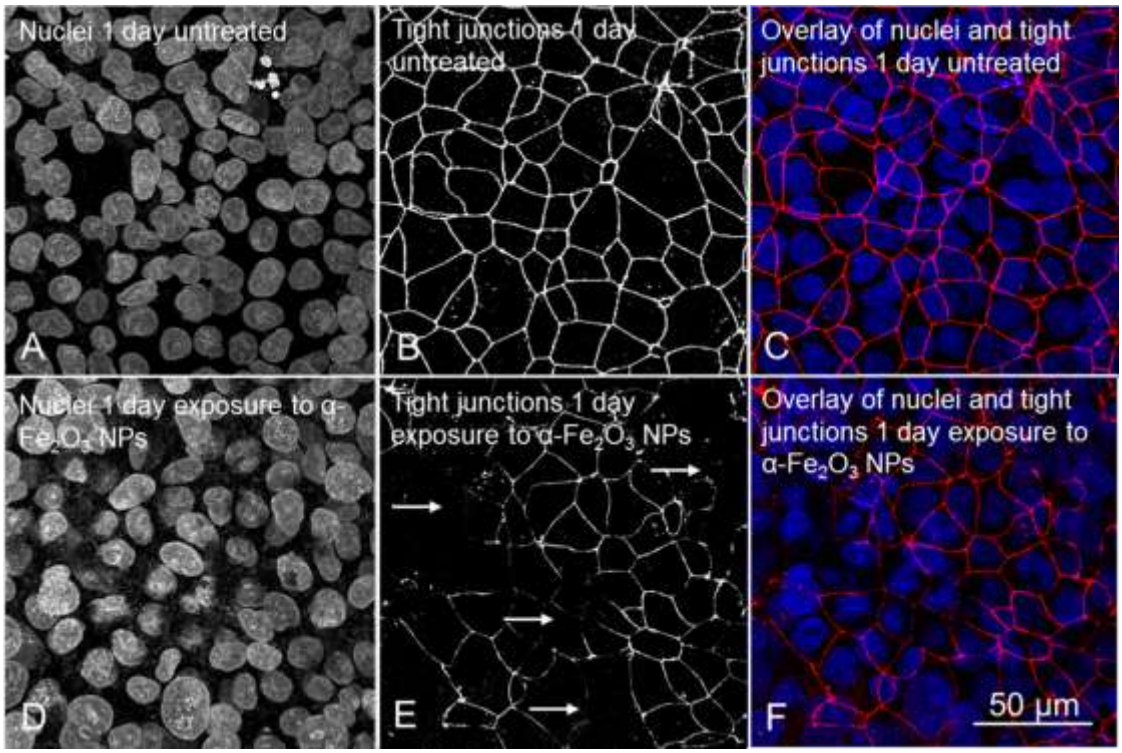

Figure 22. Tight junctions, as measured by ZO-1 immunofluorescence, are perturbed in 78nm treated specimens. (A) Untreated, healthy BeWo epithelia display the typical honeycomb arrangement of ZO-1 at the intercellular junctions and this appears contiguous across the epithelium. (B) After a 24 hour exposure to 78 nm α-Fe_2O_3 at a concentration of 100 µg/mL tight junctions are disrupted. The distribution of ZO-1 is non-contiguous throughout the epithelium, and in some areas ZO-1 appears absent (white arrows). All specimens were images through the entire z-axis at 0.5 µm increments, and shown are maximum projection images. In both the untreated and NP-treated specimens, the epithelia were treated as replicate samples and grown for 3 days prior to NP exposure. The scale bar is shown in F.

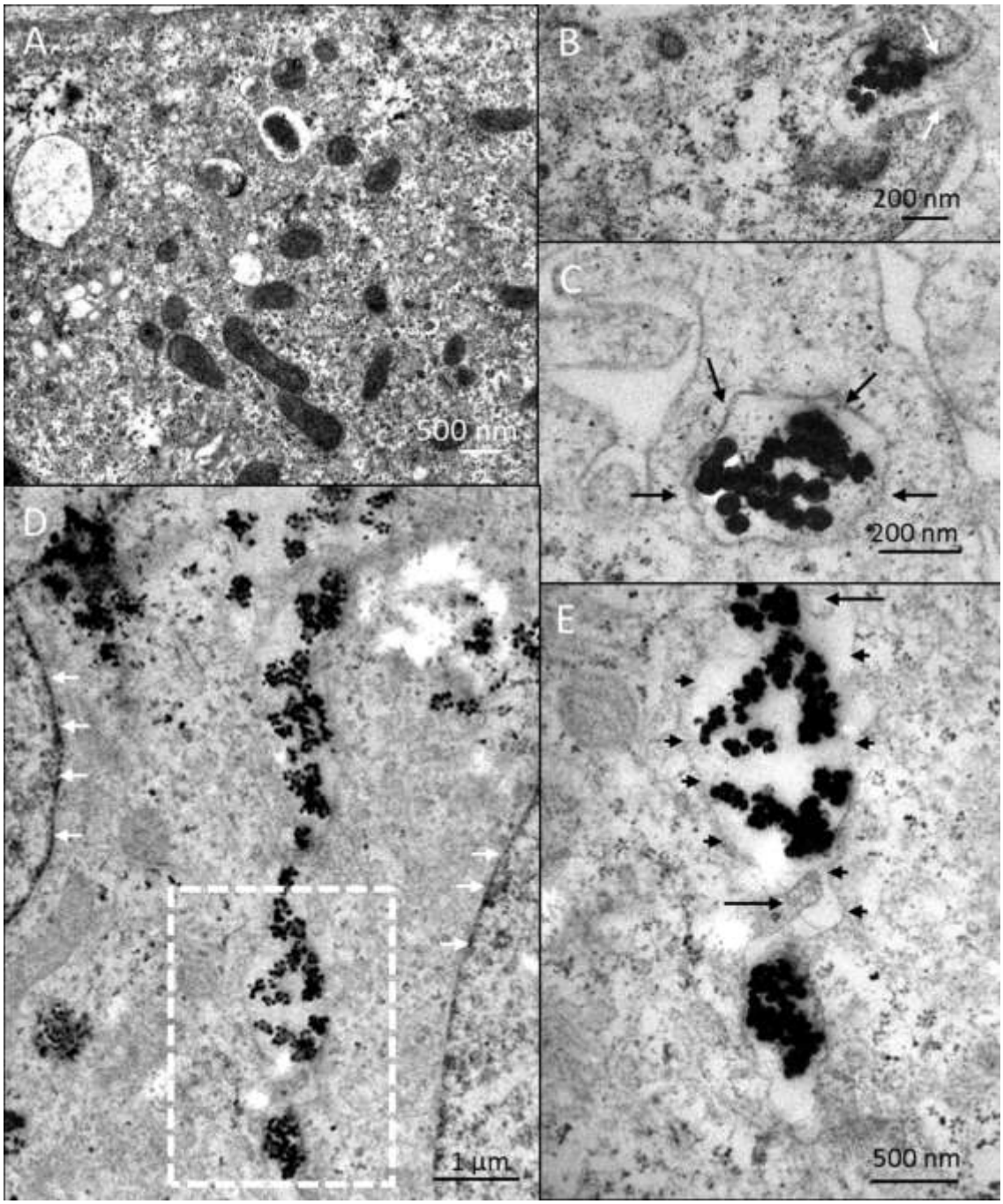

Figure 23. TEM analysis of intra- and extracellular NP localization in BeWo epithelia. (A) Numerous endocytotic, secretory granules and electron dense mitochondria can be seen in untreated BeWo epithelia. (B) After a single 4 hour exposure to the 78 nm α-Fe_2O_3 NPs at 100 µg/mL these NPs can be seen in the extracellular space and beginning to endocytose via large membrane invaginations that surround agglomerated NPs. The white arrows point to large membrane protrusions surrounding NPs. (C) At 4 hours the NPs appear to be contained in membrane-bound vesicles at the apical region of the cells.

The black arrows point to the electron-dense membrane surrounding the NPs. (D) After 8 hours in culture NPs are seen in the lateral margins between two cells. The white arrows point to the two different nuclei. (E) The micrograph represents a magnification of the region of interest shown as a white box in D. NPs can clearly been seen as non-membrane-bound and further interdigitating microvilli are present between the two cells. The black short arrows point to the membrane of the cell, while the long black arrows point to interdigitating microvilli. The scale bars are shown at the lower right corner of each micrograph.

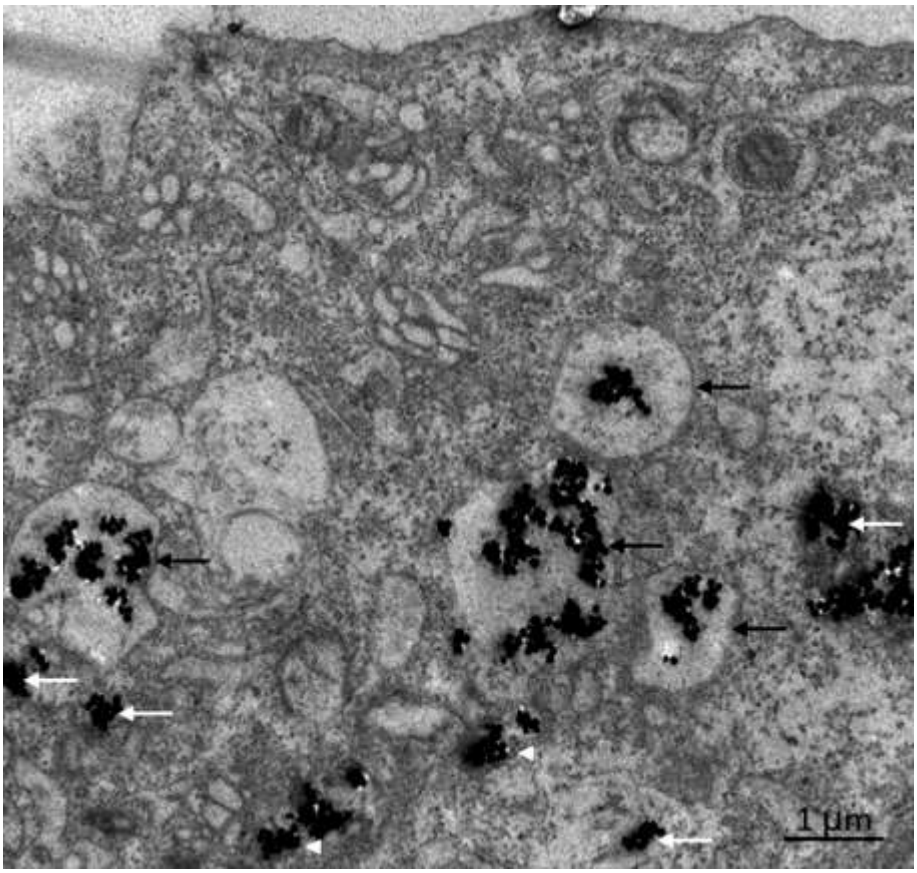

Figure 24. NPs represent at least 3 discrete "populations" of intracellular NPs. After 16 hours of exposure to 78 nm α-Fe_2O_3 NPs appear as three discrete populations, that is, some NPs appear clearly membrane-bound as indicated by black arrows. The second population of NPs appear non-membrane-bound (white arrows). The third group are in vesicles that may be rupturing (white arrowheads). The scale bar is shown at the lower right corner of each micrograph (1 µm).

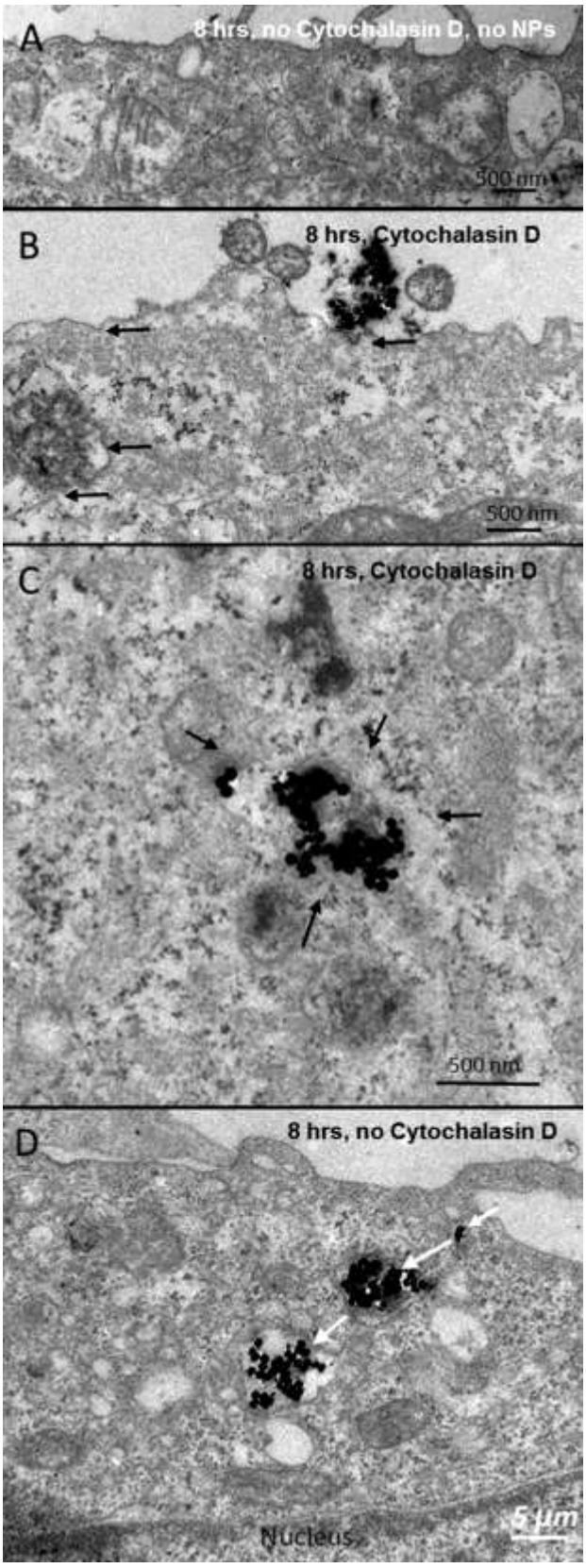
A
8 hrs, no Cytochalasin D, no NPs
500 nm
B
8 hrs, Cytochalasin D
500 nm
C
8 hrs, Cytochalasin D
500 nm
D
8 hrs, no Cytochalasin D
Nucleus
5 µm

Figure 25. NP internalization is largely, but not completely, inhibited by disruption of actin-mediated endocytosis. (A) Untreated specimens have clearly distinguishable membrane-bound vesicles with apical microlli projections. (B) After treatment with cytochalasin D for one hour prior to, and during the duration of NP exposure (8 hrs) NP endocytosis appears to be disrupted. Black arrows point to clearly identifiable cell membranes. The nanoparticle agglomerates appear to decorate the apical surface of the cells. (C) Low concentrations of NPs appear internalized at this time point (8 hrs.). However, electron-dense membranes surrounding the NPs were not clearly observed. (D) When the NPs are dosed without Cytochalasin D inhibition of actin, there appears many more

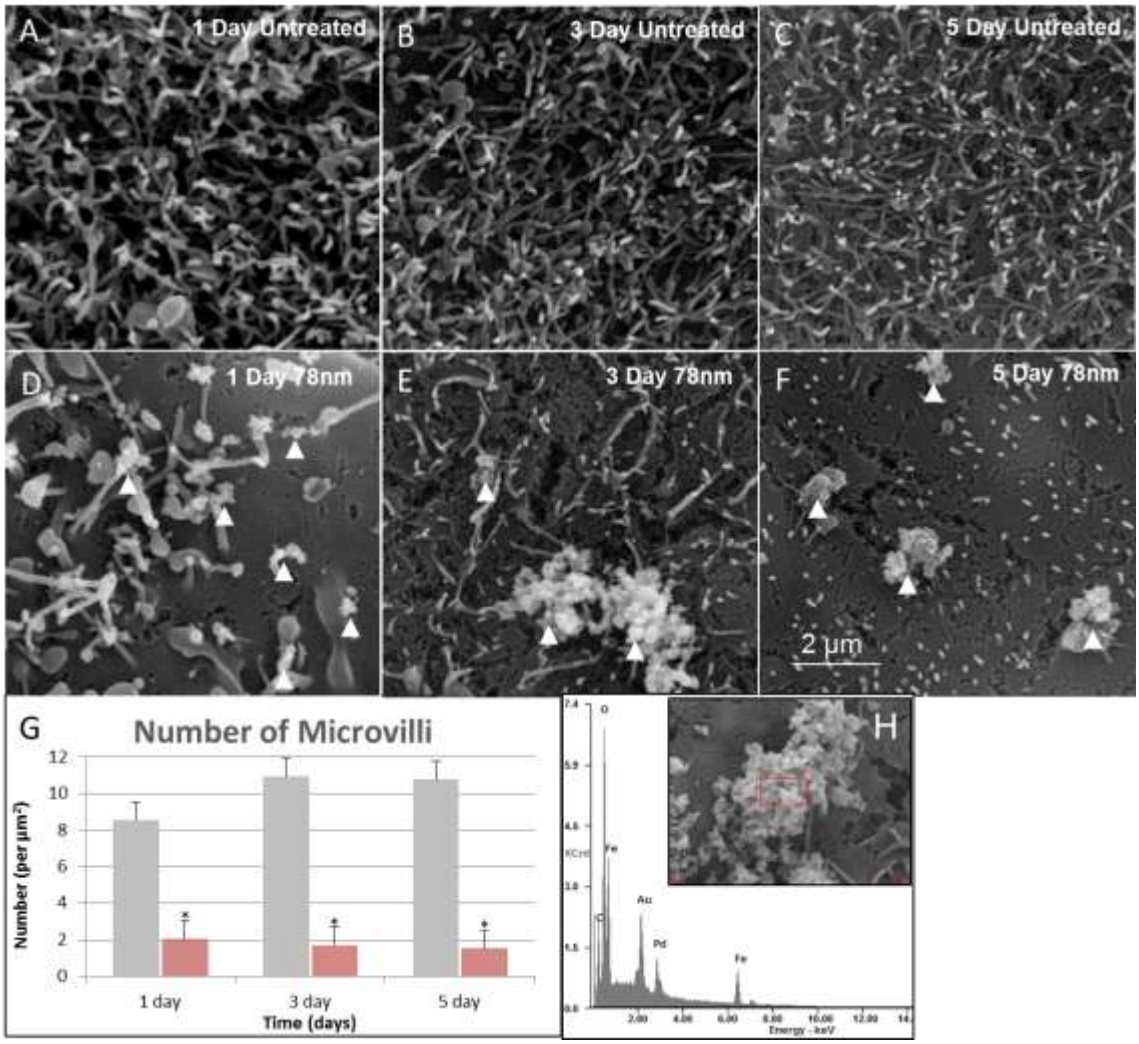

Figure 26. Scanning electron microscopy reveals the effects on the brush-border of BeWo cells. (A-C) In untreated cells, there are well developed microvilli on the apical surface at days 1, 3, and 5, respectively. (D-F) However, after treatment with α-Fe_2O_3 NPs, the apical brush-border is nearly abolished ($p<0.001$). The arrowheads point to NP clusters. (G) The histogram shown quantitation of microvilli. The number of microvilli is significantly fewer as a result of NP exposure. Each image was taken at identical magnification and thus the scale bar in F (2 µm) can be compared across micrographs. Error bars represent mean ± standard error. No fewer than 5 micrographs were scored representing 5 randomly chosen areas of 1 μm^2 per micrograph in four independent experiments.

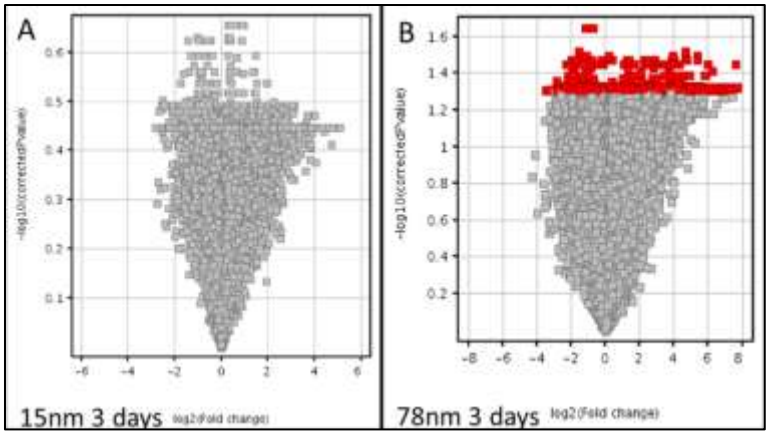

Figure 27. DNA microarray analysis indicates that exposure to 78 nm α-Fe_2O_3 evokes statistically significant changes at the level of the gene at 72 hours post-exposure. (A) The volcano plot indicates that exposure to 15 nm α-Fe_2O_3 NPs only slightly changes the fold-expression of any number of 44,000 genes, none of which are statistically significant. (B) Exposure to the 78 nm diameters results in a number of statistically significant ($p \leq 0.05$) changes in expression (red). The experiment was conducted as biological triplicate on the same day.

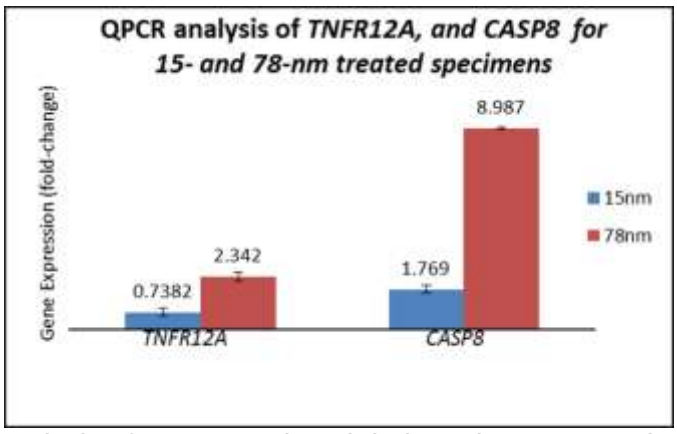

Figure 28. QPCR analysis of cDNA employed during microarray analysis has a similar expression profile for *TNFR12A* and *CASP8*. Similar results to those obtained during microarray analysis show that 15 nm exposed specimens show modest changes in expression, whereas epithelia exposed to the 78 nm diameter have large changes in gene expression. Error bars represent standard deviation. Relative gene expression was normalized by the α-tubulin housekeeping gene *TUBA1A* and calculated by the ΔΔCt method.

Hydrodynamic Diameter (DLS)	Diameter (TEM)	Polydispersive Index	ζ-potential	ζ-potential standard deviation
15 nm	15 nm	0.3	-12 mV	26.8 mV
51 nm	50 nm	0.12	-7.5 mV	42.2 mV
94 nm	78 nm	0.25	-12.2 mV	18.5 mV

Table 3. The physico-chemical characteristics of α-Fe_2O_3 NPs of the three diameters: 15-, 50- and 78-nm. The narrow polydispersive index of the nanomaterial indicates a homogenous diameter of NPs. Zeta-potential measurements indicate uniformly stable, positively charged nanomaterial. All measurements were conducted in culture medium containing serum.

Relevance	GenBank Accession	Gene	Description	Fold-Change
Tight Junctions	[NM_148960]	*CLDN19*	Claudin 19	-4.82
Adherens Junctions	[NM_015669]	*PCDHB5*	Protocadherin α5	-7.36
	[NM_018930]	*PCDHB10*	Protocadherin α10	-4.30
	[NM_018932]	*PCDHB12*	Protocadherin α12	-3.87
	[NM_018933]	*PCDHB13*	Protocadherin α13	-2.03
	[NM_018934]	*PCDHB14*	Protocadherin β14	-4.69
	[NM_032101]	*PCDHGB7*	Protocadherin αb,7	-3.64

Table 4. Microarray analysis indicates that 78 nm α-Fe_2O_3 NPs elicit down regulation of mRNA encoding proteins responsible for intercellular junctions. Exposure to 78 nm α-Fe_2O_3 NPs at a concentration of 100 µg/mL results in down regulation of genes essential for junctional integrity at the 3 day time point. Claudin 19, a component of tight junctions is down regulated nearly 5-fold. In addition, a number of protocadherins are down regulated ranging from 2 to 7-fold. All data shown represent specimens conducted as biolgical triplicate where $p \leq 0.05$.

Relevance	GenBank Accession	Gene	Description	Fold-Change
Actin Associated	[NM_001102]	*ACTN1*	Actinin, alpha 1	+2.10
	[NM_001104]	*ACTN3*	Actinin, alpha 3	+2.80
	[NM_006135]	*CAPZA1*	Actin Capping Protein	+5.80
	[NM_001043352]	*TPM3*	Tropomyosin 3	+4.32
	[NM_007284]	*TWF2*	Twinfilin homolog 2	+4.90
	[NM_004723]	*ARHGEF2*	Rho/Rac GEF 2	+3.37
	[NM_001005360]	*DNM2*	Dynamin	+3.65
Cytoskeleton	[NM_001614]	*ACTG1*	Actin, Gamma	+3.33
	[NM_002273]	*KRT8*	Keratin 8	+6.66
	[NM_002282]	*KRT83*	Keratin 83	+9.86
Apoptosis	[NM_004346]	*CASP3*	Caspase 3	+2.80
	[NM_033358]	*CASP8*	Caspase 8	+5.36
	[NM_013374]	*PDCD6IP*	Programmed cell death 6	+3.89
	[NM_021138]	*TRAF2*	TNF associated factor 2	+3.69
	[NM_001250]	*CD40*	TNF receptor 5	+2.39
	[NM_004394]	*DAP*	Death associated protein	+4.59
	[NM_016639]	*TNFRSF12A*	TNF receptor 12A	+2.88
	[NM_005938]	*FOXO4*	Forkhead	+4.16
	[NM_019885]	*CYP26B1*	Cytochrome P450 B1	+3.76
	[NM_007355]	*HSP90AB1*	Heat shock protein 90 A	+4.73
	[NM_138578]	*BCL2L1*	BCL2-like 1	+2.18
	[NM_022105]	*DIDO1*	Death inducer-obliterator 1	+3.06

Table 5. Microarray analysis indicates that 78 nm α-Fe_2O_3 NPs up regulate gene involved in apoptosis, and actin bundling and organization. Exposure to 78 nm α-Fe_2O_3 NPs at a concentration of 100 µg/mL results in up regulation of genes essential for actin organization and bundling such as CapZ, γ-actin, among others. Apoptosis appears to be the cause of cell death as initiator and executor caspases are upregulated as well as the receptors responsible for their activation. All data shown represent specimens conducted as biological triplicate where $p \leq 0.05$.

CHAPTER 6
CONCLUSIONS

General

This Dissertation described a novel nanotoxicology paradigm that is referred to as brush border disruption. Brush border disruption was first noted in 2010, in the study published by Koeneman and coworkers as a reorganization and reduction in the total number of microvilli from the surface of human intestinal cell *in vitro*, and has since been shown to be independent of *in vitro* sedimentation (Chapter 4). Further, this Dissertation shows that the correct analytical methods (Chapter 2 and 3) and brush border expressing cell line (Chapter 2) are necessary for proper interpretation of experimental results. Indeed, this assertion is borne out from independent studies (Fisichella et al., 2012; Koeneman et al., 2010) that clearly show major differences in the techniques employed to investigate human intestinal brush border disruption as a consequence of TiO_2 NP exposure. This Dissertation suggests also that brush border disruption is not limited to models of the intestine, but occurs also in human placenta cells *in vitro*. The subsequent paragraphs substantiate the former claims, provide additional insights into the putative mechanisms responsible for brush border disruption, and shed light on the relevance of brush border disruption within the context of disease.

Brush Border Disruption as a Consequence of TiO_2 NP Exposure: The Need for the Appropriate Cell Lines and Analytical Techniques

At present it appears that the choice of brush border expressing cell models and subsequent analytical techniques are important for proper interpretation of experimental results. Differences in cell lines and analytical techniques necessary to show brush border disruption as a consequence of NP exposure was identified first as a consequence of the study by Fishchella and coworkers (2012), but has since become more widespread (Aliaa Rasheed Al-Jubory, 2013). The study (Fisichella et al., 2012)

was conducted in order to identify whether or not TiO_2 NPs that are common components of sunscreens affect human intestinal cells *in vitro* while attempting to mimic the changes in physiological environment that the particles encounter (i.e., the "lifecycle") prior to *in vitro* exposure. Although the choice of material may be considered more relevant than TiO_2 sources employed elsewhere, the study approached this biological problem (i.e., brush border disruption and exposure assessment) from a materials science perspective as will be described in the proceeding text.

The human intestinal cell line, Caco-2, was first established by Fogh and coworkers (Fogh, Fogh, & Orfeo, 1977) and deposed at American Type Culture Collection (ATCC) with the designation HTB-37™. Subsequent studies showed that this cell line, when grown under the appropriate conditions, spontaneously differentiated into cell that maintained some of the *in vivo* morphological and biochemical features (Hidalgo et al., 1989). Most notably, HTB-37™ formed microvilli, junctions and contained enzymes that are found in normal tissue in the body. However, since HTB-37™ was originally derived from a human colon adenocarcinoma, a number of differences from normal human intestinal absorptive cells were observed. This led Peterson and Mooseker (M. Peterson & Mooseker, 1992) to further subclone the HTB-37™ cell line into two different monoclonal cell lines that were referred to as "brush border expressing" (BBe). Subcloning was conducted because the authors noted morphologically heterogenous brush borders, in addition to a number of biochemical differences related to brush border differentiation (M. Peterson & Mooseker, 1992; M. D. Peterson et al., 1993; M. D. Peterson & Mooseker, 1993). The BBe1 subclone of HTB-37™ was deposited at ATCC with the designation CRL-2102™. When grown correctly, the Caco-2 BBe1 and 2 cell lines develop a well-ordered array of microvilli, and demonstrate villin localization exclusively at the apical brush border (M. D. Peterson et al., 1993). Since the

characteristics chosen by Peterson and Mooseker more closely resemble normal human intestinal cells, and permit a normal sequence of brush border morphogenesis, it appears as if the most appropriate choice of human intestinal cells that can be used to investigate *in vitro* brush border disruption as a consequence of NP exposure is Caco-2 BBe1. However, and despite offering these cautions to the scientific community (J.J. Faust, Zhang, Koeneman, Chen, & Capco, 2012), the use of HTB-37™ appears to be the favored choice by investigators within the nanotoxicology field (Aliaa Rasheed Al-Jubory, 2013; Fisichella et al., 2012).

The choice of cell lines is not the only difference that has been noted in studies investigating brush border disruption. Another difference results due analytical techniques employed to visualize NPs and microvilli. Although "super-resolution" light microscopy techniques are becoming available, investigators have used electron microscopes in order to examine the fine detail of biological structures and NPs with high resolution. Electron microscopy is conducted with the specimen in a vacuum and thus necessitates a number of procedural steps (described in Chapter 2) to permit high resolution visualization of the specimen in a near-native state. For SEM this includes cytological fixation of the specimen, dehydration, drying, and coating of the specimen with metals. Deviations from the procedure can result in a number of artifacts that severely cloud experimental interpretation. For example, omitting the secondary fixative OsO_4 will result in removal of the lipid-based membranes, drying the specimen in air will depress fine surface feature, and choosing to omit sputter coating can result in charge buildup and poor image quality due to lack of conductivity and fewer secondary electrons relative to metal coated specimens, respectively. Thus if the investigator is interested in preserving near-native morphology of the sample as is necessary for brush border

analysis and procuring high quality images, procedures described in Chapter 2 are essential.

There are few very rare exceptions to the aforementioned microscopy preparation that deal with spectral analysis to confirm the presence of the NPs, particularly when NP used in the analysis are isolated directly from food. This is due to the fact that inorganic NPs are often themselves metal. For example, the study by Reed and coworkers (2014) analyzed the effects of exposure to 8 different drink supplements that claimed to contain NPs. The NPs included the following elements: copper, gold, iridium, palladium, platinum, silica, silver and zinc. The authors confirmed the existence of NPs and their elemental composition in the drink supplements, and subsequently exposed Caco-2 BBe1 cells to the supplements containing NPs. One drawback to the analysis was the fact that sputter coating with palladium and gold made it impossible to definitively show the elemental composition of surface agglomerated palladium and gold NPs, since the coating material was the same elemental composition as the NPs. Furthermore, it is a fact that some of the surface agglomerated NPs could be washed away during dehydration and critical point drying. For these reason, and from a purist materials standpoint, investigators have elected to forgo critical point drying and sputter coating specimens with metals in order to analyze the material composition through the use of energy dispersive x-ray spectroscopy. Omitting these procedures permits materials analysis, but imparts artifacts that do not allow analysis of microvilli on the cell surface, as was shown in Appendix, Supplemental Figure 1. Therefore, without the correct explanation for experimental results that apparently suffered from technical artifacts due to studies not recognizing the need to employ two or more independent methodologies for sample preparation under these very rare circumstances (Fisichella et al., 2012), it is impossible to make claims that NPs may or may not affect the brush border. Further,

studies conducted in this Dissertation proved the elemental composition of iron oxide and titanium NPs can be identified since these elements were not used during specimen preparation. Therefore, it behooves those investigators that wish to study changes that occur to brush border microvilli as a consequence of NP exposure to adopt methods that permit near-native organization of brush border microvilli. Separately, if NPs employed for brush border disruption are made from elements that are used also in specimen preparation for SEM, the investigator can choose to modify the procedures described in Chapter 2 in order to analyze elemental composition at the expense of artifacts described in Appendix, Supplemental Figure 1 of this Dissertation.

Brush border disruption is not the only event where differences have been observed as a consequence of incorrect methodologies employed to analyze such events. Studies have claimed that environmentally degraded TiO_2 NPs that are components of sunscreens are not internalized by Caco-2 cells (Fisichella et al., 2012) at concentrations as high as 100 μg/mL (i.e., 100 ppm). This comes as a surprise given Chapter 4 and 5 which clearly showed internalization of both TiO_2 particles as well as iron oxide (i.e., α-Fe_2O_3) NPs. The surprise of this discrepancy is further underscored by the fact that food grade TiO_2 particles, as shown in Chapter 4, were internalized at concentrations as low as 350 ng/mL (i.e., 350 ppb) and shown elsewhere employing semiconductor-grade TiO_2 NPs (Aliaa R Al-Jubory & Handy, 2013; Koeneman et al., 2010). Thus, in addition to the correct electron microscopy procedures it may be necessary for investigators to employ redundant methodologies to show the extent of particle internalization. For example, and permitting feasibility, investigations should consider showing internalization via TEM analysis coupled with ICP-MS as replicate experiments. As others have suggested this definitively indicates the presence of NPs in cells (Yamashita et al., 2011).

Consolidating Data from Brush Border Disruption in Intestinal and Placenta Models: The Putative Mechanism(s) Accounting for NP-Induced Brush Border Disruption

What mechanistic events account for brush border disruption? It is unlikely that a single mechanism exists to explain such an event. Rather, data shown in this Dissertation suggest a multimodal response that culminates in a reorganization and subsequent loss of brush border microvilli *in vitro*. Brush border disruption could result from either a change in cellular biochemistry as a cellular response to the material or alternatively could occur due to inherent physico-chemical properties of the material itself. As will be described in the proceeding text, evidence exists that NPs could induce short-term changes in the architecture of microvilli or long term changes that are typified as a loss in the total number of microvilli.

It was shown in this Dissertation and elsewhere (Koeneman et al., 2010) that NPs decorate the free-surface of brush border expressing cells. Furthermore, studies have shown that exposure to NPs results in changes in the level of $[Ca^{2+}]i$ (Gitrowski, Al-Jubory, & Handy, 2014; Koeneman et al., 2010). The most probably mechanism underlying the NP-induced increase in Ca^{2+} is the fact that NPs can reorganize lipid bilayers (B. Wang et al., 2008). This in turn could lead to leaky membranes and Ca^{2+} influx from the extracellular environment. It is known that the level of Ca^{2+} inside the cell is in the micro- or even nanomolar range, whereas extracellular Ca^{2+} is in the millimolar range. Rapidly increasing the level of $[Ca^{2+}]i$ could result in activation of Ca^{2+}-sensitive enzymes. One such enzyme, Villin, is highly versatile and stoichiometrically the major bundling protein of the microvillus core. In the nanomolar and micromolar range villin is an actin capping and bundling protein, respectively (Friederich, Pringault, Arpin, & Louvard, 1990). However, in the millimolar range, which might occur due to NP-induced changes in Ca^{2+}, villin severs actin bundles.

Severing of actin filaments over the short term results in microvilli that appear morphologically limp (De Beauregard et al., 1995) as was reported in this Dissertation. Thus, villin appears to be a good candidate responsible for brush border disruption via NP-induced changes in the level of $[Ca^{2+}]i$. This putative mechanism requires only that NPs decorate the surface of the cell, and could happen within minutes. Such an event represents a short term mechanism that could be dependent on the physico-chemical parameters of NPs.

Short term changes that are dependent on the physico-chemical parameters of the material may not be the only causal agents responsible for brush border disruption as a result of NP exposure. Chapters in this Dissertation clearly showed micrographs that illustrated NP internalization of food grade TiO_2 and α-Fe_2O_3 in intestinal and placenta brush border expressing cell models, respectively. Internalization by cells commonly results in reorganization of the cortical cytoskeleton. This includes deformation of the plasma membrane, reorganization of the cortical actin network, and internalization of material. Once NPs are internalized they are enclosed by plasma membrane in the form of membrane vesicles. Membrane vesicles in the form of endosomes can fuse with lysosomes in an effort to digest the inorganic material. High frequency of NP internalization alone could result in an imbalance in the normal cortical actin network. This is because the most abundant protein that composes the brush border cytoskeleton is actin (Mooseker, 1985; Tilney & Mooseker, 1971), and actin filaments are necessary for various forms of internalization (i.e., phagocytosis, pinocytosis, and receptor-mediated endocytosis) of material by the cell. Furthermore, it is known that membranes from endocytosed material are recycled rather dynamically and continuously. If less membrane was available to the brush border, the possibility exists that the cytoskeletal apparatus responsible for maintaining the length of the microvilli, could be affected as

well. This hypothesis is supported by studies which clearly showed that the application of exogenous lipids results in longer microvilli (Margolis & Bergelson, 1979; Poole, Meder, Simons, & Müller, 2004). These data suggest that an alternative mechanism that could account for brush border disruption is dependent on exclusively a change in the normal physiology of the cell through the concerted changes in the cortical cytoskeleton and endomembrane system.

However, studies have reported also that NPs can escape membrane-bound vesicles (Verma & Stellacci, 2010). NP escape is supported by investigations that have shown single or small agglomerated NPs within the cytoplasm of the cell Chapter 5. Moreover, NPs are known to attract proteins to their surface because of the electric double layer formed as a result of the inherent charge of some NPs. Recent studies have shown that SiO_2 NPs attract cytoskeletal or cytosolic proteins once internalized (Lesniak et al., 2012). As described in Chapter 5, low and high affinity adsorption of proteins to the NP surface results in formation of the NP protein corona. If internalized NPs are free floating in the cytoplasm and not confined in membrane vesicles, it is possible that the normal localization of protein(s) necessary to maintain the architecture of the brush border cytoskeleton could be compromised due to adsorption of proteins to the NP surface. This in turn could lead to changes in the normal ratios of proteins necessary for the normal shape and length of microvilli. This hypothesis is corroborated by studies that have shown that the brush border cytoskeleton is not as static as one might imagine (Stidwill et al., 1984). Indeed, pulse-chase experiments revealed turnover of the individual proteins in the brush border on the order of hours to days (Stidwill et al., 1984). Furthermore, fluorescence recovery after photobleaching has shed light on proteins treadmilling within microvilli (Tyska & Mooseker, 2002). These facts indicate

that one potential mechanism responsible for brush border disruption as a long term response could be sequestration of proteins via the NP corona.

It has been noted by others (Bement & Mooseker, 1996) that the brush border cytoskeleton is intimately interconnected with the zonula adherens. In fact, studies that have investigated brush border morphogenesis point out microvilli elongation first at the cell periphery and later at interior regions. Although it remains to be shown, one could envision formation of the terminal web first at the established cell-cell junctions as an anchoring point for terminal web assembly followed by slower polymerization of the interior voids to bridge adjacent adherens junctions. This would create a contiguous terminal web region necessary for microvilli elongation over the entire surface of the cell. Chapter 5 of this Dissertation showed changes in barrier function of the epithelium due to the tight junctions after exposure to α-Fe_2O_3 NPs. More importantly, α-Fe_2O_3 NPs were found between the lateral margins of two adjacent cells. This wedging effect of the NPs between cells could permit disassembly of adherens junctions. Since junctions are necessary for epithelial cell polarity in addition to a fortified terminal web capable of sustaining a brush border, changes in cell-cell junctions could account for disruption of the brush border due to NP exposure.

One major finding of Chapter 5 was that exposure to α-Fe_2O_3 NPs resulted in changes in gene expression. The most intriguing finding related to brush border disruption was upregulation of the gene responsible for production of the actin capping protein, CapZ. This was fascinating because early studies by Bretscher and Weber (1995) showed that CapZ is a component of the placenta brush border. More recent studies conducted in the Tyska laboratory further showed that CapZ is a component of isolated intestinal brush borders via shotgun mass spectrometry analysis (McConnell, Benesh, Mao, Tabb, & Tyska, 2011). In the event that mRNA is translated from upregulated

CAPZA gene uncontrolled filament capping at microvilli plus tips (i.e., barbed, plus ends) could ensue as a result of an increase in CapZ protein. Increases in CapZ protein could fragment not only the actin filaments that give rise to long microvilli, but may begin disassembly of other actin-based structures. Further, since the proteins that constitute brush border microvilli are dynamic and constantly turned over, the effects of CapZ may be potentiated by the normal treadmilling processes. Although the aforementioned statements have yet to be shown, upregulation of CapZ may be a pivotal event involved in NP-induced brush border disruption. Since gene transcription usually occurs on the order of hours to days, this putative mechanism may represent a long term effect of NP exposure.

One recent study has revealed the existence of intermicrovilli protocadherins as a means of organizing and imparting mechanical integrity to microvilli during brush border morphogenesis (Crawley et al., 2014). The authors employed the Caco-2 BBe1 cell model and analyzed the organization of brush border microvilli during the 20 days required for morphogenesis through the use of scanning electron microscopy. The number of microvilli on the surface of the epithelia is consistent with results reported in this Dissertation and shown elsewhere (Koeneman et al., 2010; M. D. Peterson & Mooseker, 1993). However, the authors (Crawley et al., 2014) serendipitously noted the existence of intermicrovillar connections when view in high magnification (their figure 1). They further employed quick freeze deep etch techniques followed by TEM of replicas to image the brush border cytoskeleton for both Caco-2 BBe1 and mouse small intestine as has been done elsewhere (Chandler & Sharp, 2014; Hirokawa & Heuser, 1981; Larabell & Chandler, 1988). Although this technique provides unparalleled views of the brush border cytoskeleton, it is difficult to definitively show the location of the intermicrovilli connections since the bird's eye view shown (Crawley et al., 2014) might be

misinterpreted as intermediate filaments or myosin II that is known to interconnect microvilli at their bases. For this reason the authors employed immuno-EM and showed colloidal gold localized at the tip regions of the microvilli. Since the antibody was raised again protocadherin-24, and the secondary antibody conjugated to colloidal gold only interacted with the primary antibody, the authors definitively showed intermicrovilli protocadherins at the tips of adjacent microvilli. At the time Chapter 5 of this Dissertation was published, the existence of protocadherins as intermicrovillar connections as a regulator of brush border morphogenesis was not known. However, exposure to iron oxide NPs in the placenta model resulted in a number of protocadherins down regulated. Since this new study (Crawley et al., 2014) revealed a role for protocadherins in brush border assembly, and microarray analysis of placenta extracts previously exposed to iron oxide NPs resulted in down regulation of protocadherins as shown in Chapter 5, the possibility exists that NPs may affect intermicrovillar protocadherins as a rapid short term change that results in brush border disruption.

NP-Induced Brush Border Disruption May Occur In Vivo: Models Commonly Use as Surrogates for Humans

Studies conducted in this Dissertation focused on NP exposure utilizing cell culture models of the intestinal epithelium and the trophoblast layer in the placenta as first steps. The choice of these cell systems were based on a number of criteria include cost relative to animals model, ethical concerns associated with animal euthanasia, availability of human tissue, and complexity of the experimental system. However, to date, brush border disruption has not been shown using *in vivo* systems. There exist a number of animal models that can be used in the laboratory in order to extrapolate effects that may occur in humans. These models include simple worms and flies to mice, rats and pigs. One *in vivo* model that has become an attractive option widely used in the

laboratory is the fruit fly *Drosophila melanogaster* (Drosophila). The GI tract of Drosophila have similar anatomical features to humans including a gut associated immune system, a well ordered brush border expressing intestinal epithelium, stem cells capable of renewing the absorptive epithelium, and local changes in pH (Apidianakis & Rahme, 2011; van der Flier & Clevers, 2009). Furthermore, Drosophila are inexpensive, reproduce rapidly, and have been used as a model of the brush border cytoskeleton (Morgan, Heintzelman, & Mooseker, 1995). For these reasons Drosophila represented one option that could be used in order to determine if brush border disruption occurs *in vivo*. However, the fatal flaw of employing Drosophila as a means to investigate *in vivo* brush border disruption as a consequence of NP exposure was the fact that Drosophila secretes a peritrophic membrane (PM) that encapsulates the bolus. The PM is a highly ordered protein based structure composed of chitin, proteoglycans, and digestive enzymes (D. G. King, 1988). Depending on the species, the PM is secreted either at the foregut or at the midgut. The PM acts as a thick barrier between the bolus and the absorptive epithelium that is not found in humans. Rather humans secrete mucus from from Brunner's glands and goblet cells interspersed within the absorptive epithelium. These mucus secretions in humans are necessary to protect the epithelium from the low pH contents secreted from the stomach, but do not encapsulate the bolus as a highly ordered sieve as is the case for the PM. In addition to mechanical protection, the PM acts to sequester bacteria and unwanted molecules from the adsorptive epithelium. Studies have shown that the pore size of the PM is at maximum 10 nm in diameter. As a consequence, NPs that are commonly added to human foods, such as food grade TiO_2, are omitted from direct interaction with the absorptive epithelium since the smallest NP is around 20 nm in diameter (Figure 29). These data suggest two things related to NP-induced brush border disruption; 1) it is essential that the NPs interact directly with the

brush border if brush border disruption is to occur; 2) leaching of ions from the NPs as was a control for studies conducted in Chapter 4 does not account for brush border disruption.

Although Drosophila does not permit studies related to brush border disruption, the fact that there are similar changes in pH to humans suggests that Drosophila may be a simple model that can be used in order to identify physico-chemical changes that occur as the material passes through the GI tract. Studies conducted in this Dissertation show changes is zeta-potential as an effect of pH. Moreover, gastric pH could result in changes in the agglomeration state of the material or surface etching. Etching due to changes in pH could make primary particle diameter smaller. Future investigations should consider exploiting the physiology of the GI tract of Drosophila in order to identify physico-chemical changes during the life-cycle of the material.

Drosophila is not the only model organism that is used in the laboratory setting. Often investigators employ mice or rats in order to extrapolate to the human condition. In fact, studies that established the mechanisms responsible for brush border morphogenesis were conducted in model systems such as chicken (Chambers & Grey, 1979), frog (Bonneville & Weinstock, 1970), and even salamander (Tilney & Cardell, 1970). In addition, investigators have developed established protocols to isolate intact brush borders from mouse and rat for experimental purposes. Although mouse and rat could be the next logical candidates in order to investigate *in vivo* brush border disruption due to NP exposure, investigators have stated that human brush borders are fragile compared to avian models (Carboni et al., 1987). The fragility of human brush borders suggests a change in the architecture of the brush border cytoskeleton in humans compared to avian models and rodents. Although changes in the brush border cytoskeleton of humans compared to avian models and rodents remains ill-defined, the

fact that human brush borders are fragile suggests also that human brush borders might be sensitive to NP exposure. However, it is known also that changes in diet affect the length of rodent brush border microvilli. For example, microvilli are known to elongate during feeding conditions, and retract during fasting (Palay & Karlin, 1959). Furthermore, lectins were shown to result in elongation of rodent brush border microvilli (Hagen, Trier, & Dambrauskas, 1994). Since these events have not been confirmed in humans, one might consider microvilli length as a defining criterion brush border disruption in rodents. This is because of the durability of rodent brush borders compared to humans, and the fact that retraction of microvilli would result in a decrease in surface area. One caveat to retraction as a criterion for change in rodents is the fact that the length of microvilli are known to be long in the small intestine (i.e., approximately 1 μm), but short (200-500 nm) in the large intestine. Furthermore, the number of microvilli can vary depending on the degree of differentiation that occurs as enterocytes migrate from the crypts to the villi. However, the change in normal length in the small intestine might be an indicator later disease.

NP-Induced Brush Border Disruption Mimics the Effects of Exposure to Enteropathic Bacteria

There exist striking similarities between the effects observed after *in vitro* NP exposure compared to disease states associated with infection of enteropathic bacteria. For starter, once enteropathic bacteria infect host tissue, they actively attach to the intestinal epithelium, reorganize the actin cytoskeleton in the host cells, and consequently reduce the number of microvilli on the surface of the cell. Moreover, acute (i.e., short term; hours) exposure to enteropathic bacteria results in leaky tight junctions. Finally, membrane vesicle shedding via microvilli which is known to occur *in vivo* (McConnell et al., 2009) in response to bacterial infection (Shifrin Jr et al., 2012), may

occur during *in vitro* exposure to NPs. The proceeding text compare results observed in this Dissertation to results observed after exposure to enteropathic bacteria (i.e., *E. Coli*, *C. Difficile*, etc.).

The results described in this Dissertation highlight a novel nanotoxicology paradigm referred to as NP-induced brush border disruption. Disruption is defined on the basis of a net loss and disordered array of brush border microvilli as a consequence of NP exposure. However, for some time it has been known that the early events associate with infection of enteropathic microorganisms results in a large reduction in the number of microvilli on the surface of the cell (Celli, Deng, & Finlay, 2000; Manjarrez-Hernandez, Aitken, Baldwin, Williams, & Knutton, 1992). Within the microbiology community the event of reducing the number of microvilli on the surface of the enterocytes as a consequence of bacterial infection is referred to as brush border effacement. Effacement occurs after adherence of the bacteria, transfer of bacterial proteins into the host cell, and reorganization of the host brush border cytoskeleton. Furthermore, although there are subtle differences in the molecular strategies responsible for bacterial invasion, independent mechanisms culminate in activation of Rho GTPase-mediated actin reorganization. For enteropathic E. coli (EPEC) these events include attachment, effacement and intimate attachment. In order for the bacterial cell to strongly attach to the enterocyte, the bacterium must inject Tir into the host cell. Injection of Tir into the enterocyte results in dimerization of Tir and permits ligand receptor interaction between the bacterial intimin and now host Tir (Kenny et al., 1997). Signal transduction events by way of Fyn and Abl phosphorylation of Nck recruit N-WASP and Arp 2/3 proteins required to reform the actin meshwork in the form of a pedestal. During this process, the EPEC secreting proteins EspA and EspB are necessary for activation of signal transduction events in the host cell in order to efface microvilli.

Once secreted by the bacterium, these proteins active second messangers such as Ca^{2+} and IP_3 though activation of phospholipase C (Kenny et al., 1997), which could lead to PKC activation. The relevance of PKC activation as a causal agent for reorganization of microvilli remains to be elucidated. However, there is a remarkable degree of similarity between scanning electron micrographs illustrating brush border effacement via enteropathic microorganisms (Dean, Maresca, Schüller, Phillips, & Kenny, 2006), and images shown of NP-induced brush border disruption shown in this Dissertation (Chapters 2-5).

Reducing the number of brush border microvilli on the apical surface of the cell is not the only similarity that may exists between these two models. It has been shown that enteropathic bacterial infection results in leaky tight junctions. Tight junctions exist as a molecular seal between the lumen and the underlying blood supply. The loss of the tight junctions results in unregulated flux between the two separated compartments, which results in severe diarrhea. Following EPEC infection, there is an immediate, albeit transient disruption of tight junctions as measured by decreases in TEER (Collington, Booth, & Knutton, 1998). Moreover, studies have shown that occludins and claudins shift from the detergent resistance fraction to the soluble fraction when analyzed via Western Blott (Donnenberg, Kaper, & Finlay, 1997). These data suggest that the tight junction proteins claudin and occludin are no longer attached to the cytoskeleton as part of their normal function. How does EPEC-induced tight junction reorganization mimic effects observed in this dissertation? Chapter 5 of this dissertation showed the apparent loss of tight junctions between placenta cells as measure via immunocytoshemical analysis of ZO-1 as a consequence of exposure to iron oxide NPs. The apparent loss of epithelial integrity (ZO-1 label) was also confirmed via TEER. Moreover, microarray data showed nearly a 5-fold decrease in *CLDN19* expression, which encodes claudin-19.

Unpublished studies conducted employing the Caco-2 BBe1 cell model suggest that food grade TiO_2 exposure also remodels junctions. However, instead of decreases in TEER and the absence of tight junctions, under the aforementioned conditions junctions apparently undergo a remodeling that results in massive junction undulations as evidenced by immunolocalization of ZO-1 (Figure 30, A B) and surface views (Figure 30, C D). This change in junctions as a response to food grade TiO_2 further corresponds to a significant increase in resistance.

How does one consolidate apparently opposing results? Studies have shown transient increases in TEER as a consequence of low levels of reactive oxygen species (Rao, 2007; Sheth, Seth, Thangavel, Basuroy, & Rao, 2004). Food grade TiO_2 was proven to be the anatase crystal structure as shown in Chapter 3. One major difference between anatase and rutile TiO_2 is the fact that anatase, has greater catalytic properties that result in the production of ROS and toxicity (Braydich-Stolle et al., 2009; Jiang et al., 2008; Sayes et al., 2006). Low levels of ROS production could be a mechanistic clue that accounts for junction undulation, which would result in tight junctions with more surface area compared to non-undulating junctions. Furthermore, ROS indicators showed large increases in placenta cells after exposure to large iron oxide NPs. These same indicators were unable to report ROS after exposure to food grade TiO_2 after exposure to the Caco-2 BBe1 cell mode. Taken together, these data suggest that low levels of ROS may reorganize junctions and increase TEER as an early mechanism to prevent free flow of ions, whereas high levels of ROS associated with exposure to large iron oxide NPs results in the loss of TEER and tight junctions.

Changes to the cytoskeleton may not be the only similarity between intestinal epithelia exposed to NPs and separately enteropathic bacteria. Investigators have shown that membrane shedding through microvilli is dependent on MYO1A (McConnell &

Tyska, 2007). However, the relevance of this event has only recently come to fruition. A recent study showed that exposure to enteropathic bacteria resulted in membrane shedding from microvilli (McConnell et al., 2009). It was further found that these membranes contained lysozyme and intestinal alkaline phosphatase, and actively attached to enteropathic bacteria *in vivo*. The authors of the report (Shifrin Jr et al., 2012) suggested that membrane shedding was a protective event that resulted in clearance of enteropathic bacteria from the gut. Chapter 4 of this Dissertation showed electron-dense spherical material encompassing surface aggregated NPs that looked like vesicles. Moreover, surface views via SEM showed evidence of 100-200 nm vesicles intermingled within agglomerated TiO_2. Although these surface vesicles have yet to be characterized, the notably similarities between those observed after exposure to enteropathic bacteria and those found after exposure to NPs suggest that the cells within the epithelium actively secrete vesicle as a putative clearing mechanism.

Collectively these similarities suggest that the epithelium may use related mechanism in defense of exposure to NPs. The fact that results described in this Dissertation mimic the early events of exposure to enteropathic bacteria open the door to studies where redundancies between these two systems can be noted. Further, although the studies described in this Dissertation have not been proven *in vivo* the similarities noted suggest common clinical manifestations of disease.

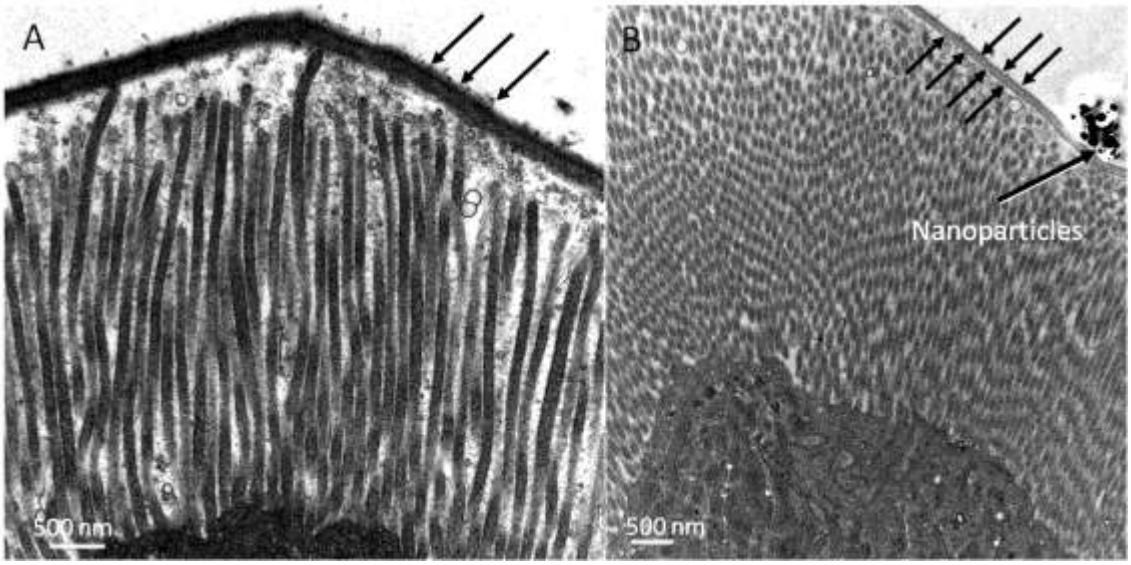

Figure 29. The peritrophic membrane in Drosophila exclude food grade TiO from the brush border. (A) Untreated control brush borders isolated from Drosophila midgut epithelium reveal a thick, electron-dense peritrophic membrane that covers the brush border microvilli. (B) The peritrophic membrane excludes food grade TiO_2 NPs from the brush border microvilli. The black arrows point to the peritrophic membrane, while the black and white arrow points to the nanomaterial. The scale bar in each micrograph is 500 nm.

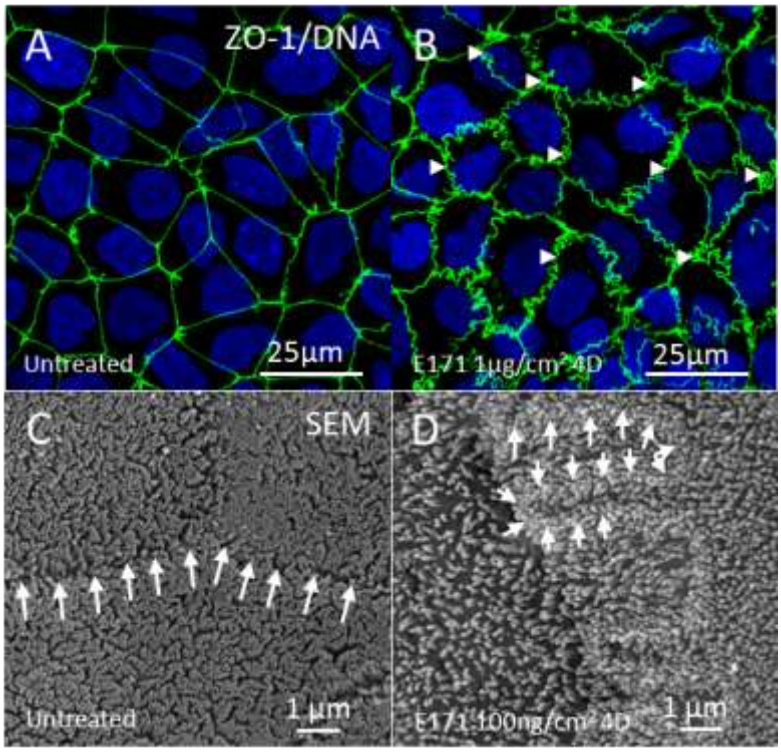

Figure 30. Exposure to food grade TiO_2 results in undulating tight junctions. (A) Laser scanning confocal analysis of the normal honeycomb organization of the tight junctions. (B) Exposure to food grade (E171 coded) TiO_2 results in undulations in tight junctions. (C) Replicate untreated control samples were imaged with the scanning scope and the junctions, outlined by white arrows, appear linear, whereas (D) sampled exposed to food grade (E171 coded) undulate (white arrows).

REFERENCES

Abbott, L. C., & Maynard, A. D. (2010). Exposure assessment approaches for engineered nanomaterials. *Risk Analysis, 30*(11), 1634-1644.

Achler, C., Filmer, D., Merte, C., & Drenckhahn, D. (1989). Role of microtubules in polarized delivery of apical membrane proteins to the brush border of the intestinal epithelium. *J Cell Biol, 109*(1), 179-189.

Al-Jubory, A. R. (2013). Titanium dioxide nanoparticle uptake across the isolated perfused intestine of rainbow trout: physiological mechanisms and a comparison with Caco-2 cells.

Al-Jubory, A. R., & Handy, R. D. (2013). Uptake of titanium from TiO2 nanoparticle exposure in the isolated perfused intestine of rainbow trout: nystatin, vanadate and novel CO2-sensitive components. *Nanotoxicology, 7*(8), 1282-1301.

Amstad, E., Textor, M., & Reimhult, E. (2011). Stabilization and functionalization of iron oxide nanoparticles for biomedical applications. *Nanoscale, 3*(7), 2819-2843.

Anderson, J. M., Van Itallie, C. M., Peterson, M. D., Stevenson, B. R., Carew, E. A., & Mooseker, M. S. (1989). ZO-1 mRNA and protein expression during tight junction assembly in Caco-2 cells. *J Cell Biol, 109*(3), 1047-1056.

Apidianakis, Y., & Rahme, L. G. (2011). Drosophila melanogaster as a model for human intestinal infection and pathology. *Disease models & mechanisms, 4*(1), 21-30.

Aplin, J. (1996). The cell biology of human implantation. *Placenta, 17*(5), 269-275.

Arpin, M., & Friederich, E. (1992). Cytoskeletal components in intestinal brush border morphogenesis: an evaluation of their function *Epithelial Organization and Development* (pp. 245-271): Springer.

Arruebo, M., Fernández-Pacheco, R., Ibarra, M. R., & Santamaría, J. (2007). Magnetic nanoparticles for drug delivery. *Nano Today, 2*(3), 22-32.

Artursson, P., Palm, K., & Luthman, K. (2012). Caco-2 monolayers in experimental and theoretical predictions of drug transport. *Advanced drug delivery reviews*.

Athinarayanan, J., Periasamy, V. S., Alsaif, M. A., Al-Warthan, A. A., & Alshatwi, A. A. (2014). Presence of nanosilica (E551) in commercial food products: TNF-mediated oxidative stress and altered cell cycle progression in human lung fibroblast cells. *Cell Biol Toxicol, 30*(2), 89-100.

Auffan, M., Rose, J., Bottero, J.-Y., Lowry, G. V., Jolivet, J.-P., & Wiesner, M. R. (2009). Towards a definition of inorganic nanoparticles from an environmental, health and safety perspective. *Nature nanotechnology, 4*(10), 634-641.

Bachman, B. J., & Vasile, M. J. (1989). Ion bombardment of polyimide films. *Journal of Vacuum Science & Technology A: Vacuum, Surfaces, and Films, 7*(4), 2709-2716.

Bartles, J. R., Zheng, L., Li, A., Wierda, A., & Chen, B. (1998). Small espin: a third actin-bundling protein and potential forked protein ortholog in brush border microvilli. *J Cell Biol, 143*(1), 107-119.

Begg, D. A., Rodewald, R., & Rebhun, L. I. (1978). The visualization of actin filament polarity in thin sections. Evidence for the uniform polarity of membrane-associated filaments. *J Cell Biol, 79*(3), 846-852.

Bement, W. M., Forscher, P., & Mooseker, M. S. (1993). A novel cytoskeletal structure involved in purse string wound closure and cell polarity maintenance. *J Cell Biol, 121*(3), 565-578.

Bement, W. M., & Mooseker, M. S. (1996). The cytoskeleton of the intestinal epithelium: components, assembly, and dynamic rearrangements. *The cytoskeleton: a multi-volume treatise, 3*, 359-404.

Berryman, M., Gary, R., & Bretscher, A. (1995). Ezrin oligomers are major cytoskeletal components of placental microvilli: a proposal for their involvement in cortical morphogenesis. *J Cell Biol, 131*(5), 1231-1242.

Bhabra, G., Sood, A., Fisher, B., Cartwright, L., Saunders, M., Evans, W. H., . . . Davis, S. A. (2009). Nanoparticles can cause DNA damage across a cellular barrier. *Nature nanotechnology, 4*(12), 876-883.

Blowes, D. W., Ptacek, C. J., & Jambor, J. L. (1997). In-situ remediation of Cr (VI)-contaminated groundwater using permeable reactive walls: laboratory studies. *Environmental Science & Technology, 31*(12), 3348-3357.

Blume, L. F., Denker, M., Gieseler, F., & Kunze, T. (2010). Temperature corrected transepithelial electrical resistance (TEER) measurement to quantify rapid changes in paracellular permeability. *Pharmazie, 65*(1), 19-24.

Bode, C. J., Jin, H., Rytting, E., Silverstein, P. S., Young, A. M., & Audus, K. L. (2006). In vitro models for studying trophoblast transcellular transport. *Methods Mol Med, 122*, 225-239.

Bonneville, M. A., & Weinstock, M. (1970). Brush border development in the intestinal absorptive cells of Xenopus during metamorphosis. *J Cell Biol, 44*(1), 151-171.

Braydich-Stolle, L. K., Schaeublin, N. M., Murdock, R. C., Jiang, J., Biswas, P., Schlager, J. J., & Hussain, S. M. (2009). Crystal structure mediates mode of cell death in TiO2 nanotoxicity. *Journal of nanoparticle research, 11*(6), 1361-1374.

Bretscher, A. (1983a). Microfilament organization in the cytoskeleton of the intestinal brush border. *Cell and muscle motility, 4*, 239.

Bretscher, A. (1983b). Purification of an 80,000-dalton protein that is a component of the isolated microvillus cytoskeleton, and its localization in nonmuscle cells. *J Cell Biol, 97*(2), 425-432.

Bretscher, A., Reczek, D., & Berryman, M. (1997). Ezrin: a protein requiring conformational activation to link microfilaments to the plasma membrane in the assembly of cell surface structures. *J Cell Sci, 110*(24), 3011-3018.

Bretscher, A., & Weber, K. (1978). Localization of actin and microfilament-associated proteins in the microvilli and terminal web of the intestinal brush border by immunofluorescence microscopy. *J Cell Biol, 79*(3), 839-845.

Bretscher, A., & Weber, K. (1979). Villin: the major microfilament-associated protein of the intestinal microvillus. *Proceedings of the National Academy of Sciences, 76*(5), 2321-2325.

Bretscher, A., & Weber, K. (1980a). Fimbrin, a new microfilament-associated protein present in microvilli and other cell surface structures. *J Cell Biol, 86*(1), 335-340.

Bretscher, A., & Weber, K. (1980b). Villin is a major protein of the microvillus cystoskeleton which binds both G and F actin in a calcium-dependent manner. *Cell, 20*(3), 839-847.

Brown, J. W., & McKnight, C. J. (2010). Molecular model of the microvillar cytoskeleton and organization of the brush border. *PLoS One, 5*(2), e9406.

Buyukhatipoglu, K., & Clyne, A. M. (2011). Superparamagnetic iron oxide nanoparticles change endothelial cell morphology and mechanics via reactive oxygen species formation. *Journal of Biomedical Materials Research Part A, 96*(1), 186-195.

Carboni, J., Howe, C., West, A., Barwick, K., Mooseker, M., & Morrow, J. (1987). Characterization of intestinal brush border cytoskeletal proteins of normal and neoplastic human epithelial cells. A comparison with the avian brush border. *The American journal of pathology, 129*(3), 589.

Cartwright, L., Poulsen, M. S., Nielsen, H. M., Pojana, G., Knudsen, L. E., Saunders, M., . . . Nielsen, H. (2012). In vitro placental model optimization for nanoparticle transport studies. *Int J Nanomedicine, 7*, 497.

Celli, J., Deng, W., & Finlay, B. B. (2000). Enteropathogenic Escherichia coli (EPEC) attachment to epithelial cells: exploiting the host cell cytoskeleton from the outside. *Cellular microbiology, 2*(1), 1-9.

Chambers, C., & Grey, R. D. (1979). Development of the structural components of the brush border in absorptive cells of the chick intestine. *Cell and tissue research, 204*(3), 387-405.

Chandler, D. E., & Sharp, W. P. (2014). Freeze Fracture and Freeze Etching *Electron Microscopy* (pp. 95-132): Springer.

Chaudhry, Q., Scotter, M., Blackburn, J., Ross, B., Boxall, A., Castle, L., . . . Watkins, R. (2008). Applications and implications of nanotechnologies for the food sector. *Food Additives and Contaminants, 25*(3), 241-258.

Cho, E. C., Zhang, Q., & Xia, Y. (2011). The effect of sedimentation and diffusion on cellular uptake of gold nanoparticles. *Nature nanotechnology, 6*(6), 385-391.

Clark, D., & Thomas, H. (1978). Applications of ESCA to polymer chemistry. XVII. Systematic investigation of the core levels of simple homopolymers. *Journal of Polymer Science: Polymer Chemistry Edition, 16*(4), 791-820.

Claude, P. (1978). Morphological factors influencing transepithelial permeability: A model for the resistance of thezonula occludens. *The Journal of membrane biology, 39*(2-3), 219-232.

Collington, G., Booth, I., & Knutton, S. (1998). Rapid modulation of electrolyte transport in Caco-2 cell monolayers by enteropathogenic Escherichia coli (EPEC) infection. *Gut, 42*(2), 200-207.

Coudrier, E., Kerjaschki, D., & Louvard, D. (1988). Cytoskeleton organization and submembranous interactions in intestinal and renal brush borders. *Kidney international, 34*(3), 309.

Crawley, S. W., Shifrin Jr, D. A., Grega-Larson, N. E., McConnell, R. E., Benesh, A. E., Mao, S., . . . Millis, B. A. (2014). Intestinal Brush Border Assembly Driven by Protocadherin-Based Intermicrovillar Adhesion. *Cell, 157*(2), 433-446.

Crosera, M., Bovenzi, M., Maina, G., Adami, G., Zanette, C., Florio, C., & Larese, F. F. (2009). Nanoparticle dermal absorption and toxicity: a review of the literature. *International archives of occupational and environmental health, 82*(9), 1043-1055.

Cundy, A. B., Hopkinson, L., & Whitby, R. L. (2008). Use of iron-based technologies in contaminated land and groundwater remediation: A review. *Science of the total environment, 400*(1), 42-51.

D'Angelo, R., Aresta, S., Blangy, A., Del Maestro, L., Louvard, D., & Arpin, M. (2007). Interaction of ezrin with the novel guanine nucleotide exchange factor PLEKHG6 promotes RhoG-dependent apical cytoskeleton rearrangements in epithelial cells. *Mol Biol Cell, 18*(12), 4780-4793.

Davis, J., Addison, J., Bolton, R., Donaldson, K., Jones, A., & Smith, T. (1986). The pathogenicity of long versus short fibre samples of amosite asbestos administered to rats by inhalation and intraperitoneal injection. *British journal of experimental pathology, 67*(3), 415.

De Beauregard, M. C., Pringault, E., Robine, S., & Louvard, D. (1995). Suppression of villin expression by antisense RNA impairs brush border assembly in polarized epithelial intestinal cells. *The EMBO journal, 14*(3), 409.

Dean, P., Maresca, M., Schüller, S., Phillips, A. D., & Kenny, B. (2006). Potent diarrheagenic mechanism mediated by the cooperative action of three enteropathogenic Escherichia coli-injected effector proteins. *Proc Natl Acad Sci U S A, 103*(6), 1876-1881.

Delpeux, S., Beguin, F., Benoit, R., Erre, R., Manolova, N., & Rashkov, I. (1998). Fullerene core star-like polymers—1. Preparation from fullerenes and monoazidopolyethers. *European polymer journal, 34*(7), 905-915.

Demri, B., & Muster, D. (1995). XPS study of some calcium compounds. *Journal of materials processing technology, 55*(3), 311-314.

Denker, H. W. (1993). Implantation: a cell biological paradox. *J Exp Zool, 266*(6), 541-558. doi: 10.1002/jez.1402660606

Donaldson, K., Murphy, F., Schinwald, A., Duffin, R., & Poland, C. A. (2011). Identifying the pulmonary hazard of high aspect ratio nanoparticles to enable their safety-by-design. *Nanomedicine, 6*(1), 143-156.

Donaldson, K., & Seaton, A. (2012). A short history of the toxicology of inhaled particles. *Part Fibre Toxicol, 9*(1), 1-12.

Donaldson, K., Tran, L., Jimenez, L. A., Duffin, R., Newby, D. E., Mills, N., . . . Stone, V. (2005). Combustion-derived nanoparticles: a review of their toxicology following inhalation exposure. *Part Fibre Toxicol, 2*(1), 10.

Donnenberg, M. S., Kaper, J. B., & Finlay, B. B. (1997). Interactions between enteropathogenic< i> Escherichia coli and host epithelial cells. *Trends in microbiology, 5*(3), 109-114.

Duan, Y., Liu, J., Ma, L., Li, N., Liu, H., Wang, J., . . . Zhao, X. (2010). Toxicological characteristics of nanoparticulate anatase titanium dioxide in mice. *Biomaterials, 31*(5), 894-899.

Dunphy Guzman, K. A., Taylor, M. R., & Banfield, J. F. (2006). Environmental risks of nanotechnology: National nanotechnology initiative funding, 2000-2004. *Environmental Science & Technology, 40*(5), 1401-1407.

Ehrenberg, M. S., Friedman, A. E., Finkelstein, J. N., Oberdörster, G., & McGrath, J. L. (2009). The influence of protein adsorption on nanoparticle association with cultured endothelial cells. *Biomaterials, 30*(4), 603-610.

Einstein, A. (1956). *Investigations on the Theory of the Brownian Movement*: Courier Dover Publications.

Ellis, R. E., Yuan, J., & Horvitz, H. (1991). Mechanisms and functions of cell death. *Annual review of cell biology, 7*(1), 663-698.

Faust, J.J., & Capco, D. (2012). Multifunctional scaffolds in eggs: sites for localization, signal transduction and meiotic spindle polarity. *Front Biosci (Schol Ed), 5*, 496-506.

Faust, J. J., Doudrick, K., Yang, Y., Westerhoff, P., & Capco, D. G. (2014). Food grade titanium dioxide disrupts intestinal brush border microvilli in vitro independent of sedimentation. *Cell Biol Toxicol, 30*(3), 169-188.

Faust, J. J., Zhang, W., Koeneman, B. A., Chen, Y., & Capco, D. G. (2012). Commenting on the effects of surface treated- and non-surface treated TiO(2) in the Caco-2 cell model. *Part Fibre Toxicol, 9*, 42. doi: 10.1186/1743-8977-9-42

FDA, U. (2010). Summary of color additives listed for use in the United States in food, drugs, cosmetics, and medical devices. Color additives approved for use in cosmetics part 73, subpart C: Color additives exempt from batch certification, United States Food and Drug Administration.

Ferrary, E., Cohen-Tannoudji, M., Pehau-Arnaudet, G., Lapillonne, A., Athman, R., Ruiz, T., . . . Fontaine, J.-J. (1999). In vivo, villin is required for Ca2+-dependent F-actin disruption in intestinal brush borders. *J Cell Biol, 146*(4), 819-830.

Fischer, U., Jänicke, R., & Schulze-Osthoff, K. (2003). Many cuts to ruin: a comprehensive update of caspase substrates. *Cell Death & Differentiation, 10*(1), 76-100.

Fisichella, M., Berenguer, F., Steinmetz, G., Auffan, M., Rose, J., & Prat, O. (2012). Intestinal toxicity evaluation of TiO2 degraded surface-treated nanoparticles: a combined physico-chemical and toxicogenomics approach in caco-2 cells. *Part Fibre Toxicol, 9*, 18.

Fogh, J., Fogh, J. M., & Orfeo, T. (1977). One hundred and twenty-seven cultured human tumor cell lines producing tumors in nude mice. *Journal of the National Cancer Institute, 59*(1), 221-226.

Foss Hansen, S., Larsen, B. H., Olsen, S. I., & Baun, A. (2007). Categorization framework to aid hazard identification of nanomaterials. *Nanotoxicology, 1*(3), 243-250.

Freshney, R. I. (2005). *Culture of specific cell types*: Wiley Online Library.

Friederich, E., Pringault, E., Arpin, M., & Louvard, D. (1990). From the structure to the function of villin, an actin‐binding protein of the brush border. *Bioessays, 12*(9), 403-408.

Fröhlich, E., & Roblegg, E. (2012). Models for oral uptake of nanoparticles in consumer products. *Toxicology, 291*(1), 10-17.

Fulda, S., & Debatin, K. (2006). Extrinsic versus intrinsic apoptosis pathways in anticancer chemotherapy. *Oncogene, 25*(34), 4798-4811.

Furuse, M., Itoh, M., Hirase, T., Nagafuchi, A., Yonemura, S., & Tsukita, S. (1994). Direct association of occludin with ZO-1 and its possible involvement in the localization of occludin at tight junctions. *J Cell Biol, 127*(6), 1617-1626.

Gao, X., Cui, Y., Levenson, R. M., Chung, L. W., & Nie, S. (2004). In vivo cancer targeting and imaging with semiconductor quantum dots. *Nature biotechnology, 22*(8), 969-976.

Garcia, A., Coudrier, E., Carboni, J., Anderson, J., Vandekerkhove, J., Mooseker, M., . . . Arpin, M. (1989). Partial deduced sequence of the 110-kD-calmodulin complex of the avian intestinal microvillus shows that this mechanoenzyme is a member of the myosin I family. *J Cell Biol, 109*(6), 2895-2903.

Gardner, S. D., Singamsetty, C. S., Booth, G. L., He, G.-R., & Pittman, C. U. (1995). Surface characterization of carbon fibers using angle-resolved XPS and ISS. *Carbon, 33*(5), 587-595.

Gaugain, B., Barbet, J., Capelle, N., Roques, B. P., Le Pecq, J. B., & Le Bret, M. (1978). DNA bifunctional intercalators. 2. Fluorescence properties and DNA binding interaction of an ethidium homodimer and an acridine ethidium heterodimer. Appendix: Numerical solution of McGhee and von Hippel equations for competing ligands. Biochemistry, 17(24), 5078-5088.

Gilbert, T., Le Bivic, A., Quaroni, A., & Rodriguez-Boulan, E. (1991). Microtubular organization and its involvement in the biogenetic pathways of plasma membrane proteins in Caco-2 intestinal epithelial cells. *J Cell Biol, 113*(2), 275-288.

Gitrowski, C., Al-Jubory, A. R., & Handy, R. D. (2014). Uptake of different crystal structures of TiO< sub> 2</sub> nanoparticles by Caco-2 intestinal cells. *Toxicology letters, 226*(3), 264-276.

Glenney, J. R., Glenney, P., & Weber, K. (1983). The spectrin-related molecule, TW-260/240, cross-links the actin bundles of the microvillus rootlets in the brush borders of intestinal epithelial cells. *J Cell Biol, 96*(5), 1491-1496.

Glenney Jr, J. R., Osborn, M., & Weber, K. (1982). The intracellular localization of the microvillus 110K protein, a component considered to be involved in side-on membrane attachment of F-actin. *Exp Cell Res, 138*(1), 199-205.

Granger, B., & Baker, R. F. (1950). Electron microscope investigation of the striated border of intestinal epithelium. *The Anatomical Record, 107*(4), 423-441.

Grimm-Günter, E.-M. S., Revenu, C., Ramos, S., Hurbain, I., Smyth, N., Ferrary, E., . . . Rivero, F. (2009). Plastin 1 binds to keratin and is required for terminal web assembly in the intestinal epithelium. *Mol Biol Cell, 20*(10), 2549-2562.

Grummer, R., Hohn, H. P., Mareel, M. M., & Denker, H. W. (1994). Adhesion and invasion of three human choriocarcinoma cell lines into human endometrium in a three-dimensional organ culture system. *Placenta, 15*(4), 411-429.

Guo, H., Stüben, D., & Berner, Z. (2007). Removal of arsenic from aqueous solution by natural siderite and hematite. *Applied Geochemistry, 22*(5), 1039-1051.

Gupta, A. K., & Gupta, M. (2005). Synthesis and surface engineering of iron oxide nanoparticles for biomedical applications. *Biomaterials, 26*(18), 3995-4021.

Gupta, A. K., Naregalkar, R. R., Vaidya, V. D., & Gupta, M. (2007). Recent advances on surface engineering of magnetic iron oxide nanoparticles and their biomedical applications. *Nanomedicine (Lond), 2*(1), 23-39. doi: 10.2217/17435889.2.1.23

Hagen, S. J., Trier, J. S., & Dambrauskas, R. (1994). Exposure of the rat small intestine to raw kidney beans results in reorganization of absorptive cell microvilli. *GASTROENTEROLOGY-BALTIMORE THEN PHILADELPHIA, 106*, 73-73.

Halbleib, J. M., Sääf, A. M., Brown, P. O., & Nelson, W. J. (2007). Transcriptional modulation of genes encoding structural characteristics of differentiating enterocytes during development of a polarized epithelium in vitro. *Mol Biol Cell, 18*(11), 4261-4278.

Hallagan, J., Allen, D., & Borzelleca, J. (1995). The safety and regulatory status of food, drug and cosmetics colour additives exempt from certification. *Food and chemical toxicology, 33*(6), 515-528.

Han, G., Ghosh, P., & Rotello, V. M. (2007). Functionalized gold nanoparticles for drug delivery.

Hannan, N. J., Paiva, P., Dimitriadis, E., & Salamonsen, L. A. (2010). Models for study of human embryo implantation: choice of cell lines? *Biol Reprod, 82*(2), 235-245.

He, Y. T., Wan, J., & Tokunaga, T. (2008). Kinetic stability of hematite nanoparticles: the effect of particle sizes. *Journal of nanoparticle research, 10*(2), 321-332.

Heintzelman, M. B., Hasson, T., & Mooseker, M. S. (1994). Multiple unconventional myosin domains of the intestinal brush border cytoskeleton. *J Cell Sci, 107*(12), 3535-3543.

Heintzelman, M. B., & Mooseker, M. S. (1992). Assembly of the intestinal brush border cytoskeleton. *Curr. Top. Dev. Biol, 26*, 93-122.

Hidalgo, I. J., Raub, T., & Borchardt, R. (1989). Characterization of the human colon carcinoma cell line (Caco-2) as a model system for intestinal epithelial permeability. *Gastroenterology, 96*(3), 736.

Hirokawa, N., Cheney, R. E., & Willard, M. (1983). Location of a protein of the fodrin-spectrin-TW260/240 family in the mouse intestinal brush border. *Cell, 32*(3), 953-965.

Hirokawa, N., & Heuser, J. E. (1981). Quick-freeze, deep-etch visualization of the cytoskeleton beneath surface differentiations of intestinal epithelial cells. *J Cell Biol, 91*(2), 399-409.

Hirokawa, N., Tilney, L. G., Fujiwara, K., & Heuser, J. E. (1982). Organization of actin, myosin, and intermediate filaments in the brush border of intestinal epithelial cells. *J Cell Biol, 94*(2), 425-443.

Hodgson, J. T., & Darnton, A. (2000). The quantitative risks of mesothelioma and lung cancer in relation to asbestos exposure. *Annals of Occupational Hygiene, 44*(8), 565-601.

Howarth, M., Takao, K., Hayashi, Y., & Ting, A. Y. (2005). Targeting quantum dots to surface proteins in living cells with biotin ligase. *Proc Natl Acad Sci U S A, 102*(21), 7583-7588.

Howe, C. L., & Mooseker, M. S. (1983). Characterization of the 110-kdalton actin-calmodulin-, and membrane-binding protein from microvilli of intestinal epithelial cells. *J Cell Biol, 97*(4), 974-985.

Hu, R., Gong, X., Duan, Y., Li, N., Che, Y., Cui, Y., . . . Hong, F. (2010). Neurotoxicological effects and the impairment of spatial recognition memory in mice caused by exposure to TiO2 nanoparticles. *Biomaterials, 31*(31), 8043-8050.

Huang, H.-C., Rege, K., & Heys, J. J. (2010). Spatiotemporal temperature distribution and cancer cell death in response to extracellular hyperthermia induced by gold nanorods. *ACS nano, 4*(5), 2892-2900.

Huang, X., Jain, P. K., El-Sayed, I. H., & El-Sayed, M. A. (2007). Gold nanoparticles: interesting optical properties and recent applications in cancer diagnostics and therapy.

Huang, X., Jain, P. K., El-Sayed, I. H., & El-Sayed, M. A. (2008). Plasmonic photothermal therapy (PPTT) using gold nanoparticles. *Lasers in medical science, 23*(3), 217-228.

Huppertz, B. (2011). Nanoparticles: Barrier thickness matters. *Nature nanotechnology, 6*(12), 758-759.

Initiative, N. N. (2006). What is nanotechnology. *Retrieved August, 28*, 2006.

Ishikawa, H., Bischoff, R., & Holtzer, H. (1969). Formation of arrowhead complexes with heavy meromyosin in a variety of cell types. *J Cell Biol, 43*(2), 312-328.

Jiang, J., Oberdörster, G., Elder, A., Gelein, R., Mercer, P., & Biswas, P. (2008). Does nanoparticle activity depend upon size and crystal phase? *Nanotoxicology, 2*(1), 33-42.

John, N. J., Linke, M., & Denker, H. W. (1993). Quantitation of human choriocarcinoma spheroid attachment to uterine epithelial cell monolayers. *In Vitro Cell Dev Biol Anim, 29A*(6), 461-468.

Jovov, B., Wills, N. K., & Lewis, S. A. (1991). A spectroscopic method for assessing confluence of epithelial cell cultures. *Am J Physiol, 261*(6 Pt 1), C1196-1203.

Kalive, M., Zhang, W., Chen, Y., & Capco, D. G. (2012). Human intestinal epithelial cells exhibit a cellular response indicating a potential toxicity upon exposure to hematite nanoparticles. *Cell Biol Toxicol, 28*(5), 343-368. doi: 10.1007/s10565-012-9229-7

Kalive, M., Zhang, W., Chen, Y., & Capco, D. G. (2012). Human intestinal epithelial cells exhibit a cellular response indicating a potential toxicity upon exposure to hematite nanoparticles. *Cell Biol Toxicol, 28*(5), 343-368.

Kammer, F. v. d., Legros, S., Hofmann, T., Larsen, E. H., & Loeschner, K. (2011). Separation and characterization of nanoparticles in complex food and environmental samples by field-flow fractionation. *TrAC Trends in Analytical Chemistry, 30*(3), 425-436.

Kenny, B., DeVinney, R., Stein, M., Reinscheid, D. J., Frey, E. A., & Finlay, B. B. (1997). Enteropathogenic E. coli (EPEC) transfers its receptor for intimate adherence into mammalian cells. *Cell, 91*(4), 511-520.

Kievit, F. M., & Zhang, M. (2011). Surface engineering of iron oxide nanoparticles for targeted cancer therapy. *Accounts of Chemical Research, 44*(10), 853-862.

King, B. F. (1992). Comparative studies of structure and function in mammalian placentas with special reference to maternal-fetal transfer of iron. *American Zoologist, 32*(2), 331-342.

King, D. G. (1988). Cellular organization and peritrophic membrane formation in the cardia (proventriculus) of Drosophila melanogaster. *J Morphol, 196*(3), 253-282.

Koeneman, B. A., Zhang, Y., Hristovski, K., Westerhoff, P., Chen, Y., Crittenden, J. C., & Capco, D. G. (2009). Experimental approach for an< i> in vitro</i> toxicity assay with non-aggregated quantum dots. *Toxicology in Vitro, 23*(5), 955-962.

Koeneman, B. A., Zhang, Y., Westerhoff, P., Chen, Y., Crittenden, J. C., & Capco, D. G. (2010). Toxicity and cellular responses of intestinal cells exposed to titanium dioxide. *Cell Biol Toxicol, 26*(3), 225-238.

Kokkinos, M. I., Murthi, P., Wafai, R., Thompson, E. W., & Newgreen, D. F. (2010). Cadherins in the human placenta--epithelial-mesenchymal transition (EMT) and placental development. *Placenta, 31*(9), 747-755. doi: 10.1016/j.placenta.2010.06.017

Kreuter, J. (1994). Drug targeting with nanoparticles. *European journal of drug metabolism and pharmacokinetics, 19*(3), 253-256.

Kreyling, W. G., Semmler-Behnke, M., & Chaudhry, Q. (2010). A complementary definition of nanomaterial. *Nano Today, 5*(3), 165-168.

Kulvietis, V., Zalgeviciene, V., Didziapetriene, J., & Rotomskis, R. (2011). Transport of nanoparticles through the placental barrier. *The Tohoku Journal of Experimental Medicine, 225*(4), 225-234.

Larabell, C. A., & Chandler, D. E. (1988). The extracellular matrix of Xenopus laevis eggs: a quick-freeze, deep-etch analysis of its modification at fertilization. *J Cell Biol, 107*(2), 731-741.

Lee, N., Tong, M. K., Leung, P. P., Chan, V. W., Leung, S., Tam, P.-C., . . . Luk, J. M. (2006). Kidney claudin-19: localization in distal tubules and collecting ducts and dysregulation in polycystic renal disease. *FEBS Lett, 580*(3), 923.

Lesniak, A., Fenaroli, F., Monopoli, M. P., Åberg, C., Dawson, K. A., & Salvati, A. (2012). Effects of the presence or absence of a protein corona on silica nanoparticle uptake and impact on cells. *ACS nano, 6*(7), 5845-5857.

Leutwyler, W. K., Bürgi, S. L., & Burgl, H. (1996). Semiconductor clusters, nanocrystals, and quantum dots. *Science, 271*(5251), 933-937.

Li, H., van Ravenzwaay, B., Rietjens, I. M., & Louisse, J. (2013). Assessment of an in vitro transport model using BeWo b30 cells to predict placental transfer of compounds. Arch Toxicol. doi: 10.1007/s00204-013-1074-9

Lin, C.-J., Lu, Y.-T., Hsieh, C.-H., & Chien, S.-H. (2009). Surface modification of highly ordered TiO2 nanotube arrays for efficient photoelectrocatalytic water splitting. *Applied Physics Letters, 94*(11), 113102.

Lipsky, E. M., & Robinson, A. L. (2006). Effects of dilution on fine particle mass and partitioning of semivolatile organics in diesel exhaust and wood smoke. *Environmental Science & Technology, 40*(1), 155-162.

Lu, A. H., Salabas, E. e. L., & Schüth, F. (2007). Magnetic nanoparticles: synthesis, protection, functionalization, and application. *Angewandte Chemie International Edition, 46*(8), 1222-1244.

Lundqvist, M., Stigler, J., Elia, G., Lynch, I., Cedervall, T., & Dawson, K. A. (2008). Nanoparticle size and surface properties determine the protein corona with possible implications for biological impacts. *Proceedings of the National Academy of Sciences, 105*(38), 14265-14270.

Mahmoudi, M., Sant, S., Wang, B., Laurent, S., & Sen, T. (2011). Superparamagnetic iron oxide nanoparticles (SPIONs): development, surface modification and applications in chemotherapy. *Advanced drug delivery reviews, 63*(1), 24-46.

Maiorano, G., Sabella, S., Sorce, B., Brunetti, V., Malvindi, M. A., Cingolani, R., & Pompa, P. P. (2010). Effects of cell culture media on the dynamic formation of protein nanoparticle complexes and influence on the cellular response. *ACS nano, 4*(12), 7481-7491.

Maneerung, T., Tokura, S., & Rujiravanit, R. (2008). Impregnation of silver nanoparticles into bacterial cellulose for antimicrobial wound dressing. *Carbohydrate polymers, 72*(1), 43-51.

Manjarrez-Hernandez, H., Aitken, A., Baldwin, T., Williams, P., & Knutton, S. (1992). Intestinal epithelial cell protein phosphorylation in enteropathogenic Escherichia coli diarrhoea. *The Lancet, 339*(8792), 521-523.

Mardon, H., Grewal, S., & Mills, K. (2007). *Experimental models for investigating implantation of the human embryo*. Paper presented at the Seminars in reproductive medicine.

Margolis, L. B., & Bergelson, L. D. (1979). Lipid-cell interactions. Induction of microvilli on the cell surface by liposomes. *Exp Cell Res, 119*(1), 145-150.

Matter, K., Aijaz, S., Tsapara, A., & Balda, M. S. (2005). Mammalian tight junctions in the regulation of epithelial differentiation and proliferation. *Curr Opin Cell Biol, 17*(5), 453-458.

Maynard, A. D. (2014). A decade of uncertainty. *Nature nanotechnology, 9*(3), 159-160.

McConnell, R. E., Benesh, A. E., Mao, S., Tabb, D. L., & Tyska, M. J. (2011). Proteomic analysis of the enterocyte brush border. *American Journal of Physiology-Gastrointestinal and Liver Physiology, 300*(5), G914-G926.

McConnell, R. E., Higginbotham, J. N., Shifrin, D. A., Tabb, D. L., Coffey, R. J., & Tyska, M. J. (2009). The enterocyte microvillus is a vesicle-generating organelle. *J Cell Biol, 185*(7), 1285-1298.

McConnell, R. E., & Tyska, M. J. (2007). Myosin-1a powers the sliding of apical membrane along microvillar actin bundles. *J Cell Biol, 177*(4), 671-681.

McNabb, J., & Sandborn, E. (1964). Filaments in the microvillous border of intestinal cells. *J Cell Biol, 22*(3), 701-704.

Menezes, V., Malek, A., & A Keelan, J. (2011). Nanoparticulate drug delivery in pregnancy: placental passage and fetal exposure. *Current Pharmaceutical Biotechnology, 12*(5), 731-742.

Michalet, X., Pinaud, F. F., Bentolila, L. A., Tsay, J. M., Doose, S., Li, J. J., . . . Weiss, S. (2005). Quantum dots for live cells, in vivo imaging, and diagnostics. *Science, 307*(5709), 538-544.

Milani, S., Baldelli Bombelli, F., Pitek, A. S., Dawson, K. A., & Rädler, J. (2012). Reversible versus irreversible binding of transferrin to polystyrene nanoparticles: soft and hard corona. *ACS nano, 6*(3), 2532-2541.

Miller, D., & Crane, R. K. (1961). The digestive function of the epithelium of the small intestine: II. Localization of disaccharide hydrolysis in the isolated brush border portion of intestinal epithelial cells. *Biochim Biophys Acta, 52*(2), 293-298.

Misch, D., Giebel, P., & Faust, R. (1980). Intestinal microvilli: responses to feeding and fasting. *Eur J Cell Biol, 21*(3), 269-279.

Mishra, B., Patel, B. B., & Tiwari, S. (2010). Colloidal nanocarriers: a review on formulation technology, types and applications toward targeted drug delivery. *Nanomedicine: Nanotechnology, biology and medicine, 6*(1), 9-24.

Monopoli, M. P., Åberg, C., Salvati, A., & Dawson, K. A. (2012). Biomolecular coronas provide the biological identity of nanosized materials. *Nature nanotechnology, 7*(12), 779-786.

Monopoli, M. P., Walczyk, D., Campbell, A., Elia, G., Lynch, I., Baldelli Bombelli, F., & Dawson, K. A. (2011). Physical chemical aspects of protein corona: relevance to in vitro and in vivo biological impacts of nanoparticles. *Journal of the American Chemical Society, 133*(8), 2525-2534.

Mooseker, M. S. (1976). Brush border motility. Microvillar contraction in triton-treated brush borders isolated from intestinal epithelium. *J Cell Biol, 71*(2), 417-433.

Mooseker, M. S. (1985). Organization, chemistry, and assembly of the cytoskeletal apparatus of the intestinal brush border. *Annual review of cell biology, 1*(1), 209-241.

Morck, T. J., Sorda, G., Bechi, N., Rasmussen, B. S., Nielsen, J. B., Ietta, F., . . . Knudsen, L. E. (2010). Placental transport and in vitro effects of Bisphenol A. *Reprod Toxicol, 30*(1), 131-137. doi: 10.1016/j.reprotox.2010.02.007

Morgan, N. S., Heintzelman, M. B., & Mooseker, M. S. (1995). Characterization of Myosin-IA and Myosin-IB, Two Unconventional Myosins Associated with the Drosophila Brush Border Cytoskeleton. *Dev Biol, 172*(1), 51-71.

Mukherjee, T., Squillantea, E., Gillespieb, M., & Shao, J. (2004). Transepithelial electrical resistance is not a reliable measurement of the Caco-2 monolayer integrity in Transwell. *Drug Deliv, 11*(1), 11-18. doi: 10.1080/10717540490280345

Mukherjee, T., & Staehelin, L. (1971). The fine-structural organization of the brush border of intestinal epithelial cells. *J Cell Sci, 8*(3), 573-599.

Mukherjee, T., & Williams, A. W. (1967). A comparative study of the ultrastructure of microvilli in the epithelium of small and large intestine of mice. *J Cell Biol, 34*(2), 447-461.

Mutch, D. M., Berger, A., Mansourian, R., Rytz, A., & Roberts, M.-A. (2002). The limit fold change model: a practical approach for selecting differentially expressed genes from microarray data. *BMC bioinformatics, 3*(1), 17.

Nagata, S. (1997). Apoptosis by Death Factor Review. *Cell, 88*(355-365), 392.

Nohynek, G., Dufour, E., & Roberts, M. (2008). Nanotechnology, cosmetics and the skin: is there a health risk? *Skin pharmacology and physiology, 21*(3), 136-149.

Oberdörster, G., Maynard, A., Donaldson, K., Castranova, V., Fitzpatrick, J., Ausman, K., . . . Lai, D. (2005). Principles for characterizing the potential human health effects from exposure to nanomaterials: elements of a screening strategy. *Part Fibre Toxicol, 2*(1), 8.

Oberdörster, G., Stone, V., & Donaldson, K. (2007). Toxicology of nanoparticles: a historical perspective. *Nanotoxicology, 1*(1), 2-25.

Oberdörster, G., & Utell, M. J. (2002). Ultrafine particles in the urban air: to the respiratory tract--and beyond? *Environmental health perspectives, 110*(8), A440.

Oecd. (1994). *OECD Guidelines for the Testing of Chemicals*: Organization for Economic.

Oh, J. K., & Park, J. M. (2011). Iron oxide-based superparamagnetic polymeric nanomaterials: design, preparation, and biomedical application. *Progress in Polymer Science, 36*(1), 168-189.

Palay, S. L., & Karlin, L. J. (1959). An electron microscopic study of the intestinal villus I. The fasting animal. *The Journal of Biophysical and Biochemical Cytology, 5*(3), 363-371.

Patterson, A. (1939). The Scherrer formula for X-ray particle size determination. *Physical review, 56*(10), 978.

Pattillo, R. A., & Gey, G. O. (1968). The establishment of a cell line of human hormone-synthesizing trophoblastic cells in vitro. *Cancer Res, 28*(7), 1231-1236.

Penners, N., & Koopal, L. (1986). Preparation and optical properties of homodisperse haematite hydrosols. Colloids and Surfaces, 19(4), 337-349.

Peterson, M., & Mooseker, M. (1992). Characterization of the enterocyte-like brush border cytoskeleton of the C2BBe clones of the human intestinal cell line, Caco-2. *J Cell Sci, 102*(3), 581-600.

Peterson, M. D., Bement, W. M., & Mooseker, M. S. (1993). An in vitro model for the analysis of intestinal brush border assembly. II. Changes in expression and localization of brush border proteins during cell contact-induced brush border assembly in Caco-2BBe cells. *J Cell Sci, 105*(2), 461-472.

Peterson, M. D., & Mooseker, M. S. (1993). An in vitro model for the analysis of intestinal brush border assembly. I. Ultrastructural analysis of cell contact-induced brush border assembly in Caco-2BBe cells. *J Cell Sci, 105*(2), 445-460.

Pietroiusti, A., Campagnolo, L., & Fadeel, B. (2012). Interactions of Engineered Nanoparticles with Organs Protected by Internal Biological Barriers. *Small*.

Pijnenborg, R. (1990). Trophoblast invasion and placentation in the human: morphological aspects *Trophoblast Invasion and Endometrial Receptivity* (pp. 33-47): Springer.

Poole, K., Meder, D., Simons, K., & Müller, D. (2004). The effect of raft lipid depletion on microvilli formation in MDCK cells, visualized by atomic force microscopy. *FEBS Lett, 565*(1), 53-58.

Powell, J. J., Faria, N., Thomas-McKay, E., & Pele, L. C. (2010). Origin and fate of dietary nanoparticles and microparticles in the gastrointestinal tract. *Journal of autoimmunity, 34*(3), J226-J233.

Quackenbush, J. (2002). Microarray data normalization and transformation. *Nature genetics, 32*, 496-501.

Rai, M., Yadav, A., & Gade, A. (2009). Silver nanoparticles as a new generation of antimicrobials. *Biotechnology advances, 27*(1), 76-83.

Rampon, C., Bouillot, S., Climescu-Haulica, A., Prandini, M.-H., Cand, F., Vandenbrouck, Y., & Huber, P. (2008). Protocadherin 12 deficiency alters morphogenesis and transcriptional profile of the placenta. *Physiological genomics, 34*(2), 193-204.

Rao, R. (2007). Oxidative stress-induced disruption of epithelial and endothelial tight junctions. *Frontiers in bioscience: a journal and virtual library, 13*, 7210-7226.

Rasband, W. S. (2008). ImageJ. *http://rsbweb. nih. gov/ij/*.

Reed, J. C. (2000). Mechanisms of apoptosis. *The American journal of pathology, 157*(5), 1415-1430.

Reed, R. B., Faust, J., Yang, Y., Doudrick, K., Capco, D., Hristovski, K. D., & Westerhoff, P. (2014). Characterization of nanomaterials in metal colloid-containing dietary supplement drinks and assessment of their potential interactions after ingestion. *ACS Sustainable Chemistry & Engineering*.

Regulations, C. F. (2000). Title 21. *Chapter I (revised)*.

Resch-Genger, U., Grabolle, M., Cavaliere-Jaricot, S., Nitschke, R., & Nann, T. (2008). Quantum dots versus organic dyes as fluorescent labels. *Nature methods, 5*(9), 763-775.

Revenu, C., Ubelmann, F., Hurbain, I., El-Marjou, F., Dingli, F., Loew, D., . . . Rivero, F. (2012). A new role for the architecture of microvillar actin bundles in apical retention of membrane proteins. *Mol Biol Cell, 23*(2), 324-336.

Roco, M. C. (2007). National nanotechnology initiative-past, present, future. *Handbook on nanoscience, engineering and technology, 2*.

Rytting, E., & Audus, K. L. (2005). Novel organic cation transporter 2-mediated carnitine uptake in placental choriocarcinoma (BeWo) cells. *J Pharmacol Exp Ther, 312*(1), 192-198. doi: 10.1124/jpet.104.072363

Rytting, E., & Audus, K. L. (2007). Effects of low oxygen levels on the expression and function of transporter OCTN2 in BeWo cells. *J Pharm Pharmacol, 59*(8), 1095-1102. doi: 10.1211/jpp.59.8.0006

Sadrieh, N., Wokovich, A. M., Gopee, N. V., Zheng, J., Haines, D., Parmiter, D., . . . McNeil, S. E. (2010). Lack of significant dermal penetration of titanium dioxide (TiO2) from sunscreen formulations containing nano-and sub-micron-size TiO2 particles. *Toxicological Sciences*, kfq041.

Saunders, M. (2009). Transplacental transport of nanomaterials. *Wiley Interdiscip Rev Nanomed Nanobiotechnol, 1*(6), 671-684. doi: 10.1002/wnan.53

Sayes, C. M., Wahi, R., Kurian, P. A., Liu, Y., West, J. L., Ausman, K. D., . . . Colvin, V. L. (2006). Correlating nanoscale titania structure with toxicity: a cytotoxicity and inflammatory response study with human dermal fibroblasts and human lung epithelial cells. *Toxicological Sciences, 92*(1), 174-185.

Schrödinger, E. (2009). Encyclopedia Britannica,(2009). *Encyclopedia Britannica, online, 18*.

Selikoff, I. J., Churg, J., & Hammond, E. C. (1964). Asbestos exposure and neoplasia. *Jama, 188*(1), 22-26.

Semmler-Behnke, M., Fertsch, S., Schmid, G., Wenk, A., & Kreyling, W. G. (2007). Uptake of 1.4 nm versus 18 nm gold nanoparticles in secondary target organs is size dependent in control and pregnant rats after intratracheal or intravenous application. *EuroNanoForum 2007*, 102.

Semmler‐Behnke, M., Kreyling, W. G., Lipka, J., Fertsch, S., Wenk, A., Takenaka, S., . . . Brandau, W. (2008). Biodistribution of 1.4‐and 18‐nm Gold Particles in Rats. *Small, 4*(12), 2108-2111.

Sheth, P., Seth, A., Thangavel, M., Basuroy, S., & Rao, R. (2004). Epidermal Growth Factor Prevents Acetaldehyde‐Induced Paracellular Permeability in Caco‐2 Cell Monolayer. *Alcoholism: Clinical and Experimental Research, 28*(5), 797-804.

Shibayama, T., Carboni, J. M., & Mooseker, M. S. (1987). Assembly of the intestinal brush border: appearance and redistribution of microvillar core proteins in developing chick enterocytes. *J Cell Biol, 105*(1), 335-344.

Shifrin Jr, D. A., McConnell, R. E., Nambiar, R., Higginbotham, J. N., Coffey, R. J., & Tyska, M. J. (2012). Enterocyte microvillus-derived vesicles detoxify bacterial products and regulate epithelial-microbial interactions. *Current Biology, 22*(7), 627-631.

Shih, P., Yung, S., & Chin, T. (1998). Thermal and corrosion behavior of P< sub> 2</sub> O< sub> 5</sub>-Na< sub> 2</sub> O-CuO glasses. *Journal of non-crystalline solids, 224*(2), 143-152.

Silverstein, S. C., Steinman, R. M., & Cohn, Z. A. (1977). Endocytosis. *Annual review of biochemistry, 46*(1), 669-722.

Singh, G., Stephan, C., Westerhoff, P., Carlander, D., & Duncan, T. V. (2014). Measurement methods to detect, characterize, and quantify engineered nanomaterials in foods. *Comprehensive Reviews in Food Science and Food Safety, 13*(4), 693-704.

Sood, A., Salih, S., Roh, D., Lacharme-Lora, L., Parry, M., Hardiman, B., . . . Gokhale, P. (2011). Signalling of DNA damage and cytokines across cell barriers exposed to nanoparticles depends on barrier thickness. *Nature nanotechnology, 6*(12), 824-833.

Stevenson, B. R., Siliciano, J. D., Mooseker, M. S., & Goodenough, D. A. (1986). Identification of ZO-1: a high molecular weight polypeptide associated with the tight junction (zonula occludens) in a variety of epithelia. *J Cell Biol, 103*(3), 755-766.

Stidwill, R. P., Wysolmerski, T., & Burgess, D. R. (1984). The brush border cytoskeleton is not static: in vivo turnover of proteins. *J Cell Biol, 98*(2), 641-645.

Sylvester, P., Westerhoff, P., Möller, T., Badruzzaman, M., & Boyd, O. (2007). A hybrid sorbent utilizing nanoparticles of hydrous iron oxide for arsenic removal from drinking water. *Environmental Engineering Science, 24*(1), 104-112.

Takeda, K., Suzuki, K.-i., Ishihara, A., Kubo-Irie, M., Fujimoto, R., Tabata, M., . . . Sugamata, M. (2009). Nanoparticles transferred from pregnant mice to their offspring can damage the genital and cranial nerve systems. *Journal of Health Science, 55*(1), 95-102.

Tanuma, S., Powell, C. J., & Penn, D. R. (1994). Calculations of electron inelastic mean free paths. V. Data for 14 organic compounds over the 50–2000 eV range. *Surface and interface analysis, 21*(3), 165-176.

Teeguarden, J. G., Hinderliter, P. M., Orr, G., Thrall, B. D., & Pounds, J. G. (2007). Particokinetics in vitro: dosimetry considerations for in vitro nanoparticle toxicity assessments. *Toxicological Sciences, 95*(2), 300-312.

Temm-Grove, C., Helbing, D., Wiegand, C., Honer, B., & Jockusch, B. (1992). The upright position of brush border-type microvilli depends on myosin filaments. *J Cell Sci, 101*(3), 599-610.

Terentyuk, G. S., Maslyakova, G. N., Khlebtsov, N. G., Akchurin, G. G., Tuchin, V. V., Maksimova, I. L., . . . Suleymanova, L. V. (2009). Laser-induced tissue hyperthermia mediated by gold nanoparticles: toward cancer phototherapy. *Journal of biomedical optics, 14*(2), 021016-021016-021019.

Thorburn, A. (2004). Death receptor-induced cell killing. *Cellular signalling, 16*(2), 139-144.

Tiede, K., Boxall, A. B., Tear, S. P., Lewis, J., David, H., & Hassellöv, M. (2008). Detection and characterization of engineered nanoparticles in food and the environment. *Food Additives and Contaminants, 25*(7), 795-821.

Tilney, L. G., & Cardell, R. R. (1970). Factors controlling the reassembly of the microvillous border of the small intestine of the salamander. *J Cell Biol, 47*(2), 408-422.

Tilney, L. G., & Mooseker, M. (1971). Actin in the brush-border of epithelial cells of the chicken intestine. *Proceedings of the National Academy of Sciences, 68*(10), 2611-2615.

Trier, J. S. (1963). Studies on small intestinal crypt epithelium I. The fine structure of the crypt epithelium of the proximal small intestine of fasting humans. *J Cell Biol, 18*(3), 599-620.

Tyska, M., & Mooseker, M. (2002). MYO1A (brush border myosin I) dynamics in the brush border of LLC-PK1-CL4 cells. *Biophysical journal, 82*(4), 1869-1883.

van der Ende, A., du Maine, A., Schwartz, A. L., & Strous, G. J. (1990). Modulation of transferrin-receptor activity and recycling after induced differentiation of BeWo choriocarcinoma cells. *Biochem J, 270*(2), 451-457.

van der Ende, A., du Maine, A., Simmons, C. F., Schwartz, A. L., & Strous, G. J. (1987). Iron metabolism in BeWo chorion carcinoma cells. Transferrin-mediated uptake and release of iron. *J Biol Chem, 262*(18), 8910-8916.

van der Flier, L. G., & Clevers, H. (2009). Stem cells, self-renewal, and differentiation in the intestinal epithelium. *Annual review of physiology, 71*, 241-260.

Verma, A., & Stellacci, F. (2010). Effect of surface properties on nanoparticle–cell interactions. *Small, 6*(1), 12-21.

Virkutyte, J., Al-Abed, S. R., & Dionysiou, D. D. (2012). Depletion of the protective aluminum hydroxide coating in TiO< sub> 2</sub>-based sunscreens by swimming pool water ingredients. *Chemical Engineering Journal*.

Wahajuddin, S. A. (2012). Superparamagnetic iron oxide nanoparticles: magnetic nanoplatforms as drug carriers. *Int J Nanomedicine, 7*, 3445.

Wang, B., Zhang, L., Bae, S. C., & Granick, S. (2008). Nanoparticle-induced surface reconstruction of phospholipid membranes. *Proceedings of the National Academy of Sciences, 105*(47), 18171-18175.

Wang, J., Zhou, G., Chen, C., Yu, H., Wang, T., Ma, Y., . . . Sun, J. (2007). Acute toxicity and biodistribution of different sized titanium dioxide particles in mice after oral administration. *Toxicology letters, 168*(2), 176-185.

Wang, Z., Lee, J. H., & Lu, Y. (2008). Label‐Free Colorimetric Detection of Lead Ions with a Nanomolar Detection Limit and Tunable Dynamic Range by using Gold Nanoparticles and DNAzyme. *Advanced Materials, 20*(17), 3263-3267.

Warheit, D. B., Hoke, R. A., Finlay, C., Donner, E. M., Reed, K. L., & Sayes, C. M. (2007). Development of a base set of toxicity tests using ultrafine TiO2 particles as a component of nanoparticle risk management. *Toxicology letters, 171*(3), 99-110.

Warheit, D. B., Sayes, C. M., Reed, K. L., & Swain, K. A. (2008). Health effects related to nanoparticle exposures: environmental, health and safety considerations for assessing hazards and risks. *Pharmacology & therapeutics, 120*(1), 35-42.

Weir, A., Westerhoff, P., Fabricius, L., Hristovski, K., & von Goetz, N. (2012). Titanium dioxide nanoparticles in food and personal care products. *Environmental Science & Technology, 46*(4), 2242-2250.

Westerhoff, P., Zhang, Y., Crittenden, J., & Chen, Y. (2008). Properties of commercial nanoparticles that affect their removal during water treatment. *Nanoscience and Nanotechnology: Environmental and Health Impacts. NJ: John Wiley and Sons*, 71-90.

Wice, B., Menton, D., Geuze, H., & Schwartz, A. L. (1990). Modulators of cyclic AMP metabolism induce syncytiotrophoblast formation in vitro. *Exp Cell Res, 186*(2), 306-316.

Wu, C., Yin, P., Zhu, X., OuYang, C., & Xie, Y. (2006). Synthesis of hematite (a-Fe2O3) nanorods: diameter-size and shape effects on their applications in magnetism, lithium ion battery, and gas sensors. *The Journal of Physical Chemistry B, 110*(36), 17806-17812.

Yamashita, K., Yoshioka, Y., Higashisaka, K., Mimura, K., Morishita, Y., Nozaki, M., . . . Nagano, K. (2011). Silica and titanium dioxide nanoparticles cause pregnancy complications in mice. *Nature nanotechnology, 6*(5), 321-328.

Young, B., Woodford, P., & O'Dowd, G. (2013). *Wheater's functional histology: a text and colour atlas*: Elsevier Health Sciences.

Zhang, W., Crittenden, J., Li, K., & Chen, Y. (2012). Attachment Efficiency of Nanoparticle Aggregation in Aqueous Dispersions: Modeling and Experimental Validation. *Environmental Science & Technology, 46*(13), 7054-7062.

Zhang, W., Hughes, J., & Chen, Y. (2012). Impacts of hematite nanoparticle exposure on biomechanical, adhesive, and surface electrical properties of Escherichia coli cells. *Applied and environmental microbiology, 78*(11), 3905-3915.

Zhang, W., Kalive, M., Capco, D. G., & Chen, Y. (2010). Adsorption of hematite nanoparticles onto Caco-2 cells and the cellular impairments: effect of particle size. *Nanotechnology, 21*(35), 355103.

Zhang, Y., Chen, Y., Westerhoff, P., Hristovski, K., & Crittenden, J. C. (2008). Stability of commercial metal oxide nanoparticles in water. *Water research, 42*(8), 2204-2212.

Zhang, Z., Kong, F., Vardhanabhuti, B., Mustapha, A., & Lin, M. (2012). Detection of engineered silver nanoparticle contamination in pears. *Journal of agricultural and food chemistry, 60*(43), 10762-10767.

Zhou, F., Kotru, S., & Pandey, R. (2002). Pulsed laser-deposited ilmenite–hematite films for application in high-temperature electronics. *Thin Solid Films, 408*(1), 33-36.

Zwaenepoel, I., Naba, A., Da Cunha, M. M. L., Del Maestro, L., Formstecher, E., Louvard, D., & Arpin, M. (2012). Ezrin regulates microvillus morphogenesis by promoting distinct activities of Eps8 proteins. *Mol Biol Cell, 23*(6), 1080-1095.

APPENDIX A

SUPPLEMENTAL FIGURE 1

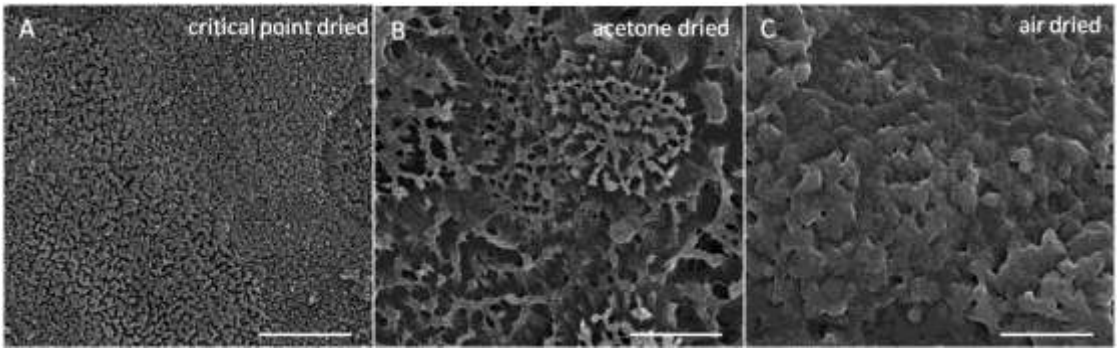

Supplemental Figure 1. Improper drying results in sample artifacts. (A) Samples that are critical point dried retain the normal organization of the brush border, and permit analysis of microvilli. (B) Samples dried with anhydrous acetone have brush borders whose microvilli are aggregated. (C) Air dried samples appear completely depressed. Neither (B) nor (C) can be analyzed for alterations in the brush border microvilli due to NP exposure since the drying techniques impart structural artifacts. Each image was originally captured at 5,000x and shown at the same magnification. The scale bars in the lower right corner are 5 µm.

APPENDIX B

SUPPLEMENTAL FIGURE 2

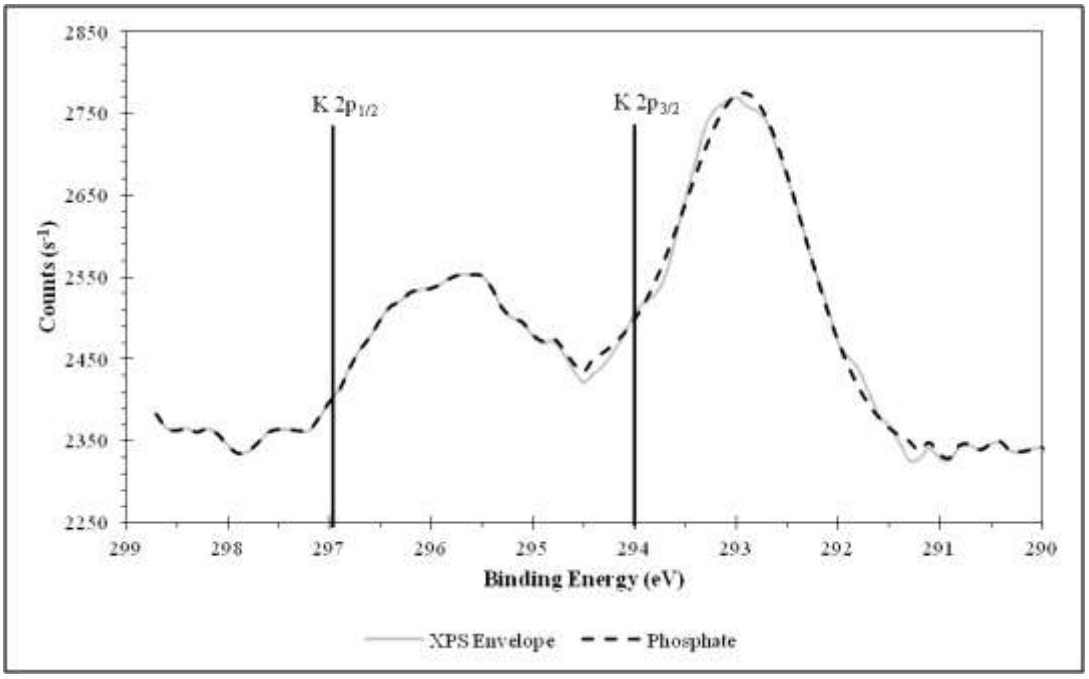

Supplemental Figure 2. XPS K 2p spectra of gum-TiO_2.

APPENDIX C

SUPPLEMENTAL FIGURE 3

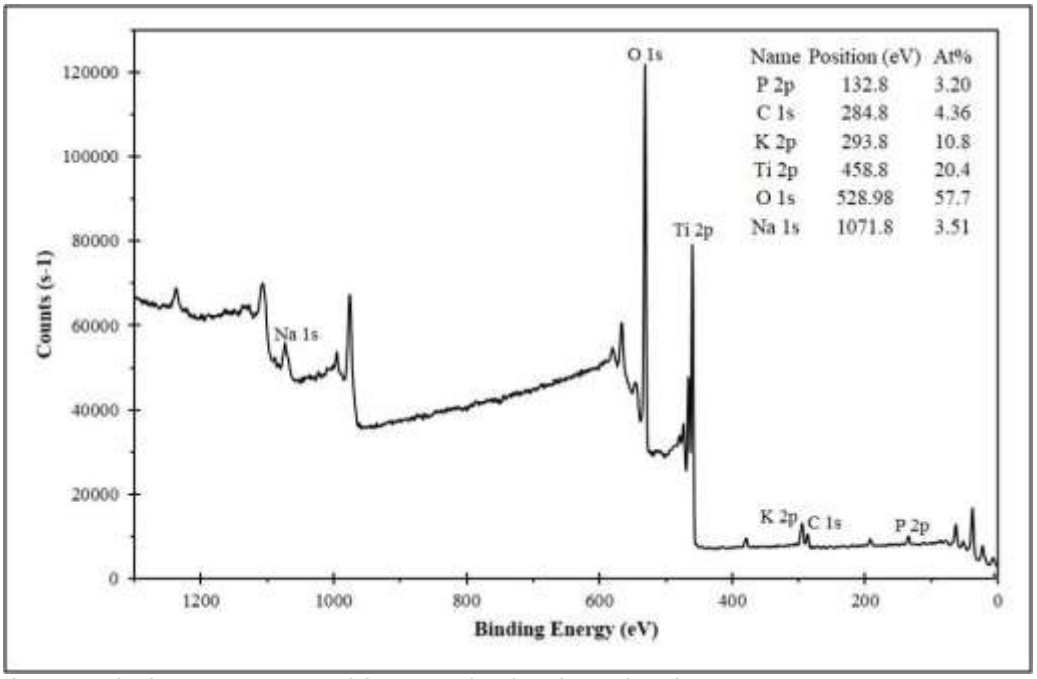

Supplemental Figure 3. XPS wide scan for food grade TiO_2.

APPENDIX D

SUPPLEMENTAL FIGURE 4

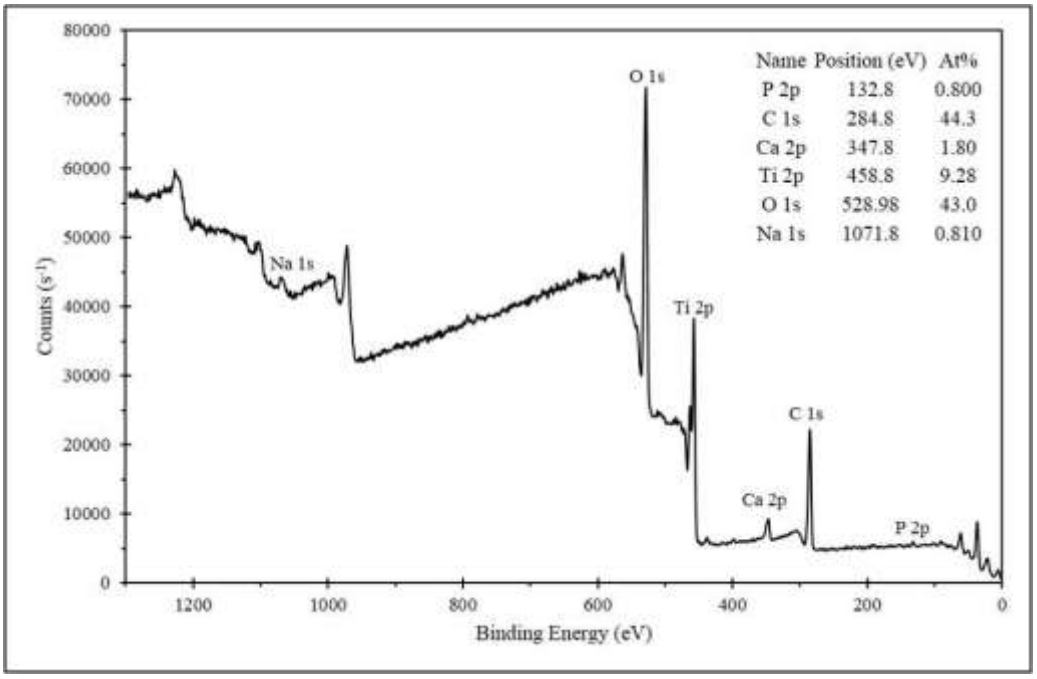

Supplemental Figure 4. XPS wide scan for gum-TiO_2.

APPENDIX E

SUPPLEMENTAL FIGURE 5

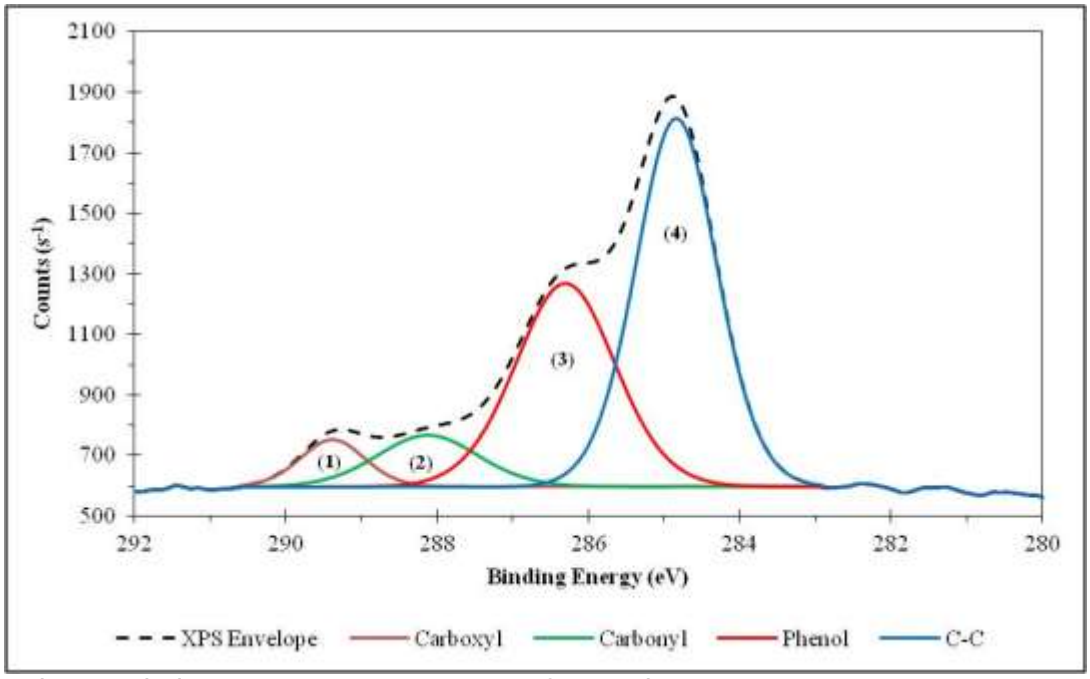

Supplemental Figure 5. XPS C 1s spectra of gum-TiO_2

APPENDIX F

SUPPLEMENTAL FIGURE 6

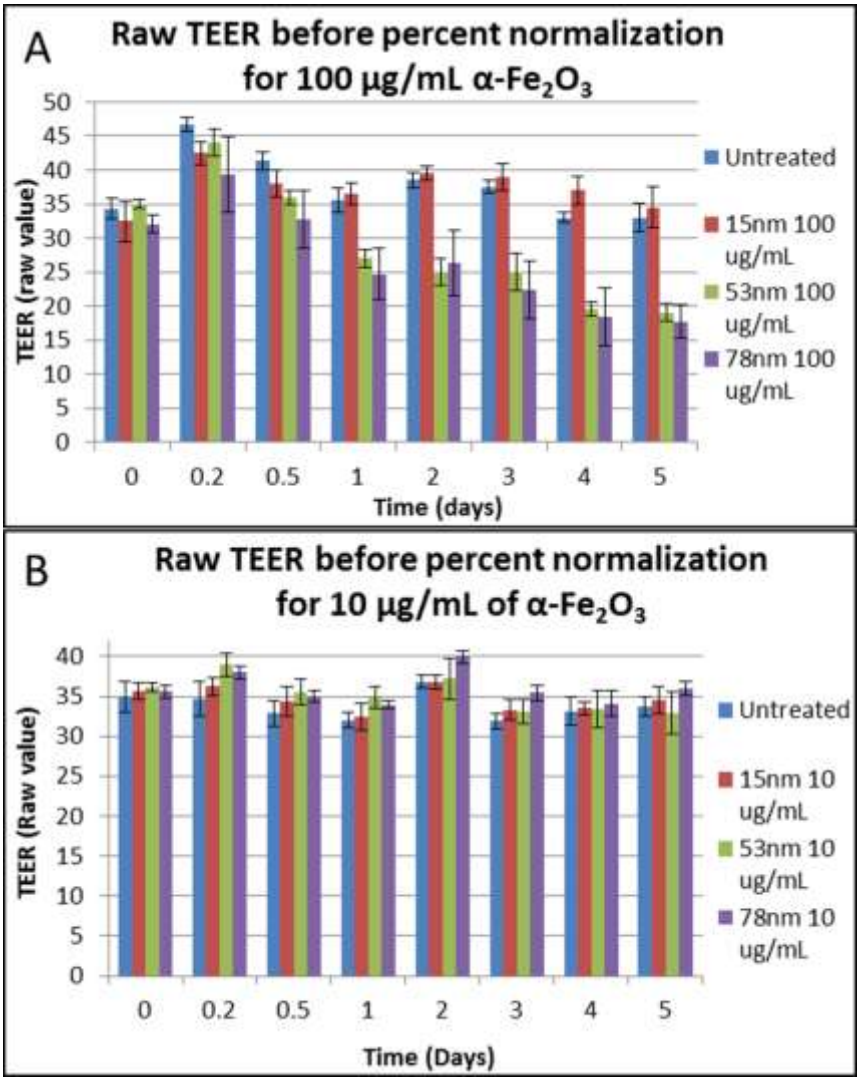

Supplemental Figure 6. Raw TEER values before percent normalization for epithelia exposed to NPs at concentrations of 100 µg/mL and 10 µg/mL. The histograms indicate that exposure to large diameter NPs result in disruption of TEER (A) The graph illustrates the change in TEER after application of different diameters of α-Fe_2O_3 at a concentration of 100 µg/mL. Both 50- and 78 nm NP treated epithelia follow the same trend, whereas the 15nm diameter exposure followed the trend of the untreated specimens. (B) Exposure to 10 µg/mL for all α-Fe_2O_3 diameters tested results in no change compared to the untreated specimens. As indicated in the Methods section, TEER levels off at its maximum value of 40 Ωcm^2 3 days after seeding BeWo cells. The NPs were applied after this 3 day culture period which is denoted as t=0 in the graphs. All experiments were conducted at least 3 independent times where n=3.

APPENDIX G

SUPPLEMENTAL FIGURE 7

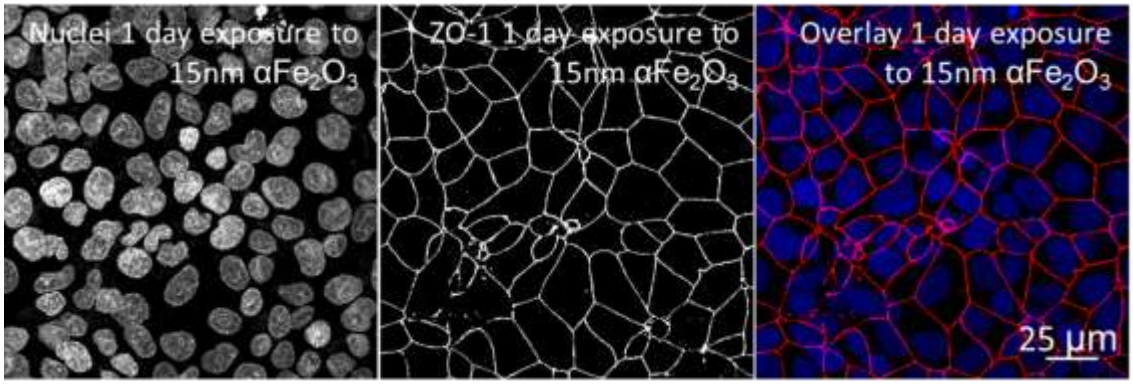

Supplemental Figure 7. Tight junctions, as measured by ZO-1 immunofluorescence, are unperturbed after exposure to 15 nm α-Fe_2O_3 NPs at a 100 µg/mL concentration at the 1 day time point.

APPENDIX H

SUPPLEMENTAL FIGURE 8

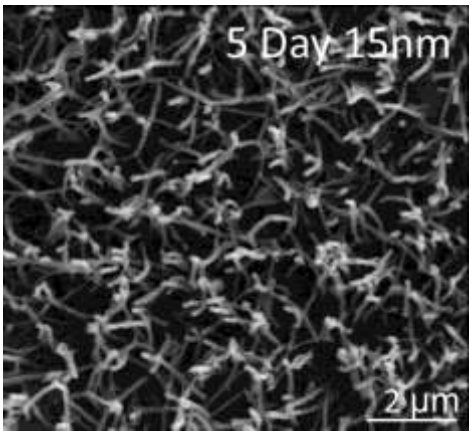

Supplemental Figure 8. Morphological analysis of microvilli in 15 nm-treated specimens indicates no change in the number and structure of the microvilli. After exposure to 15 nm NPs the microvilli remain erect and appear to contain a similar number of microvilli compared to controls.